2011

Analytical design method for cold production of heavy oil with bottom water using Bilateral Sink Wells

Wenting Qin
Louisiana State University and Agricultural and Mechanical College, wqin1@lsu.edu

ANALYTICAL DESIGN METHOD FOR COLD PRODUCTION OF HEAVY OIL WITH BOTTOM WATER USING BILATERAL SINK WELLS

A Dissertation

Submitted to the Graduate Faculty of the
Louisiana State University and
Agricultural and Mechanical College
in partial fulfillment of the
requirements for the degree of
Doctor of Philosophy

in

The Craft & Hawkins Department of Petroleum Engineering

by

Wenting Qin

B.S., Southwest Petroleum University, 2003

M.S., Delft University of Technology, 2006

August 2011

ACKNOWLEDGMENTS

First and foremost, my gratitude goes to my advisors, Dr. Andrew K. Wojtanowicz and Dr. Christopher D. White. In the past four years, Dr. Andrew K. Wojtanowicz spent countless hours and endless effort helping me in my pursuit of a doctoral degree. Without his guidance, patience, and support, accomplishing this study would never have been possible. Dr. Chris White's advice and inspiration, as well as his encouragement, was essential in my last year of this research. He spent a tremendous amount of time with me discussing technical details and was always there when I needed help. I am fortunate to have had him as my supervisor.

I would also like to express my sincere appreciation to my committee member, Dr. Stephen O. Sears. Not only did I learn from his knowledge and experience in the technical aspects, I have also greatly appreciated his priceless guidance in building my writing and presentation skills. Thanks are also extended to a member of my supervising committee, Dr. Richard Hughes, for his valuable comments and suggestions on my research. Further, I would like to thank Dr. Michael W. Wascom for taking time from his busy schedule to provide strong support for my research.

Lastly, I wish to express my appreciation to all the faculty members and graduate students of the Craft and Hawkins Department of Petroleum Engineering. I will keep special memories of the time we have had together.

TABLE OF CONTENTS

ABSTRACT

Few heavy oil reservoirs with strong bottom water drives have been developed successfully because of severe water coning. Water coning tends to cause low ultimate recovery, low well productivity, and high water production. Although thermal and gravity-assisted methods might improve recovery in oil reservoirs, such methods are widely perceived as either economically unfavorable or technologically infeasible. This study proposes a new, cold production technique, called Bilateral Water Sink (BWS), to meet those challenges.

The BWS method suppresses water cresting by producing oil and water simultaneously from separate, horizontal wells completed in the oil and water zones; the oil and water completions are parallel, with the oil well directly above the water well. In conventional horizontal well production, water cresting causes water to bypass oil, making the water drive mechanism ineffective. BWS controls water invasion by altering the pressure distribution in the near-well area. With cresting suppressed, the oil completion remains water-free, allowing water to displace oil from the edges of the well drainage area to the oil completion, increasing ultimate recovery. Unlike existing heavy oil recovery methods, BWS exploits the natural reservoir energy in the bottom water drive. This makes BWS economically, technically, and environmentally appealing – especially for offshore applications, where cold production is currently the only option and oil-water separation is a problem.

In this study, BWS oil recovery is investigated analytically and numerically. A new mathematical model identifies controlling variables and project design parameters, and describes the relationships among them. The design model is used to select rates of water and oil in BWS wells for best performance. The analytical model is verified by a comparison to numerical simulations. These two approaches together provide the quantitative account of the BWS's effect on avoiding water cresting and improving oil recovery. The results show that BWS can increase

oil recovery from 10 percent to over 40 percent in a conventional case, while avoiding the problem of oil-contaminated water production. As a result, the mathematical model of BWS well behavior is shown to be a practical reservoir management tool to guide development of heavy oil reservoirs with bottom water drives.

CHAPTER 1. INTRODUCTION

1.1 Background and Motivation

The total world oil resources are estimated to be around 9 – 13 trillion barrels and heavy oil accounts for 15 percent (Alboudwarej et al 2006). As the production of conventional oil declines, recovering heavy oil becomes more important. Unfortunately, the primary recovery of heavy oil is extremely low, in the range of 5 to 15 percent (Alboudwarej et al 2006), because of the high viscosity and low mobility of oil. Heavy oil recovery is further complicated by the presence of underlying water. Due to a high water/oil mobility ratio ($M >> 1$) and a small density difference between oil and water, water coning and cresting may lead to early water breakthrough and rapidly increase water cuts to nearly 100 percent (Kasraie and Ali 1987). These factors lead to a low ultimate recovery within a range of 1 – 5 percent (Butler and Mokry 1993).

At present, thermal and gravity-assisted methods may be applied to a heavy oil reservoir with underlying bottom water, such as Steam – Assisted Gravity Drainage (SAGD) and Vapor – Assisted Petroleum Extraction (VAPEX). However, the cost of providing the heat may be high, posing an economic constraint to heavy oil production. For example, 60 – 70 percent of the Steam-Assisted Gravity Drainage OPEX are steam generation and water recycling costs (Dusseault 2006). The recovery process in gravity assisted drainage production method is very slow, because the small pressure drawdown is imposed with a reduced production rate to retain gravity dominated flow (Saskoil and Butler 1990). The relatively larger time scale attached to the oil recovery may make its application uneconomical. Even thermal methods may be economically viable in some cases. However, there are some places in which the thermal method is difficult to use, such as offshore heavy oils.

Many heavy oil reservoirs are underlain by large aquifers such as those in Canada (Kasraie and Ali 1987), offshore U.K. (Jayasekera 2000), and offshore Brazil (Marcio 2004). As such, they merit research efforts on the economical development of heavy oils with strong bottom water drives.

Motivated by an industrial need to produce heavy oil cost-effectively from strong, bottom water drive reservoirs, this study proposes a new cold production method, called Bilateral Water Sink (BWS). This technology can produce heavy oil from reservoirs at more economic rates, and avoid water coning; as a result, the process allows a maximum oil recovery. As the term suggests, the advantage of BWS technology is that steam injection is not required.

To ensure the practical application of BWS technology, fundamental mechanisms must be understood. This study develops a mathematical model to study the BWS flow system. Once the mathematical model is established, the model will predict the response of the BWS system under various operating conditions and guide assessments of operation plans.

An analytical method and numerical simulation can both provide guidance in the design of BWS. However, for practical purposes, the problem should be solved by the simplest and least costly method that will yield an adequate answer. Earlier studies (Mattax and Dalton 1990) noted that numerical simulation is still not widely used for smaller reservoirs. Neither is numerical simulation used widely in daily decision-making, even on larger reservoirs, due to the high cost of large-scale computations, as well as the long period of computational time required. In practice, the time and cost factors favor the use of analytical solutions, because a solution may take a simple form and can be easy to apply. They are accurate when all the assumptions are valid.

1.2 Hypothesis

The main hypothesis of this study is that efficient cold production of heavy oil with bottom water is feasible with the Bilateral Water Sink (BWS) technique. In the BWS technique, the top lateral produces water-free oil and the bottom lateral drains the water, thus preventing a water breakthrough to the top well, by keeping the top oil rate below the critical rate. As a result, water cresting can be completely eliminated, and oil recovery can be improved. Unlike a single horizontal well where water cresting causes water to by-pass oil, resulting in a low ultimate recovery factor; BWS prevents water invasion near the wellbore region, and consequently avoids the bypassing caused by water cresting. Moreover, instead of producing water with the oil, BWS separates the two production streams - oil and water – so produced water is oil free and subject to minimum processing prior to disposal. BWS may also enable water to play a significant role as a drive mechanism away from the well, thus stimulating primary production and recovery of oil.

A more specific formulation of the hypothesis – supported by my preliminary study – is given in Chapter 3.

1.3 Objectives

The overall study objective is to develop a new production method from theory to practice. Theoretically, the objective is to set up a mathematical model to analyze hydraulics of the BWS system and to provide adequate analytical solutions. The analytical solutions are needed for the following reasons:

- Because the essential physics of the water cresting problem are preserved, the analytical models can reveal how various parameters affect the BWS system and can identify the most influential factors.

- The analytical model may provide a valuable comparison with numerical reservoir simulators. In other words, the model may reduce/eliminate the need for tedious and costly simulations.
- The analytical models can serve as a reservoir management tool to predict the performance of BWS, as well as help operators to improve oil recovery by avoiding water cresting.

1.4 Dissertation Outline and Logic

This dissertation is divided into 7 chapters. Chapter 1 introduces the focus of this study, outlines the hypothesis, objectives and motivations, and explains logical organization of the dissertation.

Chapter 2 presents an overview of the problems encountered when producing heavy oil underlain by bottom water. It emphasizes the ineffectiveness of current industry solutions to mitigate these problems. Also presented is a literature review of present analytical models for critical rate calculation in horizontal wells. The assumptions and shortcomings of these models are also discussed.

Chapter 3 is a preliminary simulation study that compares production mechanisms of heavy oil with bottom water to the medium heavy and light oil systems. The study identifies the most important differences, reveals the mechanisms of low oil recovery and provides data needed to formulate a detailed hypothesis on the design and operation of BWS wells. The hypothesis defines the need for the analytical work that follows.

Chapter 4 develops analytical models of the critical rate in a single horizontal well system using the hodograph method and the Dupuit approximation. The improved models account for well and boundary location, the convergence of flow toward the well, and provide less restrictive

and more accurate solutions. The solutions are validated using a commercial numerical simulator for the variety of heavy/medium/light oil systems presented in Chapter 3.

Chapter 5 is a mathematical study on the "Bilateral Water Sink" system in heavy oil reservoirs. This chapter leads from the physical water cresting situation in the BWS system to a mathematical formulation and solution of critical rate in BWS wells. Again, the solution is validated by the numerical simulator.

Chapter 6 is the extension of the critical rate model in an open boundary reservoir toward a more representative reservoir case using a bounded reservoir. To provide an understanding of the concept of BWS in terms of improving oil recovery and avoiding water breakthrough. Well productivity and recovery efficiency are analyzed using this model. The design procedure of BWS is also given in this chapter to assist in developing heavy oil with bottom water.

Chapter 7 presents the conclusions, as well as a recommendations for future research.

CHAPTER 2. PROBLEM STATEMENT AND LITERATURE REVIEW

This chapter presents an overview of the difficulties encountered in heavy oil production from a bottom water drive reservoir, based on available research. This study proposes the new technology of BWS, together with a plausible mechanism for preventing water cresting, to improve oil recovery. Because analytical modeling for critical rate in a single horizontal well is deemed essential for an investigation of the fundamentals of BWS, this chapter reviews existing analytical water cresting models for a single horizontal well. This is followed by a discussion of common assumptions to simplify the boundary condition at the water-oil interface and the resulting inaccuracies.

2.1 Heavy Oil Resources Worldwide and Its Production Methods

The definitions of heavy oil vary from source to source. The U.S. Department of Energy (DOE) defines heavy oils as between API gravities 10° to 22.3°, where the API gravity and specific gravity (S.G.) are related by:

$$API = \frac{141.5}{S.G} - 131.5 \quad \text{.....(2.1)}$$

However, the API gravity is an imperfect indicator of heavy oil productivity. The key fluid property which most affects productivity and oil recovery is considered to be the in-situ, live oil viscosity. Thus, Alboudwarej (2006) emphasized the in-situ viscosity of heavy oil, and placed the viscosity of heavy oil and extra heavy oils within a range of 10 cp to more than 1,000,000 cp.

According to Alboudwarej et al. (2006), the world's total oil resources amount to roughly 9 to 13×10^{12} barrels. Conventional oil composes only about 30 percent of that amount; the rest encompass heavy oil, extra heavy oil, and bitumen (Figure 2.1). Because this study aims at investigating a new cold production method for the economic exploitation of heavy oils, which

usually flow in reservoir conditions at an uneconomic rate (Saskoil and Butler 1990), this 15 percent of the world's total oil resources is of great interest to us.

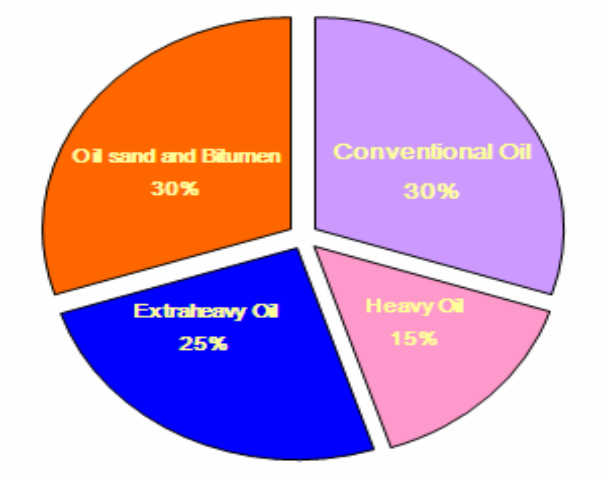

Figure 2.1 The total world oil reserves (Alboudwarej 2006)

Gaining access to new conventional oil reservoirs is difficult. On the other hand, the locations of very large deposits of heavy oil are well-known, which means little or no exploration is needed. However, the main challenge is to optimize heavy oil production with cost effective and environmentally sound methods. Many countries are now shifting national interests from conventional oil to heavy oil. Worldwide heavy oil production has increased in recent years and is expected to increase in the future (Alboudwarej 2006).

The two largest viscous oil deposits in the world are found in Canada and Venezuela. According to Dusseault (2006), Canada has the largest, heavy oil resource with some 1.7 trillion barrels of extra-heavy oil, plus 25 billion barrels of heavy oil in the 10-22.3 API gravity range, mainly located in the Canadian areas of Athabasca, Wabasca, Peace River, and Cold Lake in Alberta, as well as the Lloydminster area of Saskatchewan.

According to Curtis and Kopper (2002),Venezuela has around 1.2 trillion barrels of heavy and extra-heavy oil in the 400-mile-long Orinoco Belt in the eastern part of the country, as well as 250 billion barrels of heavy oil in other areas. In the United States, IEA (International Energy Agency) estimates that there are 100 to 180 BBO (Billion Barrels of Oil) in Alaska, with

more heavy oil in the following states: California (47 BBO), Utah (19 to 32 BBO), Alabama (6 BBO) and Texas (5 BBO). Heavy oil is also located and produced in many other countries, such as Indonesia, China, Mexico, Brazil, and Trinidad.

Most of the heavy oil deposits are in shallow, poorly consolidated sand formations with high permeability and high porosity (Ali 1997). The oil saturations also tend to be high, while formation thickness tends to measure several hundred feet. Many reservoirs in California, Western Venezuela, and Alberta have similar characteristics. According to Ali (1997), the typical value of reservoir properties is listed as below:

Table 2.1 Typical reservoir properties of heavy oil reservoirs (Ali 1997)

Properties	Value
Deposition Depth	3000 ft or less
Permeability	One to several darcies
Porosity	Around 30%
Oil saturations	50 - 80%
Formation thickness	50 to several hundred feet

Despite the above similarities, the various heavy oil resources can be markedly different in the in-situ viscosity. For example, most heavy oil viscosities in California are in the 1000 - 2000 cp range, while those in Cold Lake, Alberta, are around 100,000 cp.

Due to the inverse relationship between oil viscosity and flow rate, the primary recovery of heavy oil is extremely low, i.e., in the range of 5 to 15 percent (Alboudwarej 2006). It is evident that the principal obstacle in heavy oil recovery is high viscosity. Any reduction in viscosity will lead to an increase in the oil production. Viscosity may be lowered most effectively through the application of heat, because the viscosity decreases as the temperature increases.

Applicable thermal methods to reduce heavy oil viscosity include cyclic steam stimulation, steam flooding, steam-assisted gravity drainage (SAGD), and in-situ combustion. In

cyclic steam stimulation (CSS), steam is injected into a well for a time period from several days to several weeks. The heat is then allowed to soak into the formation surrounding the well for an additional time (weeks). Finally, the well opens for production and heated oil flows into the well with a greatly reduced viscosity. Consequently, the production rate is increased. When the rate drops below an economic limit, the cycle repeats. Recovery may approach 20 percent for CSS (Curtis and Kopper 2002). A steamflood may follow CSS to sweep oil between wells. For example, steam is injected in one well, as oil is produced in another well in a five-spot pattern. Steamflooding operations have produced recovery factors of over 70 percent (Curtis and Kopper 2002).

In steam-assisted gravity drainage (SAGD), two horizontal wells are drilled parallel to each other and separated by a constant, vertical distance of typically 16 ft. As steam is injected into the upper well, oil is produced from the lower well. Predicted recovery factors of 50 percent to 70 percent are reported (Alboudwarej 2006).

In situ combustion involves the creation of a fire front in the reservoir, together with a subsequent propagation by air injection. The burning front, or combustion zone, would move within the formation as a narrow band, consuming or displacing encountered fluids, into producing wells. The heat generated within the combustion zone is transported downstream by the burned gases, and is also conducted through the rock-fluid system (Ali 1974).

These thermal methods are widely applied to extract heavy oil, leading to successful developments in many heavy oil fields around the world. Yet the limitations of thermal methods are also widely recognized. Because steam is commonly generated with natural gas, the associated cost of steam generation and water treatment is high. In addition, large capital investments must be made in designing wells, cements, and completions for the high temperatures encountered in thermal methods. This may result in an unprofitable project.

Even if the cost issues associated with steam generation and operations can be overcome, there are situations where heavy oil is inaccessible to thermal production methods. It may be difficult to implement thermal production methods in an offshore environment, where technological and logistic aspects limit such applications. Space may not be available for equipment used to generate steam, because the equipment is heavy and large (Jayasekera 2000). Another important issue is the heat loss. Even with equipment advances such as vacuum-insulated tubulars, the heat loss above the mudline could be unacceptably large (Bunton 1999). As a result, the water temperature and water depths preclude the application of thermal production methods offshore.

At present, cold production is considered to be the only method that could be applied to offshore heavy oil (Trindade and Branco 2005).

Cold production methods may recover oil without the cost of heating, if it is possible to achieve economic rates. A lower capital expenditure makes cold production attractive compared to thermal production if cold production is viable. According to Dusseault (2006), long horizontal wells with several multi-lateral branches were used in heavy oil recovery at Faja Del Orinoco in Venezuela, with production as high as 2000-3000 stb/day.

Another cold production method is called Cold Heavy-oil Production with Sand (CHOPS). Rather than blocking sand by means of screens or gravel packs, coproduction of sand and oil is encouraged by aggressive perforation and swabbing strategies, and is sustained during production by a high drawdown. With sand ingress, productivity may increase 10 to 20 times compared to sand-free primary production. A recovery factor of 12-25 percent may be achieved, rather than the 2-8 percent without sand production (Dusseault 2006). CHOPS is used in Canada for primary production from unconsolidated sandstones containing heavy oil (Geilikman et al. 1994). Approximately 25 percent of heavy oil production in Canada was from CHOPS for 11° to

18° API heavy oils (Dusseault 2006). However, the high cost of processing or transporting the sand to shore and well servicing associated with wellbore sand cleanouts, would make sand production prohibitive, an economic concern that renders CHOPS unsuitable for offshore environmental use (Huang 1997). More recently, laboratory studies (Diaz et al. 2002) show that sand production might be controlled through exploitation of quasi-stable natural sand bridges. It is can be considered as an alternative to CHOPS for offshore developments.

The cold production method used offshore differs from the CHOPS method. Successful field cases initiated at Captain Field offshore U.K. (Jayasekera 2000) and a pilot field test at Jubarte Field offshore Brazil (Jr. and Siqueira et al. 2007) show that the most feasible production method applied in offshore heavy oils would be horizontal wells accompanied with water flooding. Horizontal wells offer two mutual benefits: first, high production rates must be maintained for offshore assets because of the high cost of offshore operations. Horizontal wells have been used to achieve high productivity in offshore U.K. wells (Jayasekera 2000). Second, using fewer but higher productivity horizontal wells may reduce the number of wells and slots required, reducing capital investment.

2.2 Water Coning and Cresting in Heavy Oil Reservoirs

Recovery from heavy oil reservoirs with underlying bottom water is difficult to manage efficiently if water coning/cresting occurs, regardless of whether the reservoir is onshore or offshore. Large wellbore pressure drawdown during the production process causes upward water movement, coning or cresting. Muskat (1947) suggested that if oil is produced at a sufficiently low rate, known as the *critical rate*, the pressure gradient caused by a viscous force may be balanced by the gravity force arising from the difference in oil and water densities. In such a case, the water cone or crest is in hydrostatic equilibrium below the region in which oil flows. On the

other hand, if the production rate exceeds the critical rate, the water-oil interface moves upward, causing water production.

In heavy oil reservoirs, the critical rate may be too low to be economically viable, and wells may produce above the critical rate. The adverse mobility ratio between heavy oil and water commonly causes early water breakthrough, possibly bypassing oil and leading to low oil recovery factors with high water production. For example, the oil field H.K. (located in Shandong, China), is a typical heavy oil reservoir with bottom water drive. Reservoir oil viscosity is 710 cp, and the current water cut is 90 percent, with only 1.0 percent recovery to date (Ju et al. 2005). Further, Stokes et al. (1978) reported in a field study at the Mount Poso steam injection project that the strong bottom water drive led to a low recovery factor, approximately 35 percent of the original oil in place.

Unfortunately, heavy oil bottom water drive reservoirs are common worldwide. Canada has heavy oil reserves of 84.9 million bbl at Alberta and Saskatchewan (Ali 1986). Many of those reservoirs are underlain by large aquifers (Saskoil and Butler 1990). Primary recovery from those reservoirs is very low, (from 1 to 5 percent; Butler and Mokry 1993) with water cut of nearly 100 percent (Kasraie and Ali 1987). In addition, many offshore heavy oil reservoirs are subject to bottom water drive. The heavy oil located on the U.K. continental shelf is approximately 10 billion barrels, with an oil viscosity ranging from 10 to 100 cp (Jayasekera 2000). Aquifers underlie most of these fields, including the Alba, Mariner, Bressay and Gannet E fields. The Jubarte field, located offshore Brazil, contains 600 million bbl of 17.1 degrees API oil with a viscosity of 14.5 cp at saturation pressure (Marcio et al. 2004). The reservoir is underlain by a very large aquifer (Marcio et al. 2004). At Bohai Bay, offshore China, it is estimated that over 74 percent of the oil is heavy, with in-situ viscosities ranging from 50 cp to 10,000 cp, and proven reserves up to 29.2 billion bbl (Zhou et al. 2008; Liu 2010). Many of these heavy oil

reservoirs have a bottom water drive. The average oil viscosity at the reservoir condition is 70 cp, and the water cut is 90 percent with only 13.5 percent recovery efficiency after 10 years of water flooding (Zhou et al. 2008).

Horizontal wells are the main method to produce offshore heavy oil. Although this development strategy may make these projects commercially viable, the water cresting problem remains. As a result, the ultimate recovery factor is generally less than 20 percent (Shecaira et al. 2002) for offshore heavy oil with bottom water.

High water production in heavy oil assets presents other technical, environmental, and economic challenges in oil-water treatment and water disposal in these offshore heavy oil developments. One difficulty of the water and oil treatment is oil-water separation. The difference in specific gravity between the produced oil and water is smaller than for medium or light crudes, causing both solids and water droplets to remain in suspension, resulting in emulsions of the heavy oil with water (Visser 1989). Further, existing technologies for oil-water separation in the production unit would require very high temperatures and a large retention time, which may be unfeasible for offshore fields (Pinto and Branco 2003).

The disposal of large amounts of produced water is another challenge. The produced water must be cleaned to less than 40 ppm oil content for overboard discharge (Jayasekera 2000); this process would require more space and load on the platforms. In addition, re-injection into the reservoir may not be possible because of the oil content in the water (Jayasekera 2000).

Attempts are made by operators to delay water breakthrough at production wells, for instance by drilling the well as close to the top of the reservoir as possible (Jayasekera 2000). Because heavy oil has a high viscosity and a relatively high density, even a structurally high well location may not sufficiently delay water breakthrough.

The difficulties of handling large volumes of produced water have motivated research to develop new technologies for oil-water separation. Downhole separation with the disposal of water has been considered. In this process, hydrocyclones separate the water from the oil and the downhole pump lifts oil to the surface, then pumping the excess water into a disposal zone. However, this requires more complex equipment downhole (Jayasekera 2000).

To date, the main strategy for recovering offshore heavy oil from bottom water drive reservoirs is to control the premature water breakthrough (Jayasekera 2000) and improve the ultimate oil recovery.

2.3 Technologies to Control Water Coning in Heavy Oil Reservoirs

We may improve recovery in bottom water drive reservoirs. One effective way is to improve the mobility ratio ($M = \frac{k_{rw} / \mu_w}{k_{ro} / \mu_o}$) by reducing oil viscosity via heating. However, thermal recovery of heavy oil with a strong bottom water drive remains problematic. Bottom water typically interferes with thermal production methods.

Karmaker and Maini (2003) noted that the water from an aquifer can migrate into the steam chamber. As a result, steam would be wasted in heating the water rather than the oil. Based on Fram and Palermo's (1996) field study, aquifers may also result in higher than desired steam chest pressure. The steam chest pressure must be maintained at or above aquifer pressure to prevent water encroachment. At higher pressure, less latent heat is available, and more steam is required to attain the desired heating of the reservoir. In addition, the heat loss may become more significant when the oil zone is in contact with the underlying aquifer, because the thermal conductivity of an aquifer is higher than that of a gas-bearing rock.

Coning, cresting and water breakthrough may be mitigated using horizontal wells. Many field cases (Sherrard 1987, Murphy 1990, Target 1992, Chen 1993) demonstrate that horizontal

wells can reduce water cresting in conventional oil reservoirs. Compared to vertical wells, horizontal wells increase inflow area, thereby enhancing well productivity. As a result, horizontal wells may have relatively high critical rates.

However, horizontal well technology is not widely accepted as a solution for heavy oil reservoirs with bottom water. In Canada, about 750 horizontal wells were drilled from 1988 until 1992. The majority of its application is for water and gas coning (Joshi 1994). However, Dusseault (2006) reported that since use of horizontal wells for cold production was initiated in Canada in the 1980s, successful cases are less frequent than failures. The researcher claimed that a "low recovery factor (seldom above 10 percent), early water breakthrough (usually impossible to plug when it happens), and short well life have combined to make this horizontal well technology have little attraction in Canada."

Besides the above methods, researchers have suggested that a horizontal well, combined with thermal and gravity-stabilized methods such as Steam-Assisted Gravity Drainage (SAGD) and Vapor-Assisted Petroleum Extraction (VAPEX) may improve recovery in heavy oil reservoirs with strong bottom water drives. Saskoil and Butler (1990) studied the SAGD process in a bottom water drive using a scaled visual model. From these experiments, an optimal recovery strategy involved placing the horizontal producer near the WOC to ensure maximum gravity drainage; the production pressure must be approximately identical, or slightly higher, than the pressure in the aquifer to prevent water coning or cresting. Sceptre's (Jespersen 1989, 1991) operation at the Tangleflags field demonstrated that the principle of gravity drainage in horizontal wells may be used in reservoirs with bottom water. However, steam costs are high in SAGD developments. Typically, 60 – 70 percent of SAGD operating expenses are steam generation and water recycling costs (Dusseault 2006). VAPEX is a nonthermal solvent-based technology (Butler and Mokry 1993). Similar to SAGD, two parallel horizontal wells are drilled

with about 16 ft vertical separation. Rather than injecting steam, a solvent is injected through the upper well. The oil viscosity may be reduced by dilution with solvents. Consequently, oil flows downwards and is produced from the lower well. It is a gravity drive system, so water coning\cresting may be prevented. However, VAPEX is a slow recovery process with low production rates. The payback period is relatively long. Finally, the high cost of the solvent is another economic concern.

Worldwide, many successful field cases (Stokes 1977, Lillie 1981, Proyer 1985) indicate that a good solution for effectively producing heavy oil with bottom water would be to decrease aquifer pressure through aquifer pumping. The principle of aquifer pumping is that aquifer lift wells – located below the oil-water contact and producing large volumes of water –decrease the pressure at oil-water contact, subsequently reducing the amount of water influx into the oil field. In California at the Mount Poso steam-injection project, recovery efficiency was improved by installing approximately 60 wells located near the OWC. Dietrich (1990) reported that at the field of South Belridge during 1997, the current operator of the Belridge project began pumping about 225,000 barrels of water per day from the Tulare zone to keep water from interfering with the ongoing steam to enhance production. Further, at the Middle Tulare project (Fram and Palermo 1996), 40 dedicated aquifer lift wells were drilled with an initial target lift rate of 525,000 barrels of water per day in 1987.

The aquifer pumping strategy lowers aquifer potential, whereas the gravity drainage approach typically maintains a high oil zone potential: either approach impedes water encroachment. The following section describes a localized version of the aquifer pumping strategy, which lowers aquifer potential near production wells using down-hole water sinks.

2.4 Down-hole Water Sink and Bilateral Water Sink Technology

The principle of Downhole Water Sink (DWS) and Bilateral Water Sink (BWS) is similar to that of aquifer pumping: it involves pumping water from the water zone to keep the OWC away from oil zone. To control water cone growth and its breakthrough, the water zone is drained through another completion in the aquifer beneath the oil-water contact (Wojtanowicz and Armenta 2004). Water and oil are produced separately from their respective zones. Fluids produced by the top completion are either free of water or have small water content, subject to drainage rate adjustments (Wojtanowicz and Armenta 2004). The concept is similar for DWS in vertical wells and BWS in horizontal wells (Figures 2.2 and 2.3).

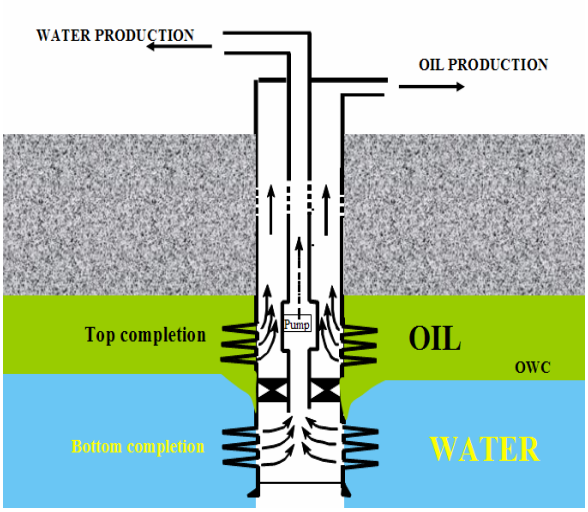

Figure 2.2 DWS water drainage-production in vertical wells (Wojtanowicz and Armenta 2004)

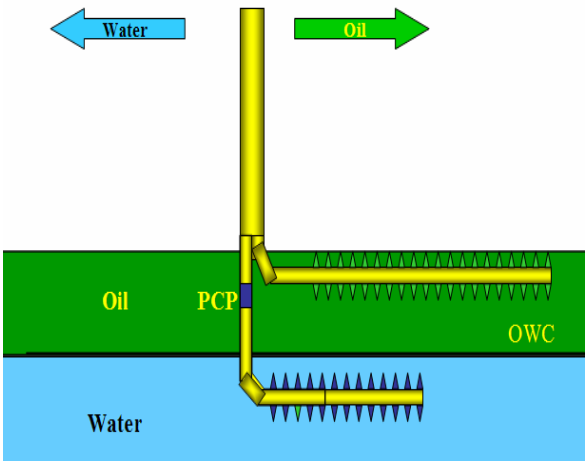

Figure 2.3 BWS water drainage-production in horizontal wells (Wojtanowicz and Armenta 2004)

The advantage of DWS and BWS over aquifer wells is the relatively low cost. Instead of drilling the aquifer wells, DWS and BWS used the same number of production wells to achieve a similar water pumping effect, albeit with more complex completions. Moreover, water sink wells localize the aquifer drawdown where it is most needed, near the oil production wells. Unlike many water control strategies, the intent in DWS and BWS is to prevent water breakthrough to wells, rather than to remediate after water breakthrough.

For the more efficient development of heavy oils, BWS appears to be more suitable than DWS. BWS uses horizontal wells with larger reservoir contact, supplemented by aquifer pumping to suppress water coning. As a result, both well productivity and recovery factors can be improved. In addition, BWS prevents the mixing of oil and water in the tubing strings and facilities; this makes BWS attractive to offshore developments, where oil-water separation is a problem. Another advantage of the BWS is that the produced water is clean and (nearly) oil-free, and could be used as an injection fluid.

Shirman and Wojtanowicz (1997) reported successful DWS field applications. However, most of the applications were in vertical wells and conventional oil reservoirs with bottom water. Qin and Wojtanowicz (2007) conducted a simulation study of a DWS vertical well application in heavy oil reservoirs, concluding that DWS could significantly reduce water production. Without DWS, the well produced 95 percent water whereas the DWS system lowered the water cut to 80 percent and raised the critical rate from 6 to 128 bpd (Figure 2.4).

Inikori and Wojtanowicz (2002) analyzed BWS in horizontal wells using numerical simulation; they found that in the conventional oil reservoir, bilateral water sinks may reduce by-passed oil and improve oil recovery by over 7 percent. They also identified and modeled the effect of wellbore friction on water cresting along the horizontal well with the water invading the upper lateral at its heel. They did not study BWS applications for heavy oil.

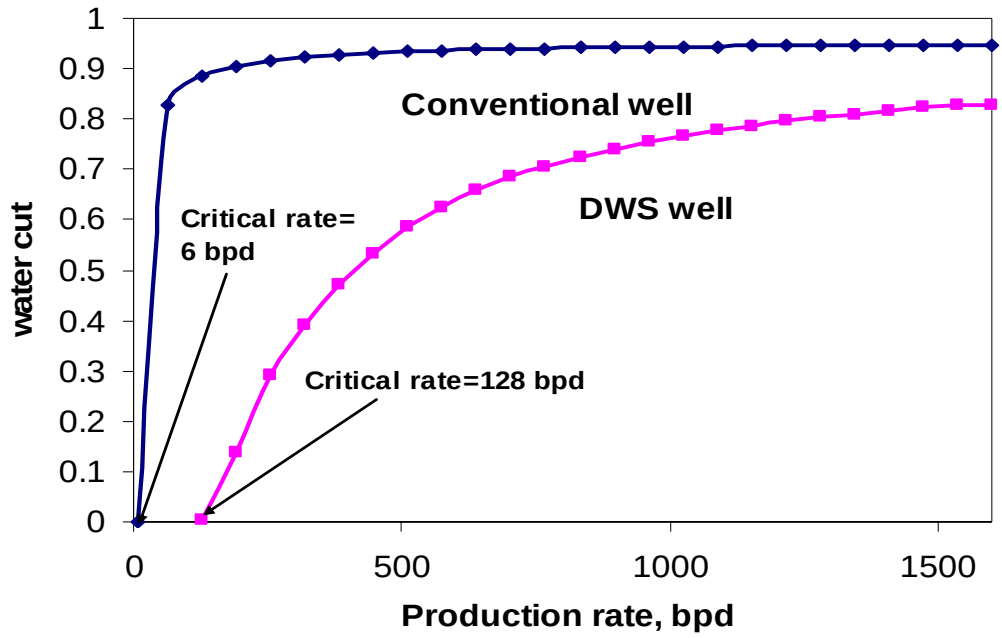

Figure 2.4 Water cut response in heavy oil reservoir for conventional well and DWS wells (Qin and Wojtanowicz 2007)

In summary, there is a lack of research on the physical mechanisms of oil recovery with BWS – particularly in heavy oil. Successful application of BWS would require an understanding of the difference between BWS use in conventional and heavy oil reservoirs. Such an understanding is one of the goals of the current research.

2.5 Analytical Modeling of Water Coning and Water Cresting

To understand BWS behavior, one must address water cresting in horizontal wells. The critical rate and water breakthrough time are the informative measures of water coning and cresting behavior. The BWS is intended to prevent water cresting, delaying or preventing water breakthrough. This study will concentrate on critical rate estimation.

Several analytical models of critical rate calculation in horizontal wells have been presented. The methods were used to solve a specific problem depending on the initial and boundary conditions. Water cresting analysis is complicated because one of the boundaries, the

oil-water interface, is itself unknown. It is therefore part of the solution being sought. Although an analytical solution to such a flow system is possible, many approximations are made to simplify the boundary condition on the interface.

In this section, we first review procedures to specify the boundary condition along the interface mathematically. Then, various analytical models for the critical rate will be presented, with discussion of the treatment of the interface boundary and comments on limitations.

2.5.1 Boundary Condition on the Interface

Laplace's equation for Φ, $\nabla\Phi^2 = 0$ is taken as the basis for describing the flow behavior of all steady-state flow systems. The equation is the governing equation in all critical rate calculations. However, the Laplace equation alone does not provide a unique solution. To obtain a particular solution corresponding to the water cresting problem in horizontal wells, the boundary conditions must be satisfied as well.

According to Bear (1972), the boundary condition on the interface is derived as follows, assuming that oil and water are completely separated by an abrupt interface, that the two fluids are incompressible, and the reservoir is homogeneous. Because the interface is stationary, the interface acts like an impervious boundary; that is, at each point on the interface, the component of the flow velocity normal to the interface is equal to zero:

$$u_n = u \bullet \boldsymbol{ln} = 0 \quad \text{.....(2.2)}$$

Where $u = -\dfrac{k}{\mu}\nabla\Phi$

Where $\boldsymbol{ln}$ is the unit normal vector for the oil-water interface.

Let Φ_o denote the potential in the oil zone and Φ_w denote the potential in the water zone, and the coordinates (x_w, z_w) and (x_o, z_o) denote points on the interface.

$$\Phi_o = p_o + \rho_o g z_o \quad (2.3)$$

$$\Phi_w = p_w + \rho_w g z_w \quad (2.4)$$

Where ρ_o and ρ_w is the density of oil and water respectively

On the interface: $p_o = p_w$, $z_o = z_w$, then we have the relationship between the coordinates z and the potential by eliminating p_o and p_w from the above two equations.

$$z_o = z_w = \frac{\Phi_w}{\Delta\gamma} - \frac{\Phi_o}{\Delta\gamma} \quad (2.5)$$

Where $\Delta\gamma = \gamma_w - \gamma_o = (\rho_w - \rho_o)g$

Because the coordinates of a point on the interface are given by Equation 2.5, the interface can be represented by a general form:

$$F(x,z) = z_o - (\frac{\Phi_w - \Phi_o}{\Delta\gamma}) = 0 \quad (2.6)$$

With the geometry of the boundary described by Equation 2.6, and $\boldsymbol{ln} = \nabla F / |\nabla F|$, the boundary condition Equation 2.2 along the interface is:

$$\frac{1}{\Delta\gamma}.\frac{1}{\mu_o}[k_o\left(\frac{\partial\Phi_o}{\partial x}\right)^2 + k_o\left(\frac{\partial\Phi_o}{\partial z}\right)^2] - \frac{1}{\Delta\gamma}.\frac{1}{\mu_o}[k_o\frac{\partial\Phi_o}{\partial x}.\frac{\partial\Phi_w}{\partial x} + k_o\frac{\partial\Phi_o}{\partial z}.\frac{\partial\Phi_w}{\partial z}] + \frac{k_o}{\mu_o}\frac{\partial\Phi_o}{\partial z} = 0$$

$$\frac{1}{\Delta\gamma}.\frac{1}{\mu_w}[k_w\left(\frac{\partial\Phi_w}{\partial x}\right)^2 + k_w\left(\frac{\partial\Phi_w}{\partial z}\right)^2] - \frac{1}{\Delta\gamma}.\frac{1}{\mu_w}[k_w\frac{\partial\Phi_o}{\partial x}.\frac{\partial\Phi_w}{\partial x} + k_w\frac{\partial\Phi_o}{\partial z}.\frac{\partial\Phi_w}{\partial z}] - \frac{k_w}{\mu_w}\frac{\partial\Phi_w}{\partial z} = 0 \quad (2.7)$$

For special cases, when the water is immobile, Equation 2.7 may be rewritten as:

$$\frac{1}{\Delta\gamma}.\frac{1}{\mu_o}[k_o\left(\frac{\partial\Phi_o}{\partial x}\right)^2 + k_o\left(\frac{\partial\Phi_o}{\partial z}\right)^2] + \frac{k_o}{\mu_o}\frac{\partial\Phi_o}{\partial z} = 0 \quad (2.8)$$

This is the boundary condition along the stable water-oil interface. The nonlinear nature of the boundary condition stem from the $(\partial\Phi_o / \partial x)^2$ and $(\partial\Phi_o / \partial z)^2$ terms. Although an exact solution of this kind of boundary can be derived by the hodograph method, many have attempted

to use the approximate solution to avoid the calculations involved. Among the many approximations, the most famous one is the Muskat (1937) approximation.

2.5.2 Muskat Approximation

The approximation made by Muskat (1937) is that the pressure distribution in the oil zone in the presence of a water cone is effectively the same as the pressure distribution without the water cone, and the water oil interface is perfectly horizontal. According to Muskat (1937):

> "Thus it cannot be solved for the cone surface unless the pressure function *p(r,z)* is known at the surface of the water cone and just within the oil zone. On the other hand, the pressure distribution in the oil zone is directly connected, at least in detail, with the shape of the static cone surface which acts like an impermeable boundary to the flow of the oil. Since this combined problem of the exact simultaneous determination of the surface of the water cone and the pressure distribution in the oil zone appears to be too difficult to permit an explicit solution, an approximation will be made."

The classic treatment of this coning problem in petroleum engineering, as presented by Muskat and Wyckoff (1947), has been widely accepted. This approach is easy to understand and simple to use, although the effect of the presence of the cone on flow restriction has been ignored.

Chaperon (1986) extended the classic treatment of the water coning phenomena as presented by Muskat and Wyckoff (1947) to horizontal wells. In her theoretical model, the basic assumptions are as follows:

- Horizontal well is located at the top of the reservoir.
- Well length is infinitely long and only applies to the two dimensional flow problem.
- No flow boundary at the top and no flow boundary at the OWC.
- Neglecting the frictional pressure loss along wellbore.

With these assumptions, she derives the shape of the water crest from the potential distribution based on this hypothetical horizontal interface, introduced as a no-flow boundary to the oil zone. In her study, the initial horizontal interface is taken as that boundary. In Figure 2.5, S is the point at the apex of the crest. While E is the point at lateral edge of the crest.

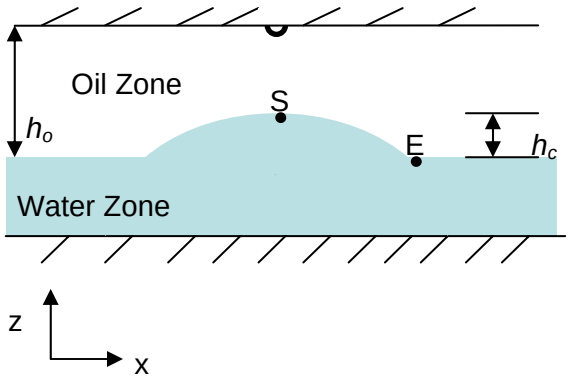

Figure 2.5 Schematic of water cresting

The steady-state potential distribution in the oil zone is obtained analytically by Houpeurt (1975) as follows in Equation 2.9, by assuming that the water crest does not exist (Figure 2.6).

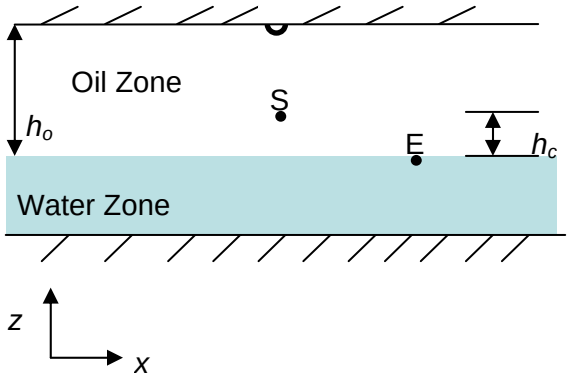

Figure 2.6 Schematic of Muskat's approach by assuming no water crest

$$\Phi_o(x,z) = \frac{q\mu_o}{2\pi L k_o} \ln(\cosh\frac{\pi x}{h_o} - \cos\frac{\pi z}{h_o}) \quad \text{.....(2.9)}$$

Together with the two equilibrium conditions,

$$\Phi_E - \Phi_S = \Delta\rho g h_c \quad \text{.....(2.10)}$$

$$\frac{d(\Phi_E - \Phi_S)}{dz} = \Delta\rho g \quad \text{.....(2.11)}$$

Chaperon (1986) derived the implicit equation for critical crest height and critical rate.

The critical crest height:

$$1-\frac{h_o-h_c}{h_o}=\frac{1-\cos\dfrac{\pi(h_o-h_c)}{h_o}}{\sin\dfrac{\pi(h_o-h_c)}{h_o}}\frac{\ln[\cosh\left(\dfrac{\pi x_e}{h_o}\right)+1]}{1-\cos\dfrac{\pi(h_o-h_c)}{h_o}} \quad \text{.....(2.12)}$$

The critical rate per unit length:

$$q_c=\frac{q}{L}=\Delta\rho g h_o\frac{k_o}{\mu_o}\frac{2\pi\left(1-\dfrac{h_o-h_c}{h_o}\right)}{\ln\left(\dfrac{\cosh\left(\dfrac{\pi x_e}{h_o}\right)+1}{1-\cos\dfrac{\pi\left(h_o-h_c\right)}{h_o}}\right)} \quad \text{.....(2.13)}$$

Because the solution neglected the flow restriction due to the presence of the water cresting, the Chaperon approximation may overestimate the critical rate.

2.5.3 Hodograph Method

The hodograph method is suitable for solving steady, two-dimensional flow problems in porous media. Hamel (1934) developed the theory of the hodograph method for the study of flow through porous media, especially with free surfaces and seepage surfaces. Henry (1959) and Bear and Dagan (1964) applied the hodograph method to salt water intrusion into fresh water aquifer, an important problem in ground water hydrology. Kidder (1956) applied the method to reservoir engineering problems.

A hodograph is a representation of a dynamic system in which the coordinates are the velocity components. The principles of the hodograph method are briefly reviewed in this section (see also Bear 1972). As mentioned earlier, the boundary condition on the interface for a homogenous reservoir is given by Equation 2.8. Inserting $u=-\frac{k_o}{\mu_o}\nabla\Phi$ into Equation 2.8, the boundary condition can be expressed in terms of flow velocity:

$$\frac{\mu_o}{k_o \Delta\gamma}\left(u_x{}^2 + u_z{}^2\right) - u_z = 0 \quad \text{(2.14)}$$

Equation 2.14 can be rewritten as:

$$u_x{}^2 + (u_z - \frac{K}{2})^2 = (\frac{K}{2})^2 \quad \text{(2.15)}$$

Where $K = \frac{k_o}{\mu_o}(\rho_w - \rho_o)g$

The hodograph of a steady surface in an isotropic porous medium is, therefore, a circle centered at (0, *K/2*), with radius *K/2*, as shown in Figure 2.7.

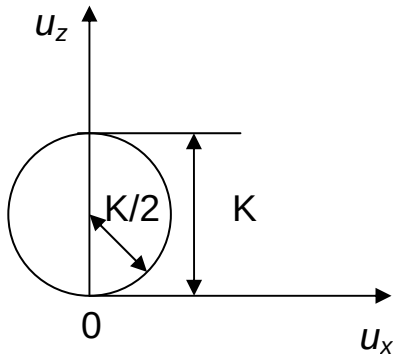

Figure 2.7 Hodograph representation of the interface (Bear 1972)

Whereas the geometric shape and the position of the interface in a physical plane are unknown, they are completely specified in the hodograph plane by circles of definite and fixed parameters. The hodograph method can provide an exact analytical solution (subject to simplifications in compressibility, phase mobility, and capillary pressure; Bear 1972).

Consider the function:

$$\overline{w} = u_x - iu_z = -\frac{\partial\Phi}{\partial x} + \frac{\partial\Phi}{\partial z}i \quad \text{(2.16)}$$

We seek to relate the hodograph plane to complex potential plane and physical plane:

Complex potential function:

$$\zeta\ (x,z) = \Phi(x,z) + i\psi(x,z) \quad \text{.....(2.17)}$$

Complex function in physical *x*-*z* plane

$$f = x + iz \quad \text{.....(2.18)}$$

We also have:

$$\frac{d\zeta}{df} = \frac{\partial\Phi}{\partial x} - i\frac{\partial\Phi}{\partial z} = -(u_x - iu_z) = -\overline{w} \quad \text{.....(2.19)}$$

Using Equation 2.19, we integrate:

$$\int_{\zeta=\zeta_0}^{\zeta} -\frac{d\zeta}{\overline{w}} = x + iz \quad \text{.....(2.20)}$$

Where $\zeta_0 = \Phi_0 + i\psi_0$ and $\zeta = \Phi\ + i\psi$

By comparing real and imaginary parts separately, we obtain the equation:

$x = x(\Phi,\Psi)$; $z = z(\Phi,\Psi)$ or

$\Phi = \Phi(x,z)$, $\Psi = \Psi(x,z)$

Once the conformal mapping relationship between the physical, complex potential and hodograph planes is known, we can use Equation 2.20 to solve the flow problem. The stepwise procedures of using a hodograph method, as summarized by Jacob and Dagan (1964), are:

- The flow region in the physical plane (f) is mapped on the hodograph plane ($\overline{w}$) by mapping its boundaries. By mapping we mean a certain kind of transformation of one plane to another plane. Points in the physical plane are mapped onto corresponding points in the hodograph plane.
- Similarly, the physical plane (f) is mapped on the complex potential (ζ) plane by mapping its boundaries.
- The flow region in both the hodograph plane and the complex potential plane are mapped

on the upper half of an auxiliary B plane.

- With B as an independent parameter, we get:

$$\frac{df}{dB} = -\frac{d\zeta}{\overline{w}dB} \quad \text{.....(2.21)}$$

After integration of Equation 2.21 along the interface, the shape and lengths of the interface may be found.

Bear and Dagan (1964) used this method to solve the water cresting problem in an infinitely large reservoir. Their detailed description of how they applied this hodograph method to the specific cases will be reviewed in this section.

Assumptions:

- Oil reservoir is homogeneous and isotropic.
- Oil is incompressible and shows a steady state flow condition.
- Sharp interface between oil and water exists.
- Friction loss along the wellbore and end point effect are negligible.

The physical plane is shown as Figure 2.8.

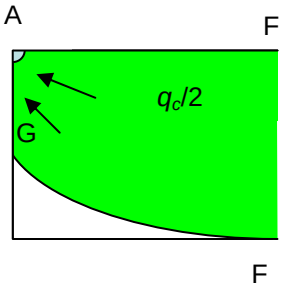

Figure 2.8 Physical plane of water cresting problem

Due to the symmetrical shape of the crest, it is sufficient to analyze the region FAGF, where A is the drain. The flow region is bounded by no flow boundary AF and free surface GF. The mapping of the flow domain FAGF onto the hodograph plane is shown in Figure 2.9.

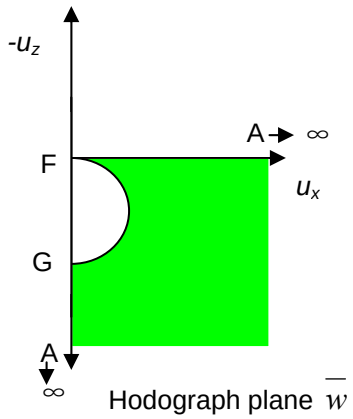

Figure 2.9 Hodograph plane for flow domain FAGF

Segment AF is a no flow boundary with vertical velocity $u_z = 0$, while segment FG, a critical free surface, is represented in the hodograph plane by a circle centered at (0, *K/2*) and with radius (*K/2*). The critical crest shape is associated with a maximum water free oil rate which is called critical rate per unit length q_c. Any rate above the critical rate will lead to water production in the well. Segment GA is a streamline which shows only vertical velocity toward to the well. A is a sink point, with infinite velocity in different directions.

The corresponding complex potential plane is shown in Figure 2.10. The physical flow region is bounded by two streamlines, line AGF and line AF in ζ plane.

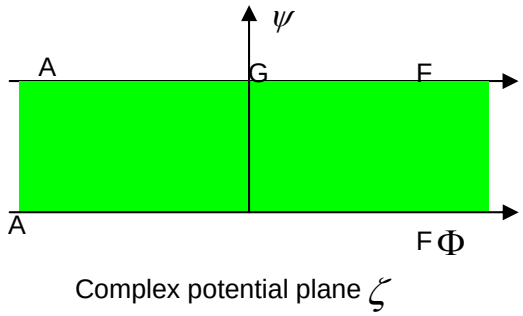

Figure 2.10 Corresponding complex potential plane

The next step is to find the relationship that maps the ζ and $\overline{w}$ planes onto an auxiliary *B* plane, shown in Figure 2.11. This can be done by using the Schwarz-Christoffel transformation.

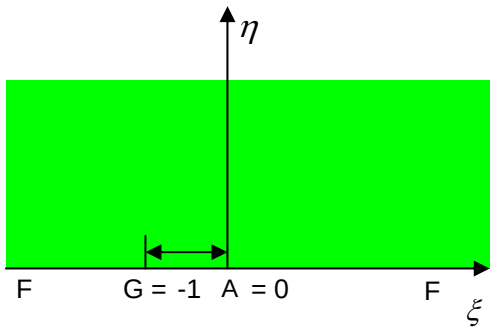

Figure 2.11 The auxiliary B plane

The ζ complex potential plane is mapped onto the B plane by using the Schwarz-Christoffel transformation:

$$\zeta = \frac{q_c}{2\pi} \ln B \quad \text{.....(2.22)}$$

The $\overline{w}$ plane is mapped onto the B plane by:

$$\overline{w} = \frac{K}{\frac{2}{\pi} arc\sinh(\sqrt{B})} \quad \text{.....(2.23)}$$

Using Equation 2.21, the relationship between the three planes can be expressed as:

$$\frac{df}{dB} = -\frac{d\zeta}{\overline{w}dB} = -\frac{q_c}{\pi^2 K}\left(\frac{arc\sinh\sqrt{B}}{B}\right)$$

$$\int_{FG} df = \int_{FG} -\frac{d\zeta}{\overline{w}dB} dB = \int_{FG} -\frac{q_c}{\pi^2 K}\left(\frac{arc\sinh\sqrt{B}}{B}\right) dB = x + iz \quad \text{.....(2.24)}$$

Integrating the Equation 2.24 along segment FG in B plane yields the following parametric equations for the interface:

$$x = \frac{2q_c\mu_o}{\pi^2 k_o \Delta\rho g}\int_0^t dt \tanh t \quad \text{.....(2.25)}$$

$$h_c = -\frac{q_c\mu_o}{\pi k_o \Delta\rho g} \ln\cosh t \quad \text{.....(2.26)}$$

Where t is a parameter and $0 < t < \infty$

Equations 2.25 and 2.26 were presented by Bear and Dagan (1964) to describe the interface equation in a reservoir with infinite thickness and infinite lateral distance. Cone\crest height tends to be infinite based on the equations. Since the solution is only restricted to the infinite reservoir case, it is not applicable to the cases where the well is produced from a confined reservoir.

Giger (1989) applied the hodograph method to a case where the reservoir is bounded by a certain thickness h_o and outer boundary at x_e. In his paper, Giger provided a general solution of the shape of the water crest by using the hodograph method presented by Efros (1963), where the parametric equations of the interface are given as:

$$x = \frac{c\theta + \varepsilon(\theta)\left\{\frac{\pi\theta^2}{4} - \frac{1}{2\pi}\left[\ln\left(1+e^{-\pi|\theta|}\right)\right]^2 - \frac{s\left[1/e^{|\theta|\pi+1}\right]}{\pi} + \frac{\pi}{12}\right\}b}{c+\ln 2} \quad \text{.....(2.27)}$$

$$z = -\left\{1 + \frac{\ln\left[\cosh\left(\frac{\pi\theta}{2}\right)\right]}{c+\ln 2}\right\} \quad \text{.....(2.28)}$$

Where b is the vertical distance between the top of the water crest and the top of the reservoir.

The critical rate from the well per unit length is:

$$q_c = \frac{\pi k_o \Delta\rho g b}{\mu_o (c+\ln 2)} \quad \text{.....(2.29)}$$

Instead of attempting to solve the above three equations, Giger showed that at a large distance from the well, the shape of the interface may be approximated by the equation of parabola:

$$y^2\left(\frac{c+\ln 2}{b}\right)^2 - x\pi\frac{c+\ln 2}{b} - \frac{\pi^2}{12} - c^2 = 0 \quad \text{.....(2.30)}$$

When $c = 0$, corresponds to the critical crest condition.

Then to solve the quadratic equation, one can obtain:

$$b = \frac{3x_e \ln 2}{\pi}\left[\sqrt{\left(1+\frac{4}{3}\frac{h_o^2}{x_e^2}\right)}-1\right] \quad \text{.....(2.31)}$$

Inserting Equation 2.31 into Equation 2.29, we can obtain the critical rate per unit length as:

$$q_c = \frac{3x_e k_0 \Delta\rho g}{\mu_o}[\sqrt{\left(1+\frac{4}{3}\frac{h_o^2}{x_e^2}\right)}-1] \quad \text{.....(2.32)}$$

Because the crest shape is estimated at a large distance from the well, Giger (1986) suggested that these solutions not be used for small values of the dimensionless drainage radius.

McCarthy (1993) solved the interface problem using the hodograph method by assuming that the crest shape intersected with the original WOC at a zero angle. This zero angle theory is true in vertical wells. For vertical wells, the pressure distribution in the oil zone is a logarithmic function. However, matters are different for the horizontal wells. At a large distance from the well, the flow is nearly linear. We can no longer assume that a water level has a horizontal asymptote.

The shape of the interface given by McCarthy is:

$$x = \frac{q_c \mu_o}{k_o \Delta\rho g h_o}\frac{2}{\pi^2}\int_0^\tau \frac{t\tanh t}{\sqrt{1+\cosh^2(\frac{t}{s})}}dt \quad \text{.....(2.33)}$$

$$z = \frac{q_c \mu_o}{k_o \Delta\rho g h_o}\frac{2}{\pi^2}\int_0^\tau \frac{\tanh t}{\sqrt{1+\cosh^2(\frac{t}{s})}}dt \quad \text{.....(2.34)}$$

Where $s = \sinh^2 \frac{\pi}{2} \frac{K}{u}$

Because Equation 2.33 cannot be solved analytically, an approximation is given by a log-linear curve fitting. After the curve fitting, the approximate solution for the critical rate is:

$$q_c = \frac{2k_o \Delta\rho g}{\mu_o} h_o \left[\frac{x_e}{h_o} + \sqrt{\left(\frac{x_e}{h_o}\right)^2 - 0.42} \right]^{-1} \quad \text{.....(2.35)}$$

Up to this point, only the case for a well located at the top has been considered. However, for more general cases where the well may be located at any location in the vertical plane, there is scant literature on this subject. According to McCarthy (1993), this problem cannot be solved analytically. This problem can be solved only numerically, because of the singularity at point B, as shown in Figure 2.12.

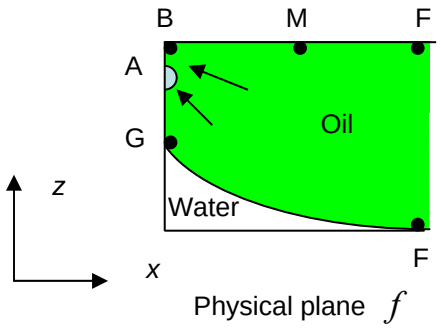

Figure 2.12 Physical plan of water cresting to a well, not located at the top (McCarthy 1993)

McCarthy (1993) proposed a procedure to solve this problem numerically. The first step is to map the physical plane f and hodograph $\overline{w}$ plane onto a semicircle in the upper-half of the auxiliary t plane.

The ζ -plane is mapped via the transformation:

$$\zeta(t) = \frac{q_c}{2\pi} \log\left[\frac{-4t}{(t+1)^2} \right] \quad \text{.....(2.36)}$$

The transformation of $\overline{w}$ plane is written as the form:

$$\overline{w(t)} = iK(t+b)^{1/2} t^{-1} \sum_{n=1}^{\infty} a_n t^{n-1} \quad \text{.....} \quad (2.37)$$

Where the coefficients a_n and b are to be found.

As before, the shape of the interface can be obtained by integrating:

$$\frac{df}{dt} = -\frac{d\zeta}{\overline{w}dt} \quad \text{.....} \quad (2.21)$$

For $t = e^{i\delta}$ $0 \le \delta < \pi$

The nonlinearity of this boundary condition on interface, together with the infinite series in Equation 2.37, makes these equations difficult to solve. After truncating the infinite series in the equation after N terms, the system of non-linear equations may be solved by using Newton's method. Despite the possibility of a numerical solution to such a system, no advantage is gained with respect to simplicity by using this method, compared to using a numerical simulator.

Guo and Lee (1992) claimed that their analytical solution may be used to determine the critical rate for a well at any location. The solution was achieved by using the hodograph method. In their paper, the physical situation was shown in Figure 2.13 and the corresponding hodograph plane was shown in Figure 2.14.

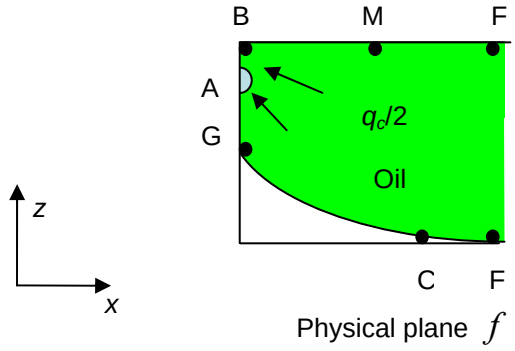

Figure 2.13 Physical plane of water cresting toward a well not located at top (Guo and Lee 1992)

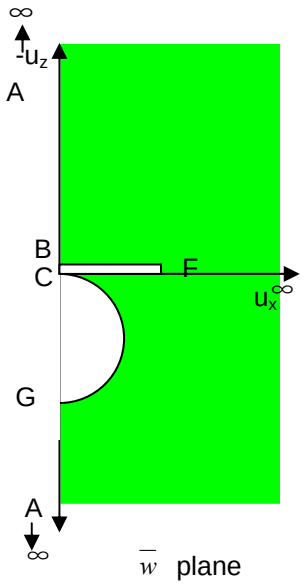

Figure 2.14 Corresponding hodograph plane in Guo and Lee's work (Guo and Lee 1992)

Based on the standard rule of the hodograph transformation introduced by Bear and Dagan (1964), the representation of point *F* should be mapped onto the hodograph plane at the origin ($u_x = 0, u_z = 0$), as shown in Figure 2.15, rather than the point *F* with velocity value $u = q_c / 2h_o$ indicated by Guo and Lee (1992). The corner point *B*, a singular point where streamlines intersect, also should be mapped at the origin. That is, two different points in the physical planes of *F* and *B* are both mapped onto the same corresponding point which is the origin. This violates the one-to-one correspondence between points in the physical and hodograph planes. To avoid this inconsistency, there must be a point *M* between *F* and *B*. Flow velocity along *FM*, reaches some maximum value at *M*, then decreases to zero (q = 0) at point *B*. This yields the cut *BMF* in the hodograph plane, as shown in Figure 2.15.

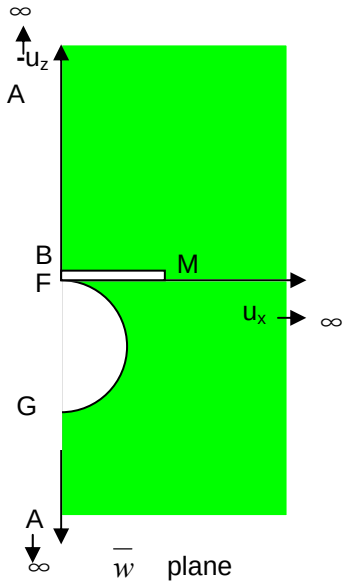

Figure 2.15 Corresponding hodograph plane, based on Bear and Dagan (1964).

Since the numerical value of the abscissas of M is unknown, the solution cannot be carried out analytically. Thus, an analytical solution to model the interface phenomena is still needed. The improved single-well model is derived in Chapter 4. In Chapter 5, the model is extended to Bilateral Water Sink (the two-well system) to determine the critical rate in two-well systems.

CHAPTER 3. QUALIFICATION OF WELL PRODUCTION MECHANISM IN HEAVY OIL

In the previous chapter, a low recovery factor is identified as the main problem encountered in the heavy oil production from a strong bottom-water-drive reservoir. Unlike for conventional oils, where the expected recovery from such reservoirs could be very high - in excess of 50 percent (Dake 1978), the expected recovery factor in heavy oil water-driven reservoirs is less than 20 percent (Shecaira et al. 2002). This chapter provides a qualitative analysis of the well productivity mechanisms specific for heavy oil reservoirs with bottom water. The objective is to understand what makes the production of heavy oil different to that of lighter oils, identify the mechanism that most hampers the well's productivity and recovery efficiency, and to identify hypothetically a technique that might remediate these mechanisms – the bilateral water sink (BWS) well completions.

The study is conducted using numerical simulation models of single horizontal well and BWS wells completed in reservoir systems with strong bottom aquifers underlying typical oil pay zones representing both conventional and heavy oils.

3.1 Simulation Model

First, a series of reservoir cases with an increasing departure from conventional oil properties toward heavy oil properties is used in simulations to study the effect of fluid properties on cresting behavior (Table 3.1).

Table 3.1 Cases for simulation runs

Oil type	Case number	API°	Oil viscosity cp	Permeability md	Porosity %
Conventional oil	1	26	2	200	20
Heavy oil 1	2	20	20	870	30
Heavy oil 2	3	14	65	5000	30
Heavy oil 3	4	14	100	5000	30

Because this study focuses on cold production, 100 cp oil is selected as an upper bounding case; i.e., any oil with in-situ viscosity above 100 cp would not be a candidate for cold production.

A two-dimensional cross section in the *x*-*z* plane perpendicular to the well axis was used in the simulation (Figure 3.1). The well is perforated at the top of the reservoir to delay the water breakthrough. The oil zone is bounded by a no-flow boundary, and the well will drain from within the bounded drainage volume. This representation is reasonable if there is a pattern of production wells, creating no-flow boundaries between wells. The water zone has a constant-potential outer boundary; there is continuous supply of reservoir energy from the natural water influx.

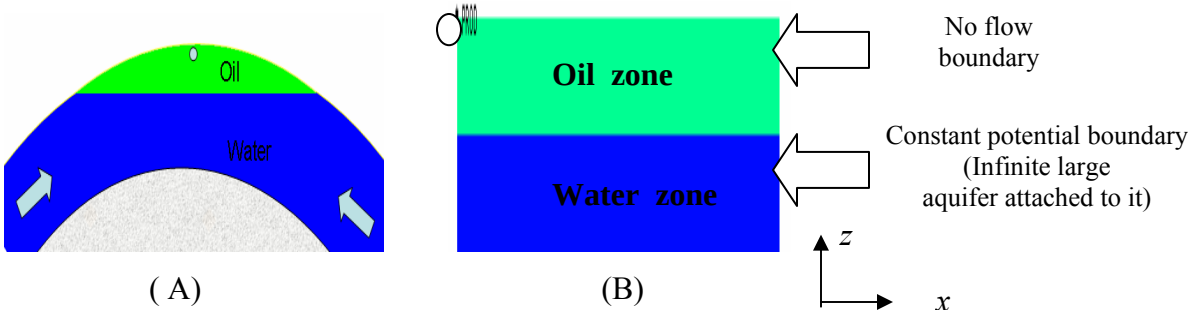

Figure 3.1 Geometry of simulation model (B) for bottom water drive reservoir (A)

All simulations are above bubble point pressure. The reservoir parameters remain constant in all the simulation runs (Table 3.2); the only variation in each run is to change the oil type by altering the value of μ and API° and their corresponding rock properties k and porosity.

Table 3.2 also gives the selected grid size. In order to capture the accuracy in terms of crest height, as well as water cut and water breakthrough times, a refined grid size with $\Delta x = 0.5$ ft is used near the well; away from the well a coarser grid was used, $\Delta x = 10$ ft. The detailed grid size sensitivity study will be presented in Chapter 4. For simplicity, straight-line relative

permeability curves are used for the segregated flow condition with a sharp oil/water interface and no capillary transition zone, so the displacement is governed by vertical equilibrium.

Table 3.2 Data set for simulation runs

Oil zone thickness	50 ft
Water zone thickness	50 ft
Reservoir distance	1000 ft
Water density	995 kg/ m^3
Water viscosity	0.96 cp
Oil compressibility	5×10^{-6} /psi
Water compressibility	3×10^{-6} /psi
Rock compressibility	4×10^{-6} /psi
Connate water saturation	0.2
Residual oil saturation	0.2
Oil relative permeability exponent	1
Water relative permeability exponent	1
Horizontal grid size	0.5 ft × 100 10 ft × 95
Horizontal grid count	195
Vertical grid size	0.5 ft
Vertical grid count	200
Production rate	0.12 stb/day/ft

3.2 Productivity Impairment Analysis

Productivity impairment is assessed by examining the water cut performance and oil recovery factor versus time (Figure 3.2) for a broad range of fluids and reservoir properties (Table 3.1).

Heavy oil water cut behavior is clearly different from the conventional oil case. In a conventional oil reservoir, water breakthrough occurs later, and the water cut gradually increases and reaches a nearly-constant value of about 60 percent. Oil continues to be recovered after water breakthrough. The relationship between the water cut and the oil recovery has been identified by Kuo (1989) through numerical simulations. However, for heavy oil (Figure 3.2), the breakthrough occurs almost immediately after production begins. After water breakthrough, the

water cut increases to 90 percent in a relatively short time span (less than a year), resulting in the loss of well productivity. In terms of oil recovery, the recovery line stays nearly as flat after water breakthrough, which implies that the high water cut render low oil recovery. The behavior of water cut and recovery plot can be more appreciated through the comparison of crest development at different production times for Case 1 (conventional oil) and Case 4 (heavy oil) obtained from numerical simulation, which reveals how crest geometry drives this water cut behavior (Figure 3.3).

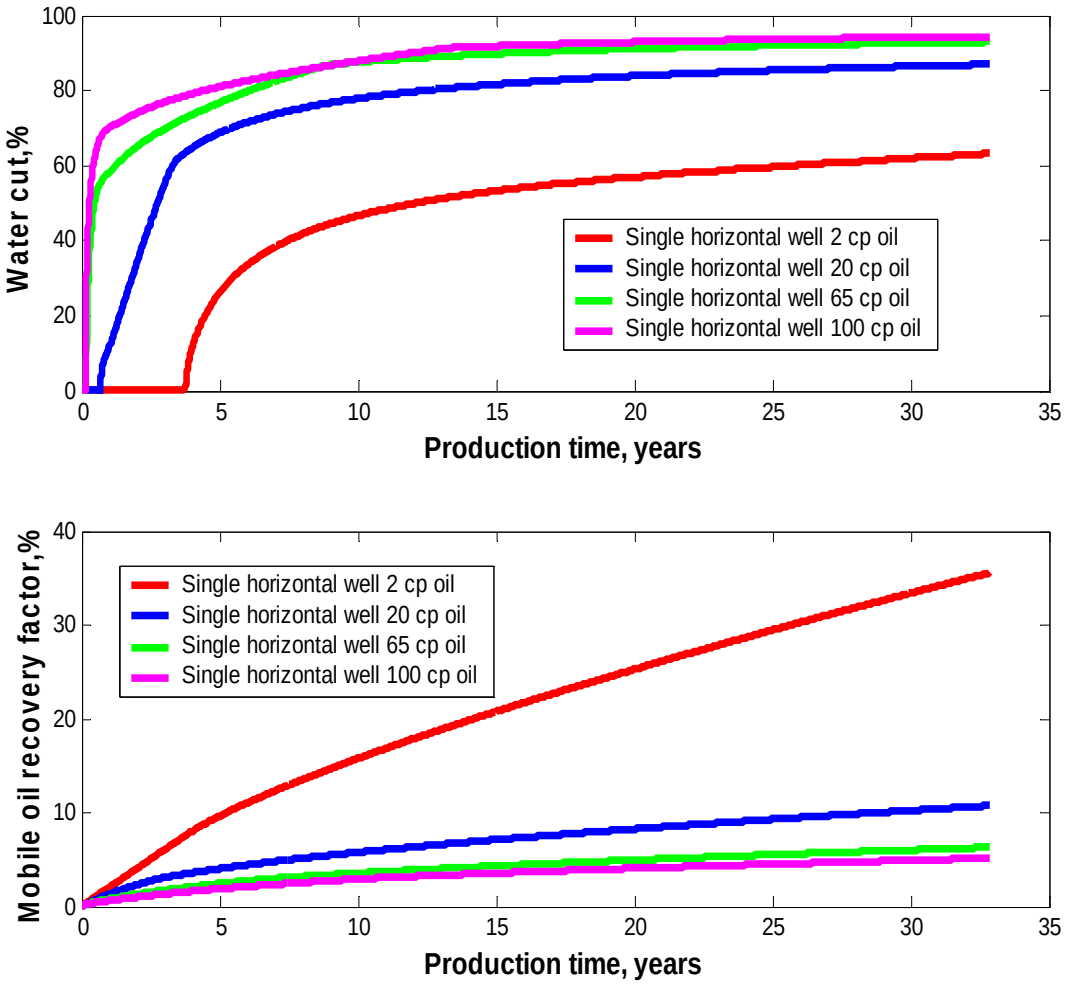

Figure 3.2 Simulation results of water cut and recovery factor vs. time

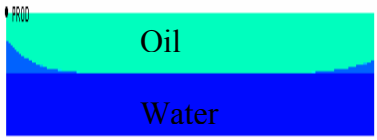

Water saturation profile for conventional oil after 2 years production
Stage 1

Water saturation profile for heavy oil after 2 years production
Stage 1

Water saturation profile for conventional oil after 4 years production
Stage 2

Water saturation profile for heavy oil after 4 years production
Stage 2

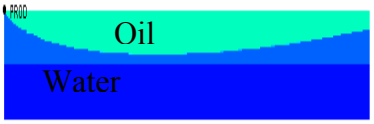

Water saturation profile for conventional oil after 33 years production
Stage 3
(A)

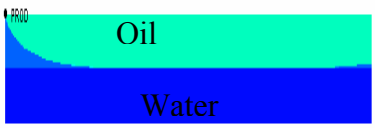

Water saturation profile for heavy oil after 33 years production
Stage 2
(B)

Figure 3.3 Water crest development comparison between conventional and heavy oil

In a conventional oil reservoir (Figure 3.3 A), three stages of crest development may be identified throughout the production life. In Stage1, the crest builds up and moves toward the well. In Stage 2, the crest reaches up to the bottom of the well, and the water breaks through into the well. In Stage 3, the crest extends laterally. This observation is consistent with the Siddiqi's (2001) experimental results using Hele-Shaw and wedge-shaped models. In the heavy oil reservoir (Figure 3.3 B), it is clear that Stage 3 is missing, which means the crest does not grow laterally after water breakthrough, and the crest shape is much narrower than that of conventional oil. Insight can be gained by examining potential profiles before water breakthrough (Figure 3.4 Case 1, conventional oil; Case 4, heavy oil) after the rate has been stabilized.

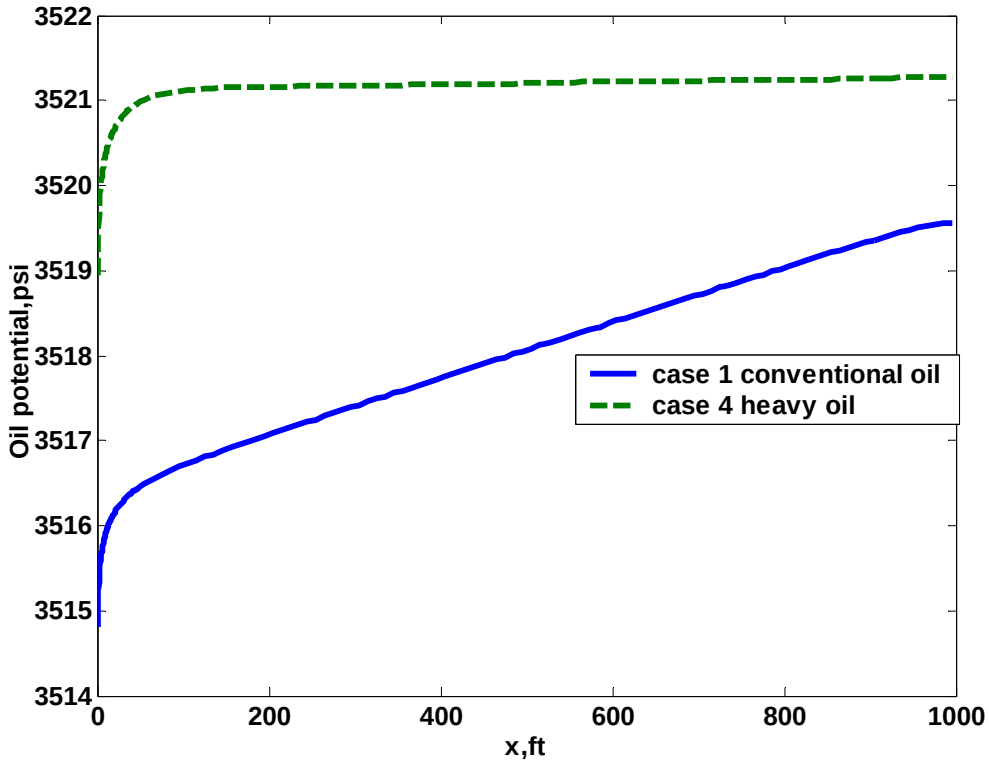

Figure 3.4 Oil potential profile comparison between Case 1 and Case 4

In conventional oil reservoir, the potential drop extends to the outer boundary (here, x_e = 1000 ft) and the whole reservoir contributes to production. However, for heavy oil, the potential is lowered only within a smaller region (here, x_i < 100 ft). The region of influence remains small regardless of how large the reservoir is. Beyond this region of influence, oil potential is nearly constant. Because the lateral extent of the crest is directly associated with the potential drop in the reservoir through $\Delta\rho gh = \Delta\Phi$, the small value of the crest width (Figure 3.3 B) is caused by a small area in which Φ drops below its original value. This implies that the oil drains only from a small region around the wellbore where $x_i < x_e$. The oil beyond the region of influence has no potential gradient driving it toward the well, and therefore will not be recovered. Not only the area subject to the potential drop is limited to vicinity of the wellbore, but also the magnitude of the potential drop is small in comparison with that of conventional oil case (Figure 3.4). Because when the well is produced at the constant liquid rate, the potential drawdown in the reservoir is

directly proportional to the drainage distance (referred to Darcy's Law). The small potential drawdown in heavy oil case results from the small drainage distance. For heavy oil to achieve high oil recovery, a new mechanism must be introduced to make the heavy oil reservoir behavior like that of a conventional oil reservoir having a large potential drawdown spread throughout the entire reservoir.

Another effect influencing the low oil recovery in heavy oil is the occurrence of water bypassing oil. For heavy oil cases after water breakthrough, because water is much less viscous than heavy oil, if water and heavy oil have the same potential gradients, water will flow at much higher rates. This may leave behind a large amount of by-passed oil. As a result, the water cut quickly rises to a very high value (Figure 3.2). The low ultimate recovery of heavy oil with bottom water drive is caused by a combination of a small drainage area and the water bypassing oil after a water breakthrough.

According to Joshi (1991), ultimate oil recovery in bottom water drive reservoirs may be increased by operating the well below or at a critical rate, which prevents water cresting and avoids this cause of by-passed oil. However, the critical rate in a single horizontal well produced from heavy oil reservoirs is usually too small to make any profit (Dusseault 2006), while recovery time largely increases. Moreover, the limited drainage area will not show a significant increase by this method. For example in Case 4 in Figure 3.4, even though all the oil within the mobilized oil region ($x_i < 100$ ft) was recovered, it only accounted for 10 percent of the original oil in place.

Here, the discussion focuses on improving the oil recovery factor in heavy oil reservoirs with bottom water drive (more detail is given in Chapter 6). Besides controlling the water crest, one should expand the drainage area to transmit a potential drop throughout the oil zone. However, existing approaches to control cresting are similar to requiring that one operate a well

below or at critical rate, not increasing the drainage area. The failure to increase the drainage area limits improvements in oil recovery. This study proposes a method that increases the drainage area and prevents water breakthrough.

3.3 Effect of Rate Increase on Recovery

Kuo (1983) conducted a numerical study of vertical wells to develop a correlation of water cut behavior after water breakthrough. He showed that regardless of the production rate, the ultimate oil recovery (limited by maximum economical water cut) was the same. Producing well at high rates could accelerate projects and shorten the well's life, rendering the same final recovery. However, his study is mainly focused on conventional oil with a mobility ratio range from 1.0 to 10.0. In this section, we will demonstrate the effect of the oil rate on heavy oil recovery by altering the production rate (q_l = 0.12, 0.24, 1.2 stb/day/ft) in numerical simulations for case 1 (conventional oil, 2 cp) and case 3 (heavy oil, 65 cp) in Tables 3.1, 3.2.

The results of recovery factor as a function of time are plotted in Figure 3.5. Similar to the Kuo (1983) results, in the case of conventional oil (2 cp oil), the increase of production rates (from 0.12 stb/day/ft to 1.2 stb/day/ft) could (theoretically) significantly increase the mobile oil recovery from 35 percent to 98 percent at the end of the project life (Figure 3.5). In contrast, for heavy oil, the high production rate doesn't significantly stimulate the recovery for the same production time. The production rate has been increased 10-fold (from 0.12 stb/d/ft to 1.2 stb/d/ft), but the recovery is small (from 6 percent to 12 percent).

The comparison shows that - for the same project duration - increasing production rate has little influence on improving oil recovery in heavy oil reservoirs. A much longer time frame would be needed to see the effects of an increased rate. However, the extended production time is not possible because of the high water cut – above the economic limit. Unlike the conventional oil case, where high ultimate oil recovery is reached sooner for a high production rate, for heavy

oil the shortening of production time with rate is irrelevant since the oil recovery factor is still less than 15 percent. This observation can be explained with Figure 3.6, showing the water cut behavior comparison for conventional and heavy oil. Because of the nature of the heavy oil, a high mobility ratio causes the water breakthrough at an early time (in couple of months), and water by-passes oil after water breakthrough, resulting in rapid increase of water cut to a very high value (over 90 percent), as shown in Figure 3.6. If we assume that a water cut of 90 percent is the economic limit for a well making profit, thereafter, the well has to be shut down. The recovery factor at 90 percent water cut is plotted in Figure 3.7, which can be regarded as the ultimate oil recovery factor. It shows the ultimate oil recovery is very small (less than 5 percent) in all the cases, and slightly decreases as production rate increases, due to the severe water cresting problem associated with a high production rate. The ultimate oil recovery that is dependent on the flow rate and high production rate will have negative impact on the oil recovery due to the early water breakthrough and high water cut in the well (Figure 3.7).

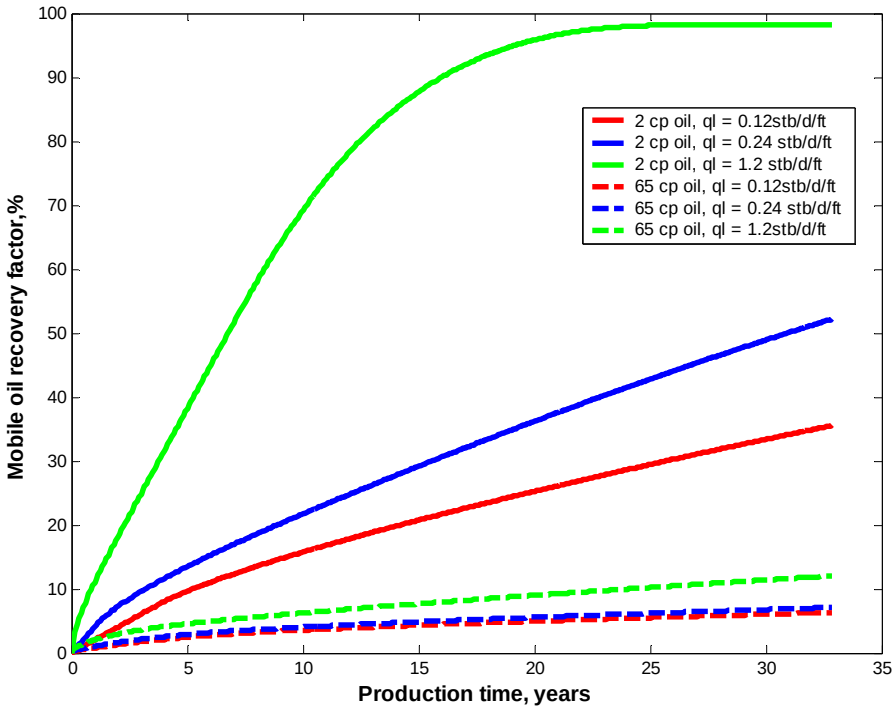

Figure 3.5 Recovery vs. production time for different production rates

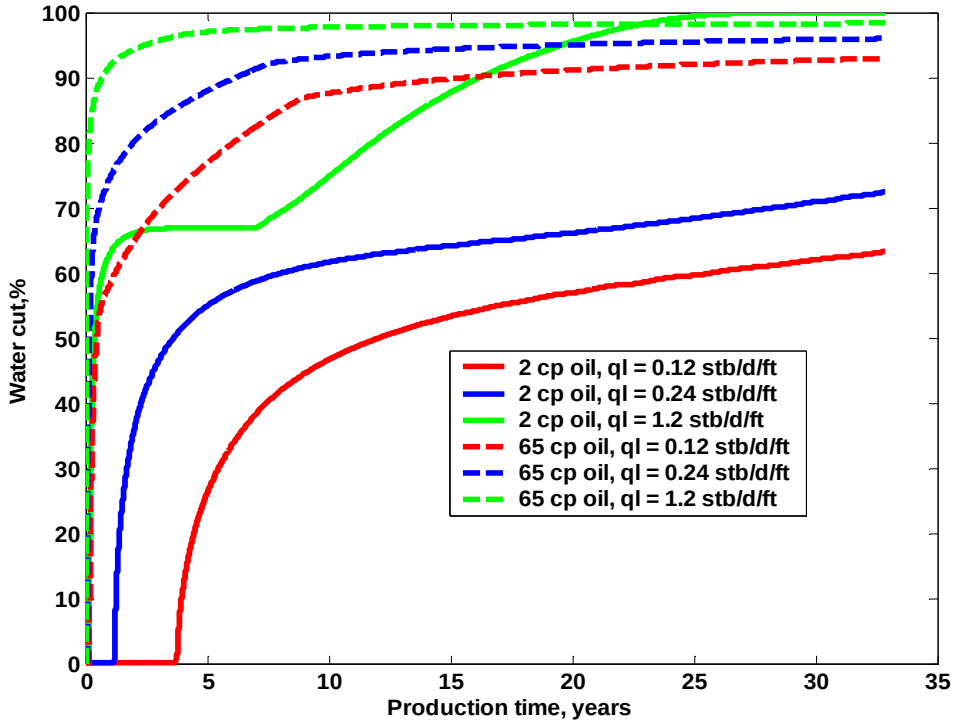

Figure 3.6 Water cut vs. production time for different production rates

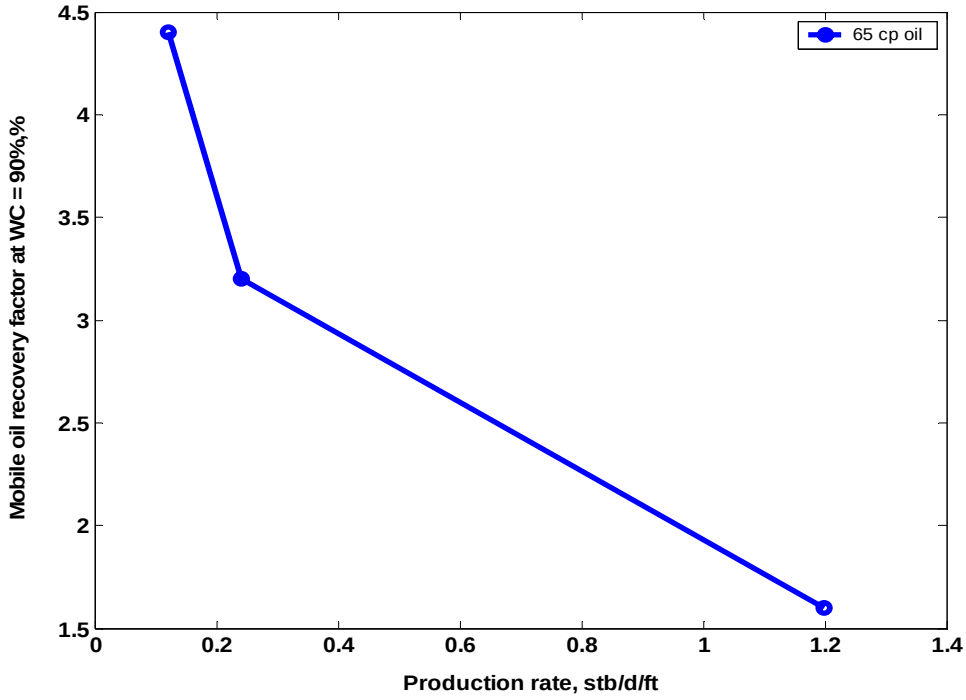

Figure 3.7 Recovery factor vs. production rates for heavy oil at water cut = 90%

Therefore, we conclude that in the heavy oil reservoirs, the maximum oil recovery could be obtained if the water breakthrough was prevented or the water cut kept below its maximum value. Of the two alternatives, the water-free production is more attractive because it eliminates a need for surface processing and separation facilities. Thus, the water-free oil production combined with a high pressure drawdown seems to be a desired cold production method for heavy oil with bottom water.

3.4 Water Crest Stabilization Time

After a well starts to produce, a transient period occurs during which the flow in the reservoir is unsteady and potential at fixed x is varied. A stabilized condition can prevail after this transient period, because the potential is maintained by the strong aquifer. During the transient period, the crest expands laterally as the distance of investigation propagates towards the outer boundary. Once the stabilized condition is achieved, the shape and the size of the crest will not vary with time, which indicates the stabilized crest condition. Plots of the flow potential distributions during the water crest development time for the four oil cases (Table 3.1) are shown in Figure 3.8. It can be seen that the potential profile in a reservoir yields different shapes at different times for conventional oil (2 cp oil). This indicates that the potential at any point in a reservoir reflects change as a function of time. A steady-state condition was not reached before water breakthrough.

In contrast, in the medium-heavy oil case (20 cp oil), the potential profile difference between various times becomes smaller, compared to the conventional oil case (2 cp oil). For heavy oil cases (65 cp and 100 cp oils), the three solid lines representing the potential distribution in a reservoir within the first 15 days are practically identical. This means the reservoir is under a stabilized flow condition from day one. Thus, the transient flow period is shorter than one day and the stabilized condition dominates the reservoir flow behavior. The

crest quickly builds up and becomes stable (Figure 3.3 B, heavy oil case). From this study, we conclude that the potential-stabilizing effect of bottom water in heavy oil is very prompt compared with the conventional oil reservoir so the stabilized-flow condition can be used for analytical modeling of well crest performance in heavy oil.

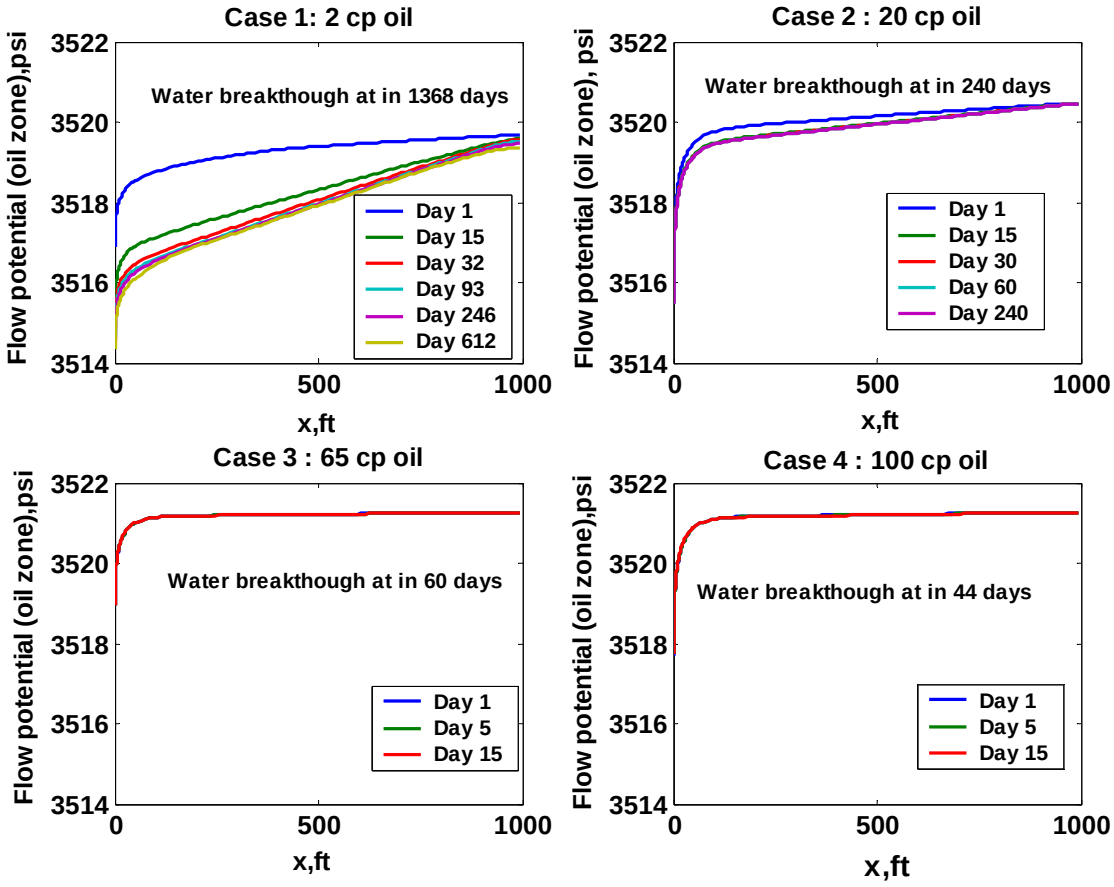

Figure 3.8 Simulation results of flow potential profile from Case 1 to Case 4

3.5 Borehole Friction Effect

Simulations show that if the well's frictional pressure loss was ignored, potential would be uniformly distributed along the wellbore, resulting in simultaneous and uniform water encroachment as shown in Figure 3.9.

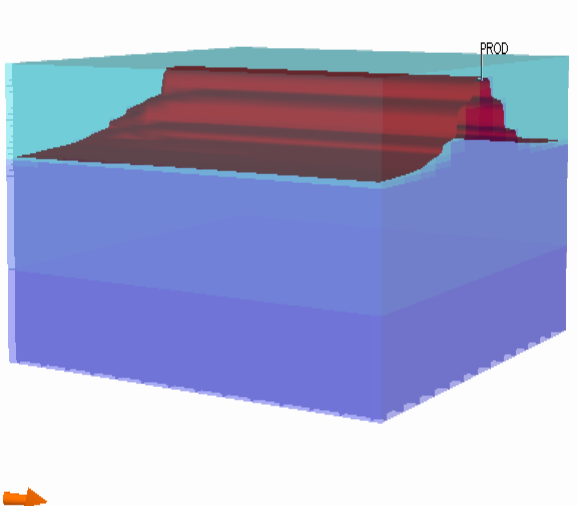

Figure 3.9 Simulated water cresting with
well friction ignored

According to Penmatcha and Aziz (1998) the friction pressure loss can be significant, so that neglecting it can lead to errors in horizontal well performance prediction. If frictional losses are not negligible, the water will tend to breakthrough first at the heel of well (where potential is lowest), then advance toward the toe (Figure 3.10). In such cases, the friction pressure drop should be included in a 3-D well model.

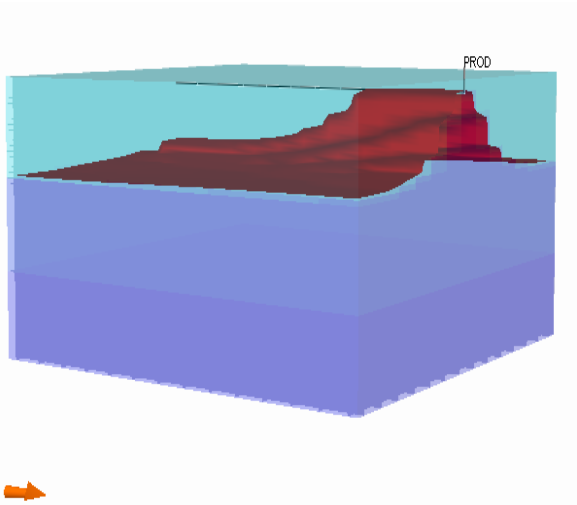

Figure 3.10 Simulated water cresting in a horizontal well with
well friction considered

To study the effect of the frictional pressure loss along a wellbore on well performance, three cases: conventional, medium heavy and heavy oil are simulated in this section. For each oil case, the frictional pressure loss is either considered (model A), or ignored (model B). The rock and fluid properties in those cases are listed in Tables 3.3 and 3.4. The well is completed across the entire reservoir, and in all the cases the well is produced at a constant rate of 5000 stb/day.

Table 3.3 Properties used in numerical simulation

Oil type	Case	API°	Oil viscosity cp	Permeability md	Porosity %
Conventional oil	1	26	2	200	20
Medium heavy oil	2	20	20	870	30
Heavy oil	3	14	65	5000	30

Table 3.4 Data set for simulation runs

Oil zone thickness	50 ft
Water zone thickness	100 ft
Reservoir extent	750 ft
Water density	995 kg/ m^3
Water viscosity	0.96 cp
Oil compressibility	5×10^{-6} /psi
Water compressibility	3×10^{-6} /psi
Rock compressibility	4.0×10^{-6} /psi
horizontal grid size	100 ft
horizontal grid count	15
Vertical grid size	3 ft
Vertical grid count	22
Well length	1500 ft
Wellbore size	0.25 ft
Production rate	5000 stb/day

The friction loss along the wellbore in model A is calculated using a correlation given by Aziz et al. (1972); their model includes fluid densities, frictional effects and kinetic energy effects. As shown in Figure 3.11, the water cut behavior and oil recovery, as a function of time, are the same for all oils in both models. Agreement between simulations of model A and model B means a validation of the assumption in neglecting frictional pressure loss along the wellbore. This agreement is due to the insignificance of the frictional pressure drop along the wellbore,

compared to the pressure drawdown in the porous media. As a result, the water cresting is uniformly distributed along well's axis (Figure 3.9). The results would be different if the well was longer, tubing was smaller, or permeability was lower.

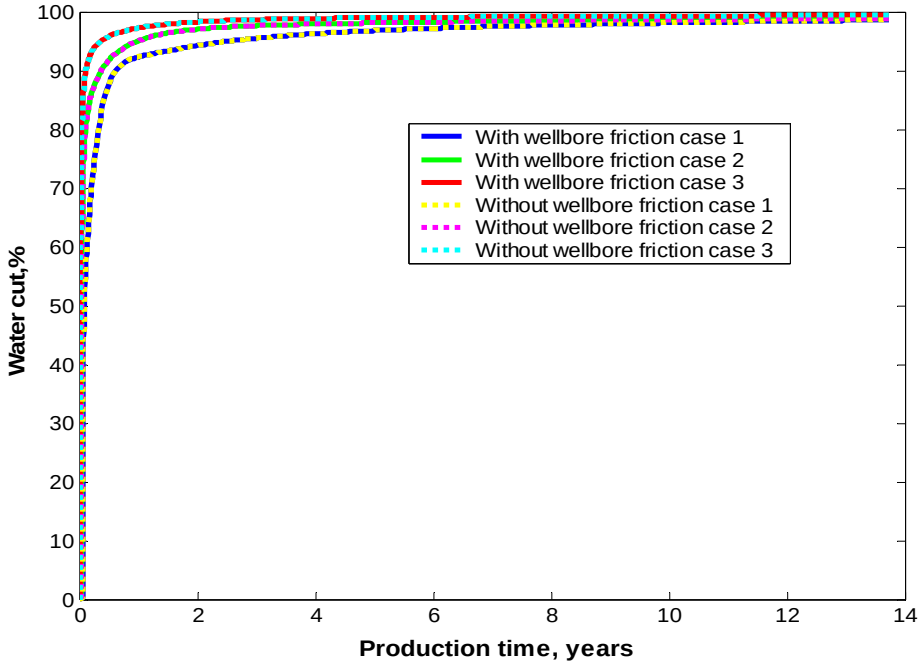

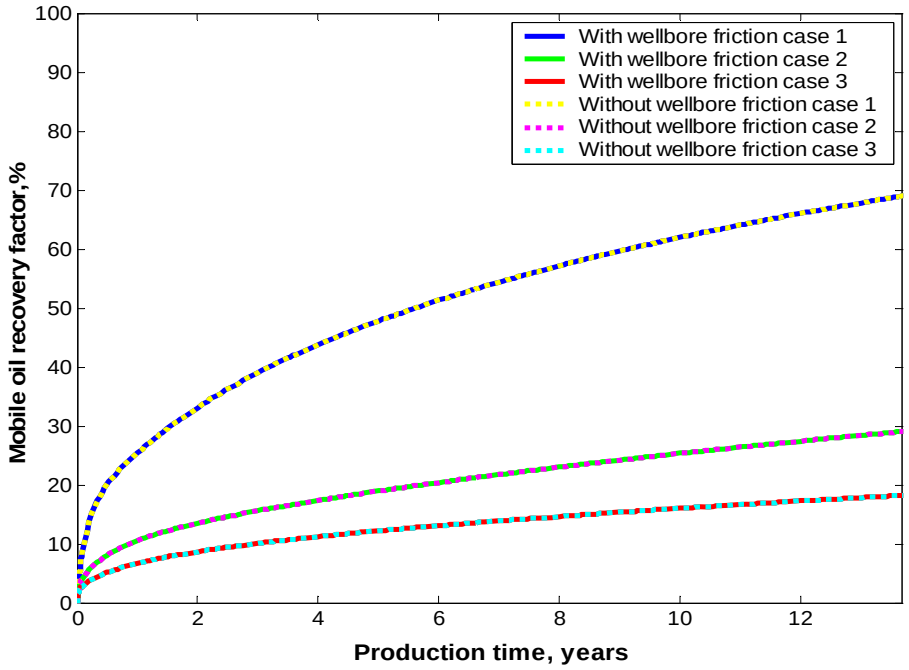

Figure 3.11 Simulation results of water cut and recovery factor with and without well friction

3.6 Feasibility of Bilateral Water Sink Wells

As concluded above, a water-free oil production combined with high pressure drawdown seems to be a desired cold production method for heavy oil with bottom water. The bilateral water sink (BWS) well technique meets the two criteria. It enables high-pressure drawdown at the top lateral while avoiding premature water breakthrough. To test the hypothesis of BWS improving oil recovery, two types of wells are simulated and compared. The first one is a single horizontal well as a base case - the case 4 in Table 3.1. The second one is a BWS well with the lower lateral (horizontal well) at the bottom of the water zone (Figure 3.12). All other properties of reservoir and boundary condition remain unchanged compared to the base case. The oil production well produced at constant liquid rate at top completion = 0.12 stb/day/ft for both cases.

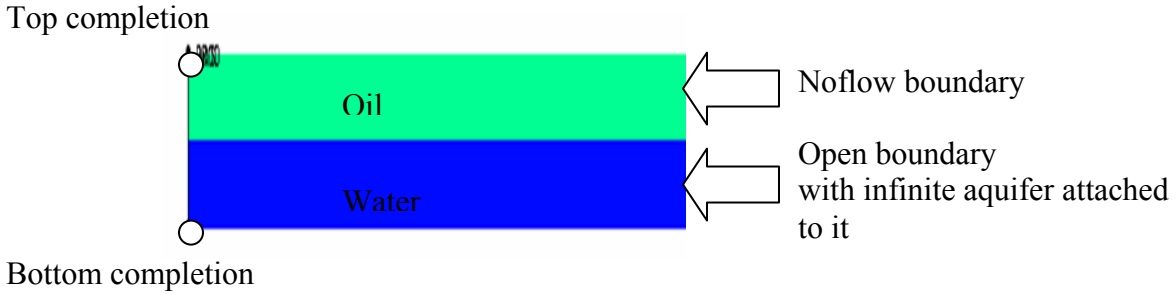

Figure 3.12 Geometry of the reservoir model for BWS

Simulation of the water-free operation of BWS is quite complicated for finding the bottom water drainage rate for the selected oil production rate at the top lateral. It requires a trial-and-error approach. We must make an initial guess and see if this water drainage rate at the lower completion can make the oil-water interface stable without water breakthrough into the well. If not, we must try gradually increasing (or decreasing) water rates until the water-free inflow condition is reached. After testing a series of rates, the water drainage rate obtained from

simulations is 12.5 bbl/day/ft. Often, more than ten simulation runs have to be made to find this rate. Each run takes several hours, which makes this approach not very efficient. Comparison of the two wells, in Figure 3.13, shows the advantage of BWS in avoiding water breakthrough, decreasing the water cut from 90 percent to 0 percent, and improving mobile oil recovery from less than 10 percent to 40 percent compared to the single lateral well. Therefore, a more direct computational method for the BWS well rates calculation is needed to avoid the trial-and-error series of numerical simulations. An analytical model and procedure for computing critical rate could provide a valuable tool to design a BWS well's operation.

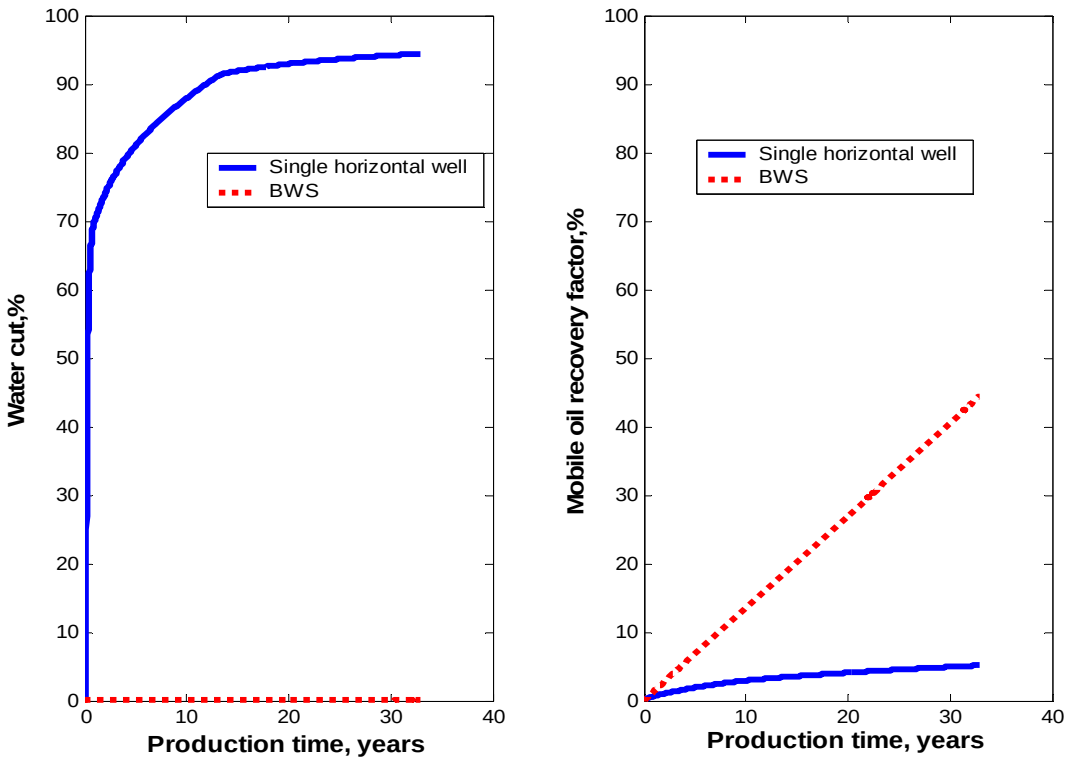

Figure 3.13 Simulated comparison of a single horizontal well with BWS

3.7 Summary

In this chapter, simulation case studies are conducted to provide insights of productivity impairment encountered in heavy oil with bottom water. Rapid water invasion to the well, small

effective drainage area (regardless the reservoir size), slow recovery, and large amount of by-passed oil have been identified as the major features of conventional single lateral well performance. Also identified are the required mechanisms for performance improvement – a water-free oil production combined with high pressure drawdown. The bilateral water sink (BWS) technology is hypothetically proposed as a potential solution to the problem. Its feasibility is demonstrated theoretically by comparing the simulated performance of BWS with a single lateral well with the same production rate in the oil pay zone. The simulation also shows a need for analytical modeling of BWS critical rates to avoid a tedious trial-and-error search with the reservoir simulator.

This chapter also provides support for simplifying assumptions that can be made in the analytical modeling of BWS critical rate. The model may be derived for steady-state flow conditions since the flow stabilization time in heavy oil is very short. Moreover, the study shows that the analytical model of critical rate can be two-dimensional since the well flow frictional effects are negligible.

CHAPTER 4. IMPROVED MODEL FOR WATER CRESTING IN HORIZONTAL WELL

The purpose of a BWS well is to increase the critical rate at the upper bilateral above the economic production rate. Therefore, designing the BWS wells would require derivation of an accurate critical rate model for a single horizontal well and upgrading the model for BWS wells. In this chapter, improved models for critical rate in a single horizontal well are built using two methods - the hodograph method and the Dupuit approximation approach. These models can improve the accuracy of the critical rate calculation with less restriction. The models are verified with numerical simulation.

4.1 Critical Rate Model by the Hodograph Method

4.1.1 Assumptions

The assumed geometry is a horizontal well with length of L – much exceeding the other two dimensions, the width, $2x_e$, and thickness, h_o, of a rectangular (cuboidal) drainage area (Figure 4.1). Radial flow near the ends of a finite-length horizontal well is neglected in this geometry; this is referred to as the end effect in this dissertation.

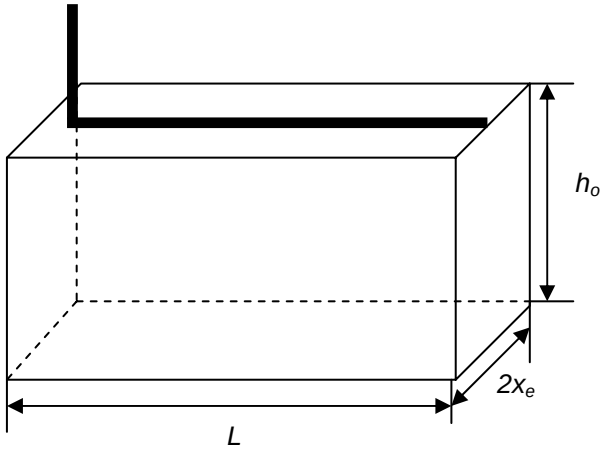

Figure 4.1 Configuration of a horizontal well in a square drainage area

The well is modeled as a line source that assumes that the wellbore radius is negligibly small and the wellbore can be treated as a line. The well is assumed to be parallel to the top and bottom boundaries. The reservoir boundary at the top of the oil pay zone is assumed to be a no-flow boundary. Also, there is constant flow potential at the lateral boundary of the drainage area, x_e. That is, the well drains a region with completely open outer boundaries laterally, and confined above and below, at steady state. In mathematical terms, these boundary conditions are

$$\Phi = \Phi_e = \text{constant at } x = x_e \quad \text{.....} \quad (4.1)$$

$$\frac{\partial \Phi}{\partial t} = 0 \quad \text{for all } x \text{ and } t \quad \text{.....} \quad (4.2)$$

This condition, in which potential is maintained in the reservoir due to the natural water influx from underlain aquifer, has been verified in Chapter 3. We also make the following additional assumptions:

- Fluids are immiscible, incompressible, and have constant viscosities.
- The permeability is homogenous and isotropic, and porosity is uniform.
- There is a sharp interface between the water and oil - the transition zone is neglected, and the end-point values of relative permeability are used. This restriction will be removed later by considering the capillary pressure transition zone and relative permeability curve.
- Friction loss along the wellbore is negligible. As discussed in the Chapter 3, the friction loss along the wellbore in heavy oil reservoirs is usually small compared to the pressure drawdown in the reservoir, and the well approaches infinite conductivity behavior.

When end effect and friction loss are neglected, the flow is the same in all the parallel planes along a horizontal well. The problem is, then, two-dimensional in the *x*-*z* plane, which is perpendicular to the axis of the well, as shown in Figure 4.2. The three-dimensional solution is

approximated via flow-per-unit length in the mathematically infinitely long horizontal well, and multiplying by the target length, L.

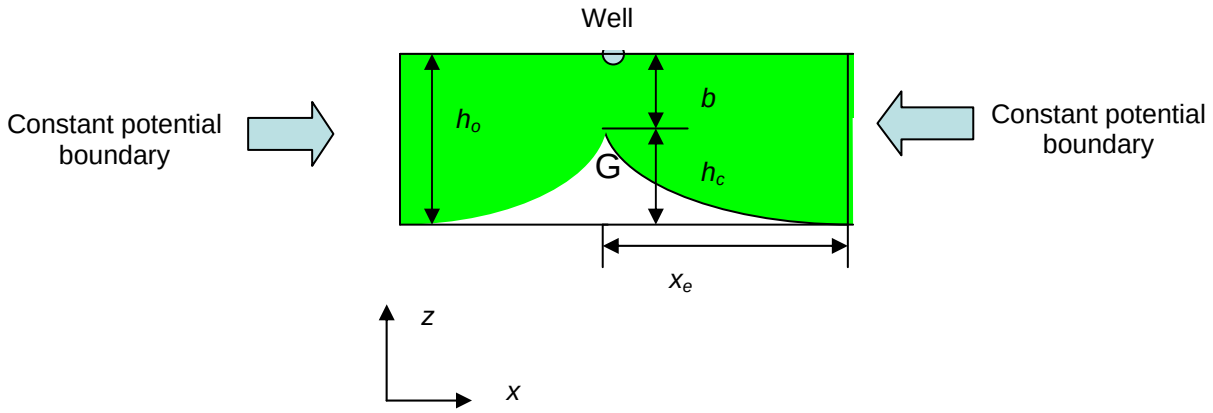

Figure 4.2 Cross-section schematic of water cresting in a horizontal well

As indicated in Figure 4.2, only the critical case is considered with the oil flowing above the OWC, while the water remains immobile. If oil rate exceeds the critical rate, the water crest becomes unstable and water will flow into the well.

4.1.2 Derivation of the Analytical Solution

Bear and Dagan (1964) describe the interface equation in a reservoir with infinite thickness and an infinite lateral extent (Figure 4.3) using Equations 2.25 and 2.26. When using these equations, the water cone would be infinitely high, because the aquifer encountered in hydrology is often infinitely large.

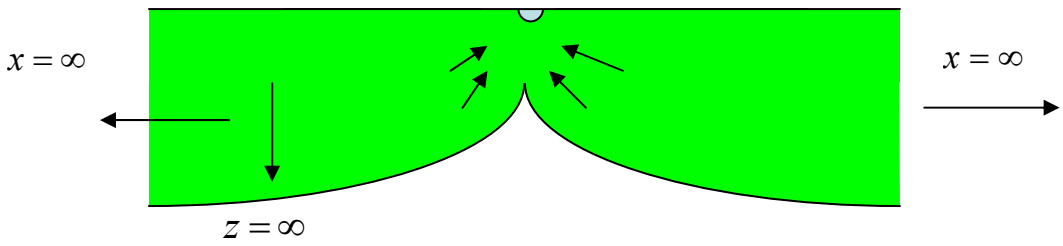

Figure 4.3 Reservoir with infinite thickness (Bear and Dagan 1964)

To calculate the critical rate and crest shape in a reservoir with oil zone thickness h_o and an outer boundary extent x_e as shown in Figure 4.2, two constraint conditions must be introduced and combined with the parametric equations given by Bear and Dagan. The two constraint conditions are:

$$h_c + b = h_o \quad (4.3)$$

$$x = x_e \quad (4.4)$$

Where:

h_c is the critical crest height;

b is the distance between the apex of the crest to the well (Figure 4.2).

To determine b, in the B plane, we integrate Equation 2.21 within

$$\int_{GA} df = \int_{GA} -\frac{d\zeta}{wdB} dB = \int_{GA} -\frac{q_c}{\pi^2 K}\left(\frac{\operatorname{arc}(\sinh\sqrt{B})}{B}\right)\ dB \text{, or} \quad (4.5)$$

$$\int_{B=-1}^{B=0} -\frac{q_c \mu_o}{\pi^2 k_o(\rho_w - \rho_o)g}\left(\frac{arc(\sinh\sqrt{B})}{B}\right) dB = x + ib \quad (4.6)$$

The integration gives,

$$\frac{bk_o(\rho_w - \rho_o)g}{\mu_o q_c} = \frac{1}{\pi}\ln 2 = 0.221. \quad (4.7)$$

Where b is expressed as :

$$b = \frac{q_c \mu_o}{k_o(\rho_w - \rho_o)g\pi}\ln 2 \quad (4.8)$$

Inserting Equations 4.8 and 2.26 into Equation 4.3 gives:

$$\frac{q_c \mu_o}{k_o(\rho_w - \rho_o)g\pi}\ln 2 + \frac{q_c \mu_o \ln\cosh t}{k_o(\rho_w - \rho_o)g\pi} = h_o \quad (4.9)$$

At the outer boundary, reservoir extent is defined by x_e; inserting Equation 2.25 into Equation 4.4 yields:

$$\frac{2\mu_o q_c}{k_o(\rho_w-\rho_o)g\pi^2}\int_0^t t\tanh t dt = x_e \quad \text{.....(4.10)}$$

Combining the above two equations, we obtain equations for calculating critical rate in a reservoir with thickness at h_o and bounded by outer distance at x_e:

$$\frac{q_c\mu_o}{k_o(\rho_w-\rho_o)g\pi}\ln 2+\frac{q_c\mu_o}{k_o(\rho_w-\rho_o)g\pi}\ln\cosh t = h_o \quad \text{.....(4.11)}$$

$$\frac{2q_c\mu_o}{k_o(\rho_w-\rho_o)g\pi^2}\int_0^t t\tanh t dt = x_e \quad \text{.....(4.12)}$$

Equations 4.11 and 4.12 can be solved simultaneously to obtain the critical rate. The critical rate q_c cannot be found analytically, but can be computed numerically. A program was developed to calculate the critical rate from Equations 4.11 and 4.12 (see Appendix A).

The solution will be expressed in dimensionless form for simplicity and generality, giving the dimensionless critical rate as a function of dimensionless distance (Table 4.1). Because dimensionless variables are used, they have the same numerical value, regardless of the units system used.

Table 4.1 Dimensionless group defined

Dimensionless group	Symbol	Equation
Dimensionless critical rate	q_{cD}	$q_{cD}=\dfrac{q_c}{\dfrac{k_o}{\mu_o}(\rho_w-\rho_o)g(h_o)}$
Dimensionless reservoir radius	x_{eD}	$x_{eD}=\dfrac{x_e}{h_o}$

Another advantage of using a dimensionless group is that the number of independent parameters is reduced. Instead of altering the value of each variable, one can vary the value of only the dimensionless group to examine the range of behavior.

In the dimensionless form, Equations 4.11 and 4.12 is:

$$q_{cD} = \frac{\pi}{\ln 2 + \ln \cosh t} \quad \text{(4.13)}$$

$$\frac{2q_{cD}}{\pi^2} \int_0^t t \tanh t \, dt = x_{eD} \quad \text{(4.14)}$$

Equations 4.13 and 4.14 can be solved numerically to obtain q_{cD} as a function of x_{eD} (Figure 4.4). The relationship between q_{cD} and x_{eD} is nonlinear. The dimensionless rate for any q_{cD} can be determined from Figure 4.4 for given value of x_{eD}. To find the actual critical rate, one can simply use the actual reservoir size to scale x_e to x_{eD}, find q_{cD}, and then compute q_c, from the dimensional critical rate formula in Table 4.1.

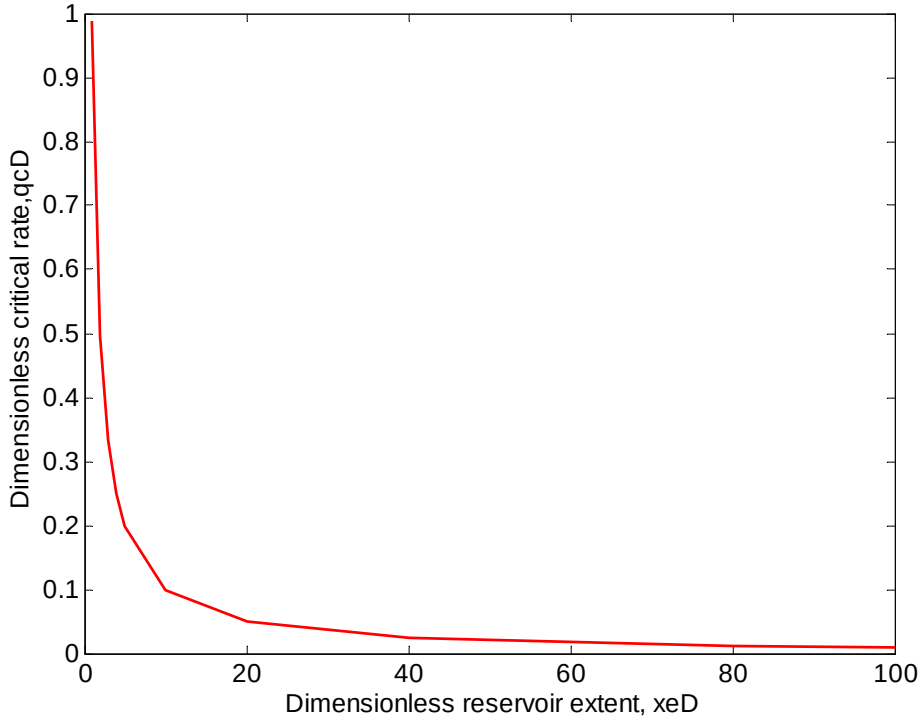

Figure 4.4 Dimensionless critical rate from hodograph method

If we plot q_{cD} vs. x_{eD} on a log-log scale (Figure 4.5), the relationship appears to be linear with the (-1) slope implying that the critical rate is proportional to the reciprocal of

dimensionless reservoir extent ($1/x_{eD}$). Figure 4.5 can be used as a simple and easy tool to predict critical rate in horizontal wells.

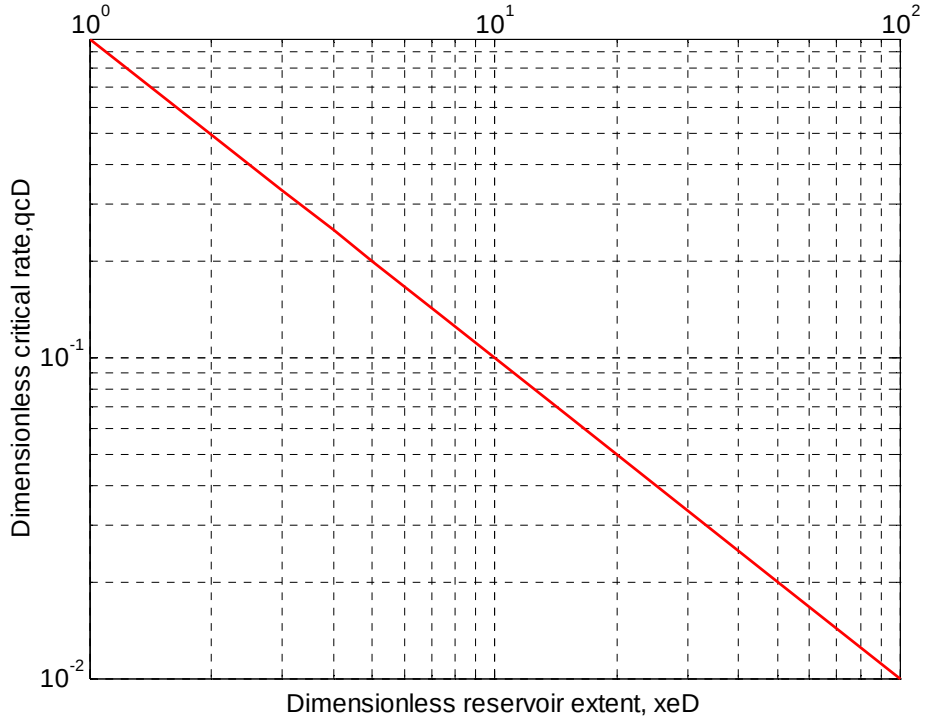

Figure 4.5 Dimensionless critical rate in log-log scale

If the effects of relative permeability and capillary pressure are not negligible, the absolute permeability k_o and oil zone thickness h_o in Equations 4.11 through 4.14 can be replaced by end-point relative permeability $k_o k_{ro}$ and an oil zone thickness above the capillary transition zone of $h_o - h_{pc}$, respectively.

The new dimensionless groups now become:

$$q_{cD} = \frac{q_c}{\frac{k_o k_{ro}}{\mu_o}(\rho_w - \rho_o)g(h_o - h_{pc})} \quad \text{(4.15)}$$

$$x_{eD} = \frac{x_e}{h_o - h_{pc}} \quad \text{(4.16)}$$

Where h_{pc} is the thickness of the capillary transition zone.

4.1.3 Verification Using Numerical Simulation

In this section, the validity the hodograph model will be tested using a numerical reservoir simulator. The numerical model (IMEX) is a black-oil model developed by CMG. Figure 4.6 shows a sketch of a reservoir with a bottom aquifer and a well perforated at the top of the reservoir. This model has a constant potential boundary obtained by injecting produced fluid into the reservoir through a vertical well. A 2D *x*-*z* model is used in this simulation.

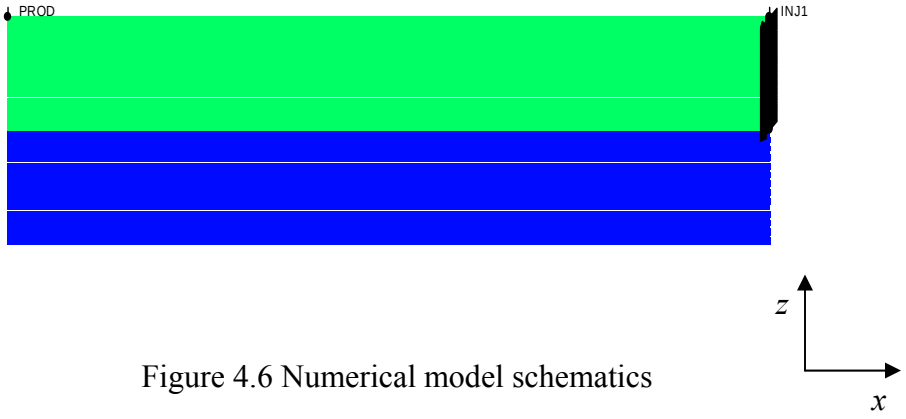

Figure 4.6 Numerical model schematics

As we discussed earlier, the only dimensionless group that affects the dimensionless critical rate q_{cD}, is the dimensionless reservoir distance x_{eD}. We varied x_{eD} from 1 to 20 in the simulations, which span the range of x_{eD} obtained for field cases (Table 4.2).

As two dimensionless variables relating the shape of the relative permeability curves, exponents n_o and n_w are included to study the effect of the shape of the water/oil relative permeability curves between end points in the simulation. Figure 4.7 shows different permeability curves with the different exponents of n_o and n_w. Capillary pressure is included in some of these cases. Figure 4.7 also gives the capillary pressure curve.

Table 4.2 Ranges of x_{eD} in actual cases (Targac et al. 2005; Gupta et al. 2008)

Oil field	Oil viscosity cp	Formation thickness ft	Well spacing ft	$x_{eD} = x_e / h_o$
West Sak	20-100	40	900-1250	11-16
Field in South Oman	90	82-99	250	1.3-1.5
Bressay, UK	65	225	933	2

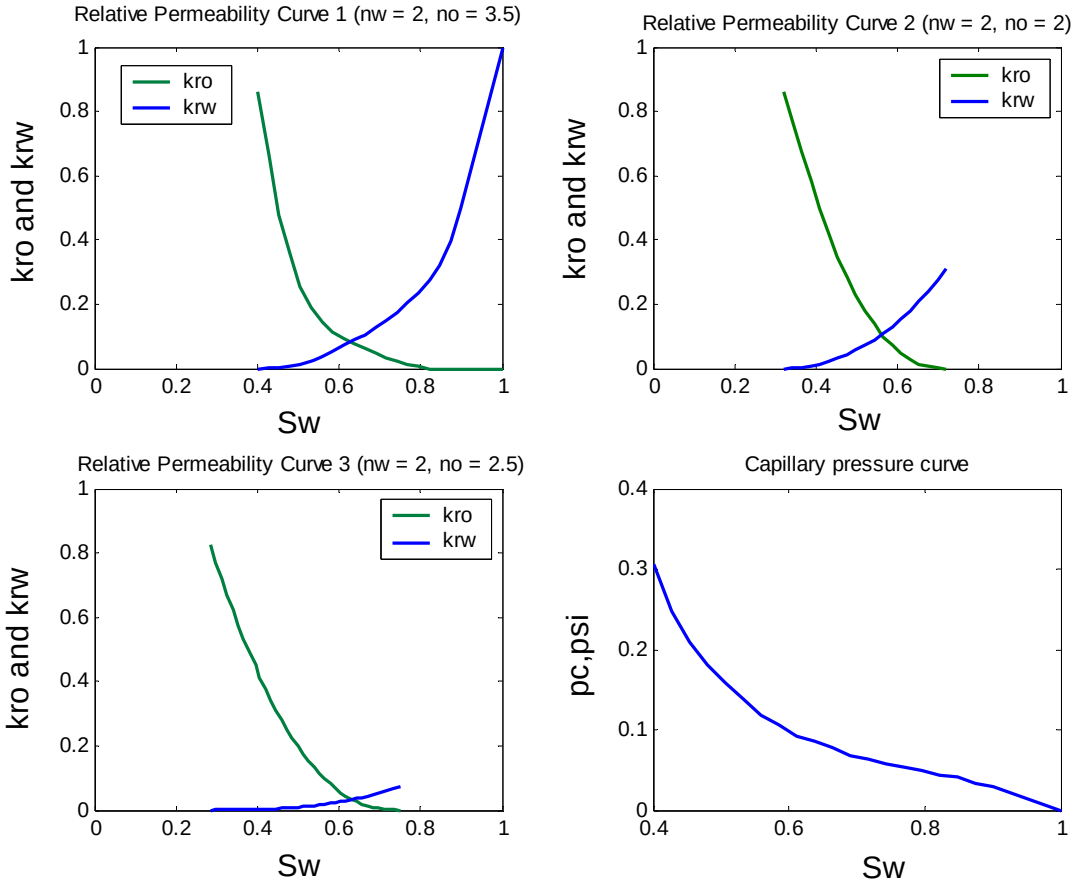

Figure 4.7 Input relative permeability curves and capillary pressure curve

The input data for all these cases are summarized in Table 4.3. All simulations were performed above the bubble point pressure and assume incompressible fluids.

Table 4.3 Summary of selected simulation cases

Cases	Oil type	k(md)	μ (cp)	ϕ (%)	$API°$	x_{eD}	n_o	n_w	p_c (psi)
1	Light oil 1	10	1.5	12	35	1.39	1	1	0
2		10	1.5	12	35	2.57	1	1	0
3		10	1.5	12	35	4.95	1	1	0
4		10	1.5	12	35	10.82	1	1	0
5		10	1.5	12	35	23.56	1	1	0
6	Light oil 2	200	2	20	26	1.39	1	1	0
7		200	2	20	26	1.39	2	3.5	0
8		200	2	20	26	1.41	1	1	0
9		200	2	20	26	1.42	2	2	0
10		200	2	20	26	1.45	2	2.5	0
11		200	2	20	26	1.83	2	3.5	0.3057
12		200	2	20	26	2.61	1	1	0
13		200	2	20	26	2.75	1	1	0
14		200	2	20	26	5.00	1	1	0
15		200	2	20	26	5.37	1	1	0
16		200	2	20	26	5.65	2	2	0
17		200	2	20	26	5.75	2	3.5	0
18		200	2	20	26	6.13	2	2	0.3057
19		200	2	20	26	10.82	1	1	0
20		200	2	20	26	10.88	1	1	0
21		200	2	20	26	21.20	1	1	0
22	Heavy oil 1	870	20	30	20	1.36	1	1	0
23		870	20	30	20	1.41	2	3.5	0
24		870	20	30	20	1.45	2	2	0
25		870	20	30	20	1.36	2	2.5	0
26		870	20	30	20	2.26	2	3.5	0.3057
27		870	20	30	20	2.66	1	1	0
28		870	20	30	20	5.33	1	1	0
29		870	20	30	20	10.95	1	1	0
30		870	20	30	20	22.61	1	1	0
31	Heavy oil 2	5000	65	30	14	1.41	1	1	0
32		5000	65	30	14	1.38	1	1	0
33		5000	65	30	14	1.41	2	3.5	0
34		5000	65	30	14	2.62	1	1	0
35		5000	65	30	14	2.72	1	1	0
36		5000	65	30	14	5.35	1	1	0
37		5000	65	30	14	5.72	1	1	0
38		5000	65	30	14	9.07	1	1	0
39		5000	65	30	14	11.62	1	1	0

Water density (995 kg/m^3) and water viscosity 0.96 (cp) are the same for all cases.

A grid sensitivity study was done to seek the best grid size. Four cases were selected to compare the cresting performance in horizontal wells under different vertical grid block sizes. The input data for these four cases are the same, except for the vertical grid block size and vertical grid blocks numbers. Table 4.4 shows the input of the data sets.

Table 4.4 Data set for simulation runs

Oil zone thickness	25 ft
Horizontal permeability	200 md
Vertical permeability	200 md
Porosity	20%
Oil density	893 kg/ m^3
Water density	995 kg/ m^3
Oil viscosity	2 cp
Water viscosity	0.96 cp
Oil compressibility	0
Water compressibility	0
Rock compressibility	0
Connate water saturation	0
Residual oil saturation	0
Oil relative permeability exponent	1
Water relative permeability exponent	1
Horizontal grid size	0.5 ft
Horizontal grid numbers	50

In all these cases, the oil thicknesses are the same, 25 ft. The cases varied from coarse grid simulation with 13 blocks between the top to bottom of the formation to refined grid with 100 blocks over the same thickness (Table 4.5).

Table 4.5 Grid patterns for the simulations of the vertical grid block size analysis

Case number	Vertical grid size (ft)	Vertical grid number
1	2	13
2	1	25
3	0.5	50
4	0.25	100

Table 4.6 shows the comparison of critical rate and critical crest height between these cases. The critical rate is obtained by varying production rates. If the production rate is above q, the well produces water. If the rate is below q, the well doesn't produce water. The rate is called a critical rate, defined as q_c.

Table 4.6 Comparison of the performance of water cresting for different vertical grid size

Case number	Vertical grid size $\triangle z$ (ft)	Vertical grid number N_z	Critical rate q_c (stb/d/ft)	Critical crest height h_c (ft)
1	2	12.5	0.12	24
2	1	25	0.12	22
3	0.5	50	0.12	21.5
4	0.25	100	0.12	21.5

The critical rate obtained from these four cases is the same, but the crest height differs from coarse grid to refined grid. That means the critical rate is less sensitive to the grid size change compared with crest height.

The case 3 with 50 blocks gives the same result as case 4 with 100 blocks for critical rate and critical crest height. Therefore, a grid size of 0.5 ft vertically is chosen to balance accuracy and speed.

The study of horizontal grid size is needed in order to avoid the use of a large number of blocks in the horizontal direction, and yet capture accuracy in the vicinity of the wellbore. A comparison between the refined grid case and coarse grid case was used. As shown in Table 4.7 from Case 1 to Case 3, the horizontal grid block size remains constant. The horizontal grid size ranges from 0.25 ft (Case 1) to 1 ft (Case 3). Case 4 is the case with a refined block size, with $\triangle x$ = 0.5 ft around the wellbore and coarse grid $\triangle x$ =10 ft elsewhere, as shown in Figure 4.8. For all situations, vertical grid size is kept the same at 0.5 ft, as earlier suggested. Table 4.7 shows a comparison in terms of critical rate and critical crest height. It can be seen that all patterns give identical results for critical rate and critical water crest height.

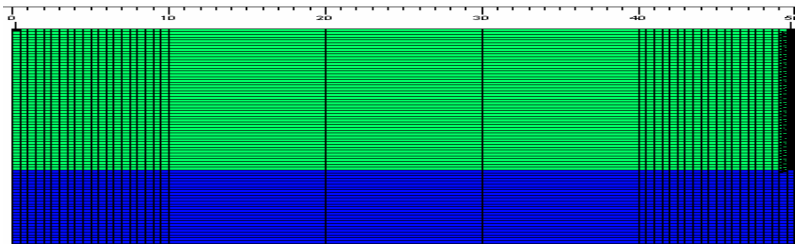

Figure 4.8 Simulation grid used in Case 4

Table 4.7 Comparison of critical rate and critical crest height under different grid patterns

Cases	Vertical grid size $\triangle z$ (ft)	Vertical grid number N_z	Horizontal Grid size $\triangle x$ (ft)	Horizontal Grid number N_x	Total grid number $N_z \times N_x$	Critical rate q_c (stb/d/ft)	Critical crest height h_c (ft)
1	0.5	50	0.25	200	10000	0.06	21.5
2	0.5	50	0.5	100	5000	0.06	21.5
3	0.5	50	1	50	2500	0.06	21.5
4	0.5	50	40×0.5, 3×10	43	2150	0.06	21.5

And oil potential distribution are very close in those cases (Figure 4.9), meaning that the influence of the horizontal grid block size on critical rate and critical water crest height is insignificant.

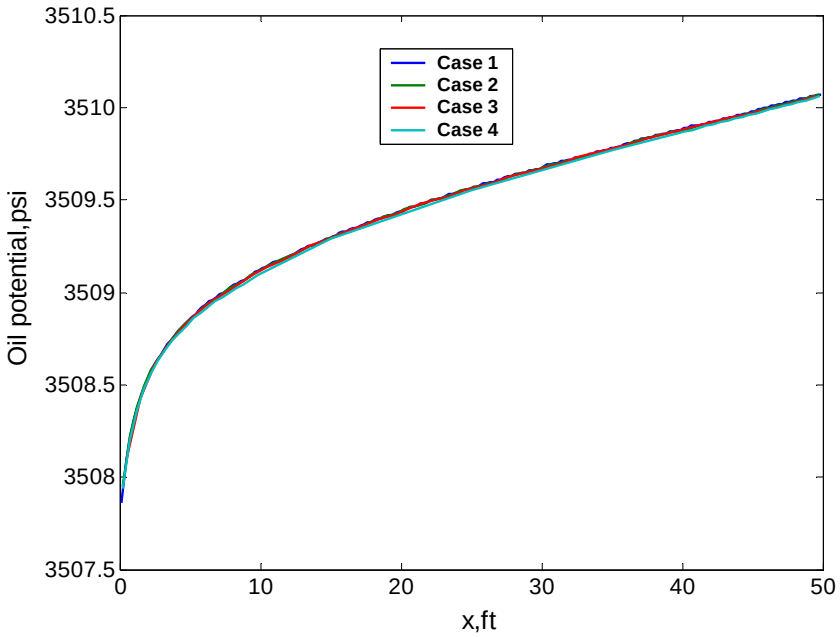

Figure 4.9 Oil potential comparisons between cases

Case 4 shows a good result when compared with a refined grid and with much less cost in time and computer storage. Therefore, this approach was used in the simulation study with refined grid around the wellbore and coarse grid elsewhere.

When the total horizontal dimension is different, then N_x is adjusted to give the value of different x_e. For instance, N_x =145 (100 ×0.5 + 45 ×10) are applied for x_e = 500 ft, while N_x =195 (100×0.5 + 95 × 10) is needed for x_e = 1000 ft.

The critical rate results are summarized in Figure 4.10, where the dimensionless critical rate is plotted vs. the dimensionless distance for all cases in Table 4.3. The solid line is the analytical solution from the hodograph method, and the points are computed by the numerical simulator. The analytical solution using the hodograph method is very similar to the results from the numerical model. Figure 4.10 also indicates that the dimensionless critical rate depends solely on the dimensionless reservoir distance, independent of rock and fluid properties, the shape of the water/oil relative permeability between end points, and the capillary pressure.

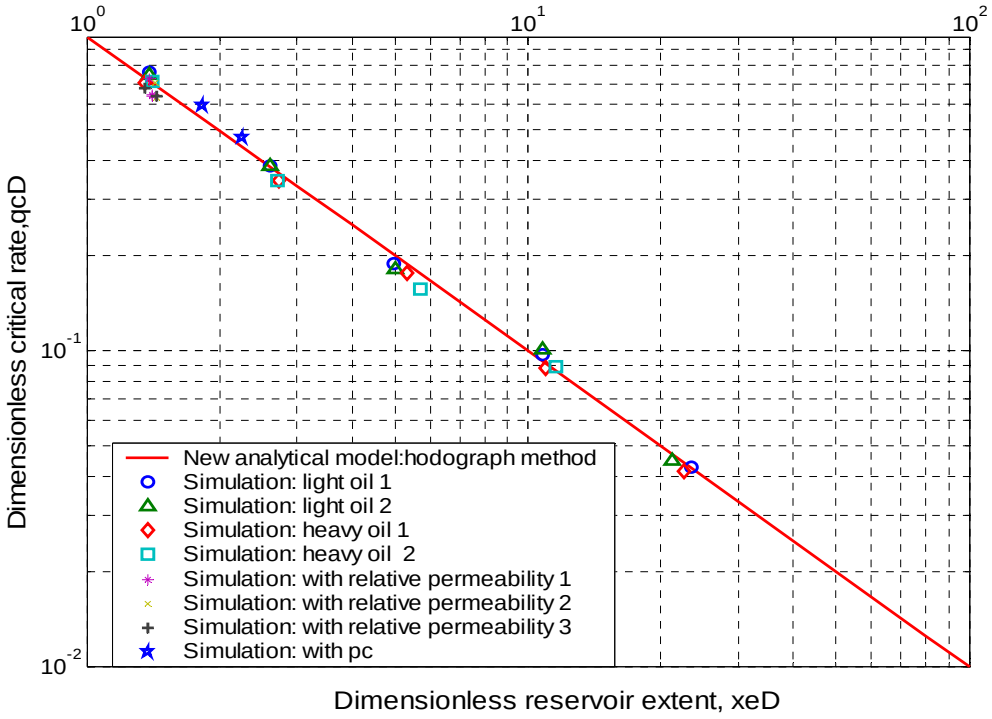

Figure 4.10 Critical rate comparisons between analytical solution and numerical simulation

The percentage deviations of the hodograph solution compared to the numerical simulation results are presented in Figure 4.11. The percentage deviation is defined as percent error:

$$\text{Percent error} = \frac{\text{Result (analytical) - result (numerical)}}{\text{Result (numerical)}} \times 100$$

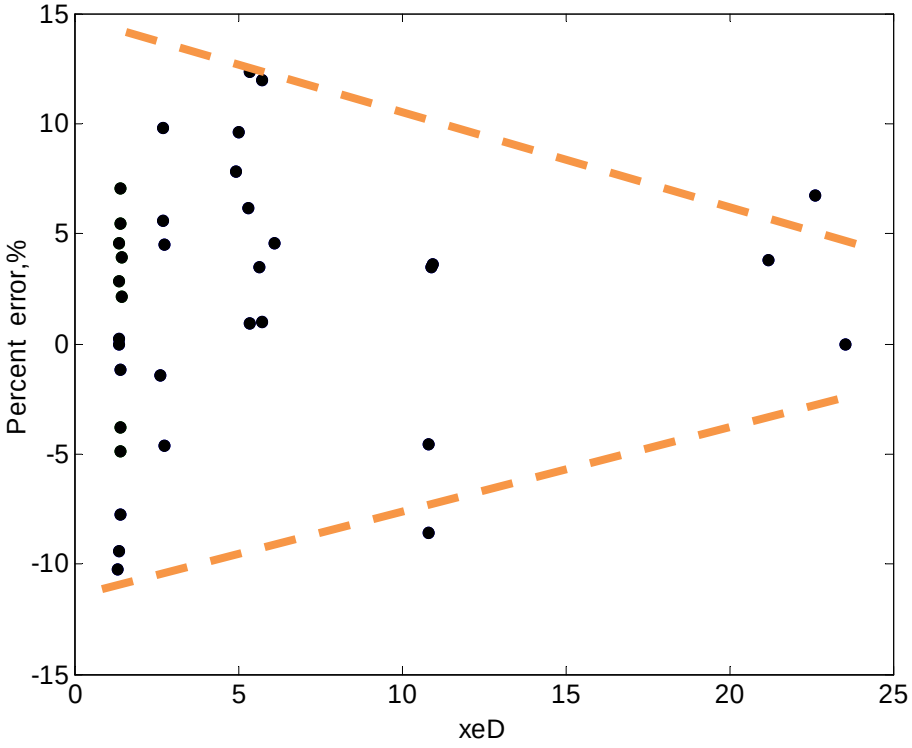

Figure 4.11 The percentage deviations

The result indicates that the new analytical solution differs by less than 10 percent from a solution obtained by the numerical simulation and the difference becomes smaller (less than 5 percent) when the dimensionless drainage distance approaches realistic values ($x_{eD} > 5$). We can conclude that the new analytical solution matches the numerical simulation. The critical rate may be determined within 10 percent accuracy through this new analytical model. Because the numerical simulation yields an approximation value of an unknown exact result, it may carry out truncation errors and round off errors, causing the deviation from the analytical solution. Also, the reservoir properties are evaluated with great uncertainty attached to their values. Porosity

may introduce an error (between 10 percent to 20 percent) and the uncertainties in residual oil saturation can introduce an error up to 20 percent (Satter, Iqbal and Buchwalter 2007), which can cause some error to estimate critical rate. Due to the above reasons, we chose 20 percent as an acceptable error range.

For Case 24, crest shape comparison is shown in Figure 4.12. The analytical crest height is 28 ft while the crest height obtained from numerical simulation is 25 ft. It can be seen that the difference between these two crests are 12 percent, within the acceptable error range (20 percent).

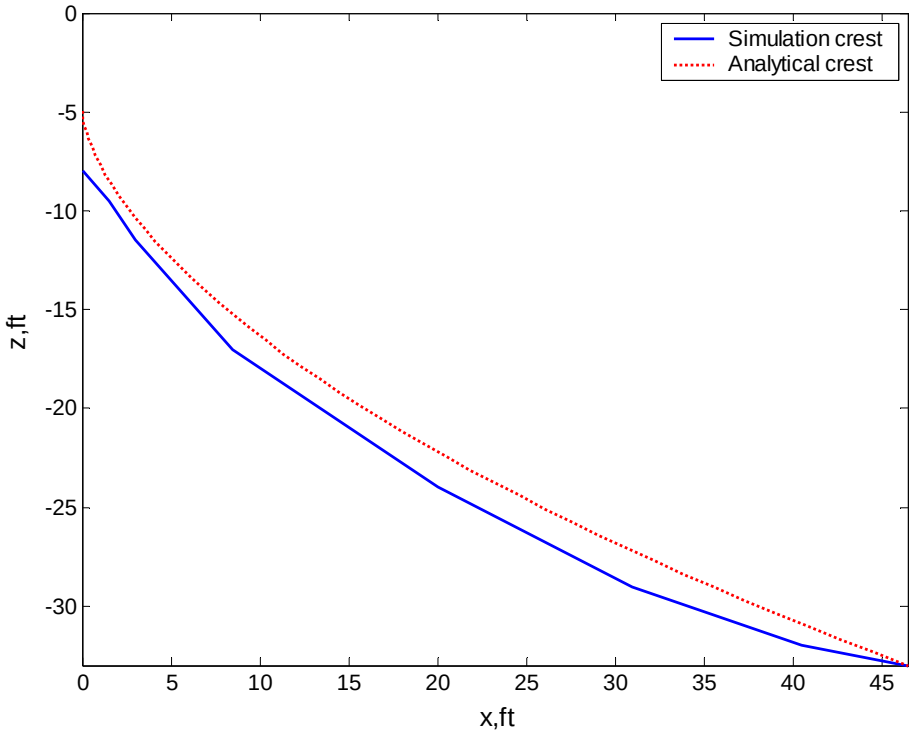

Figure 4.12 Crest shape comparison (case 24)

Figure 4.13 shows a comparison between the existing analytical solutions (Giger 1989, and Chaperon 1986, McCarthy 1993), the Dikken (1989) simulation results and the new analytical solution, derived in this work. Giger and McCarthy's model are closely matched (less than 5 percent) with only a slight discrepancy at a small dimensionless reservoir distance when compared to the analytical solution of the new model. The main advantage of the new analytical solution is a removal of the physical inconsistencies in the other models. The new model has

fewer restrictions and is more general than other models. It also shows that Chaperon's model provides a higher critical rate than other models. The differences are caused by neglecting shrinkage of the oil zone caused by the crest, therefore ignoring the effect of the crest on the flow restrictions. This study defines the error as a percentage of the difference of the analytical model from the value in the Dikken (1990) simulation study. This author plots the error as a function of x_{eD} in Figure 4.14. Without considering the crest shape, Chaperon's model can lead to a overestimation of the critical rate by up to 70 percent. The new solution is within 5 percent of the critical rates estimated in Dikken's simulations.

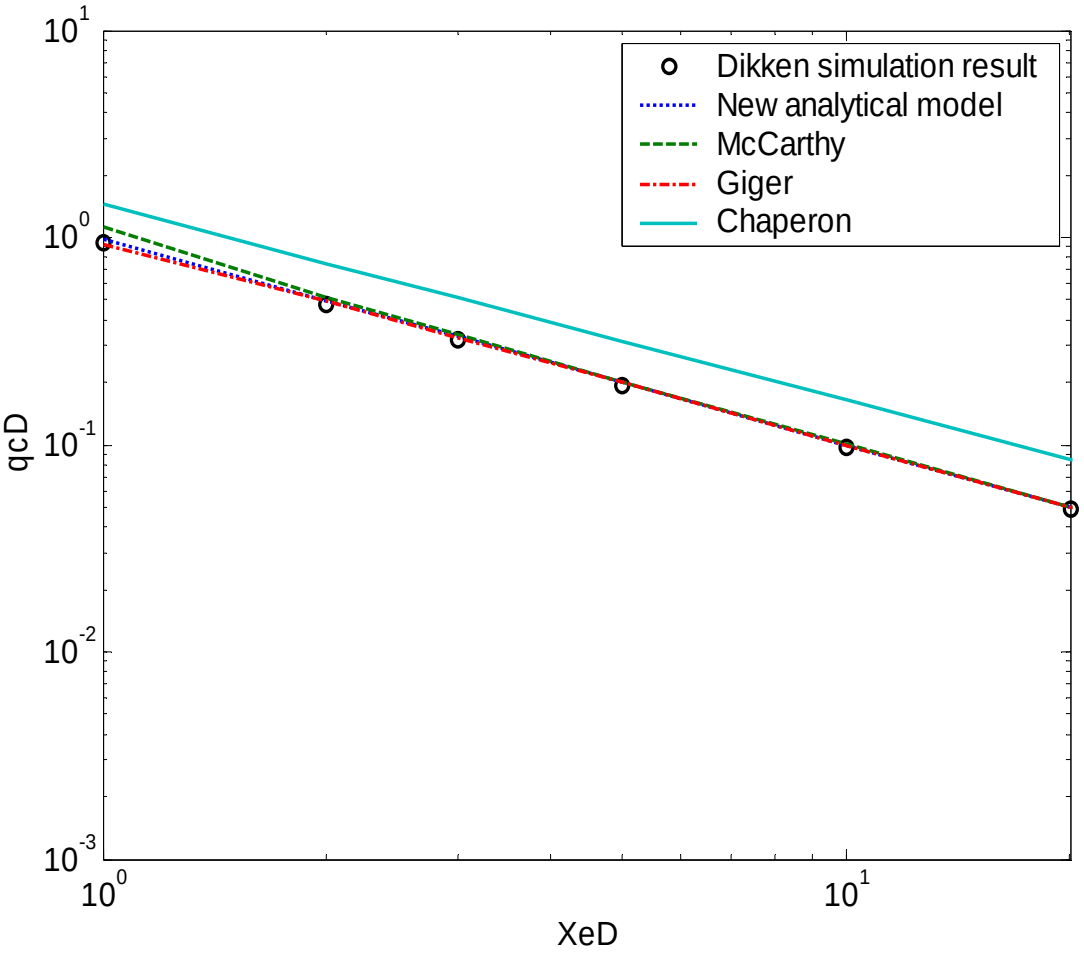

Figure 4.13 Critical rate comparison with existing models

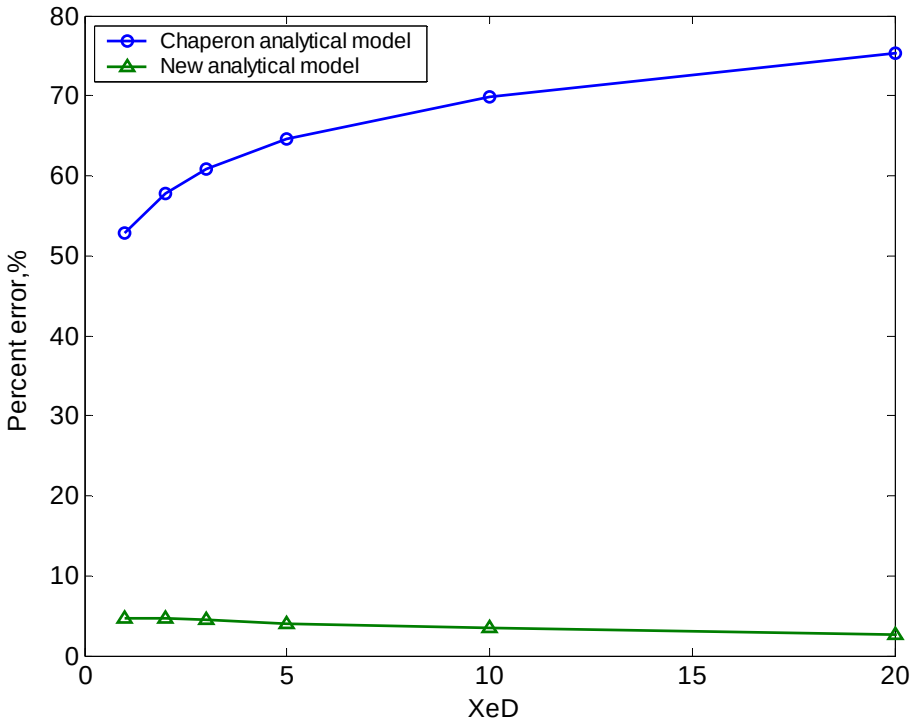

Figure 4.14 Percentage error

4.2 Critical Rate Model by Using Dupuit Approximation

4.2.1 Review of Dupuit Approximation

Although the hodograph model predicts critical rate more accurately, it remains complicated for consideration as a tool for engineering purposes. The complexity rises from the involvement of complex numbers and complex functions. One must have an understanding of the conformal mapping, complex integration, and hodograph representations of points in the physical plane before solution can be sought. For practical purposes, we must find a solution that is both accurate and simple to use. The Dupuit approximation has been widely used to solve cases in which fresh water is discharged to the sea. This section of the study applies the Dupuit approximation to the water cresting problem in horizontal wells. The validity of this approximation will be investigated against the results provided in Figure 4.10 by using the hodograph method. Despite its complexity, the hodograph is useful as a verification tool.

Dupuit (1863) published one of the first papers on solving the free surface problem in ground water flows. He developed an approximation by assuming the slope of the surface is small and the flow essentially horizontal (Figure 4.15); this is equivalent to vertical equilibrium (Coats 1967 and 1971) with uniform potentials through reservoir thickness or that the gradient of the potential is zero in the vertical direction.

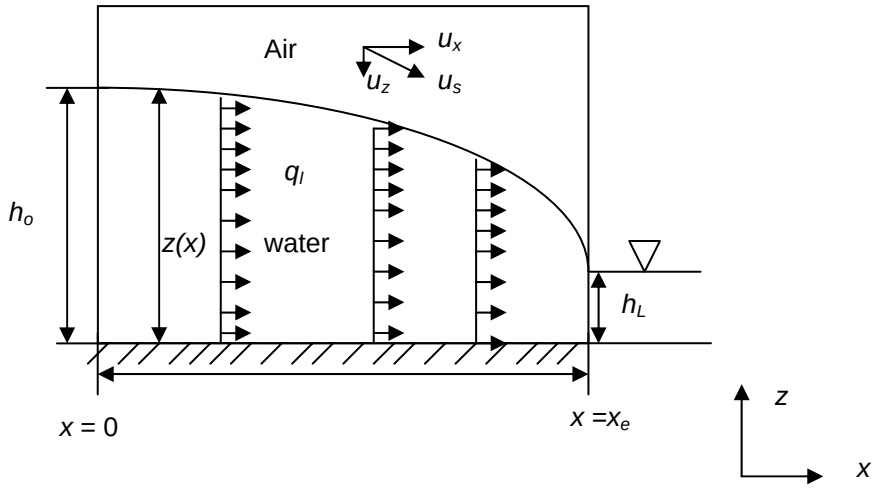

Figure 4.15 Schematic of Dupuit approximation

The flow velocity along the interface is:

$$u_s = -\frac{k}{\mu}\frac{d\Phi}{ds} \quad (4.17)$$

The term *free surface* is an isopotential surface, commonly in contact with air in groundwater flow and arbitrarily taken as $p = 0$. Therefore, $\Phi = \rho g z(x)$

Equation 4.17 may be rewritten as:

$$u_s = -\frac{k}{\mu}\frac{d\Phi}{ds} = -\frac{k\rho g}{\mu}\frac{dz(x)}{ds} \quad (4.18)$$

According to the Dupuit assumption, that flow is assumed to be horizontal, we obtain:

$$u_s = u_x = -\frac{k}{\mu}\frac{d\Phi}{dx} = -\frac{k\rho g}{\mu}\frac{dz}{dx} \quad (4.19)$$

To simplify the nonlinear boundary condition Equation 2.8 along the interface, Dupuit treated the whole flow system as a stream tube bounded by two streamlines, the free surface and the impervious bottom. By neglecting the flow variations through vertical direction, equipotential lines are vertical and conditions are expressed as average values of velocity, density, and other properties over each vertical line.

Therefore, the total flow rate through a vertical cross section per unit width is:

$$q_l = -\frac{k\rho g}{\mu} z(x) \frac{dz(x)}{dx} \quad \text{.....(4.20)}$$

By integrating Equation 4.20 with $x = 0$, $z\ (0) = h_o$; $x = x_e$, $z\ (x_e) = h_L$

We obtain:

$$q_l dx = -\frac{k\rho g}{\mu} z(x) dz \quad \text{.....(4.21)}$$

$$q_l \int_{x=0}^{x=x_e} dx = -\frac{k\rho g}{\mu} \int_{z=h_o}^{z=h_L} z dz \quad \text{.....(4.22)}$$

$$q_l = \frac{k\rho g}{\mu} (h_o^2 - h_L^2) \frac{1}{2x_e} \quad \text{.....(4.23)}$$

Equation 4.23 is known as the Dupuit-Forchheimer discharge formula. The major advantage of the Dupuit approximation is that the free surface was expressed as $z(x)$ and no longer appears as a boundary of the flow domain. The Dupuit approximation is a simple, powerful tool for engineers to solve a free surface problem (Bear 1972). Although the Dupuit-Forchheimer discharge formula as written above is only applicable to the case where the fluid surface is in contact with the atmosphere, these ground water problems are always analogous to problems encountered in petroleum engineering. With a little modification, the theory may be applied to the water-oil interface problem.

Meyer and Garder (1954) used the Dupuit approach to derive an expression for critical rate toward vertical wells, by assuming that a critical condition occurs when the cone reaches the bottom of the well (Figure 4.16).

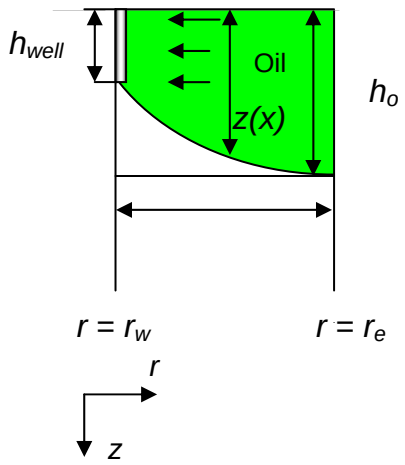

Figure 4.16 Water cone in a vertical well (Meyer and Garder 1954)

The critical rate is given by:

$$q_c = \frac{k_o \pi g(\rho_w - \rho_o)(h_o^2 - h_{well}^2)}{\mu_o \ln(\frac{r_e}{r_w})} \quad \text{..... (4.24)}$$

However, the assumption of these researchers was in conflict with the observation found through experiments conducted by Muskat and Wyckoff (1935). Muskat and Wyckoff's experimental results indicated that the critical cone remains at a certain distance below the well (Figure 4.17). The hodograph method described earlier can provide the value of that distance. Thus, the theory of Meyer and Garder is in error, since their theory assumes that the distance between the apex of the critical cone to the bottom of the well is zero.

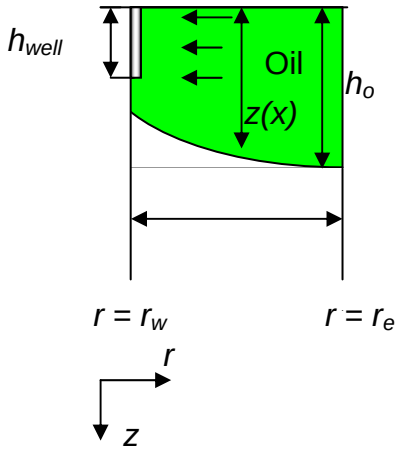

Figure 4.17 The schematic of water coning in experiments
(Muskat and Wyckoff 1935)

Joshi (1988) extended Meyer and Garder's work for vertical wells to horizontal wells to calculate critical rate using an effective wellbore radius (r_{we}) concept. According to Joshi, the critical rate in a horizontal well may be determined by substituting a horizontal-well effective wellbore radius r_{we} for r_w in Equation 4.24. Then we have:

$$q_c = \frac{k_o \pi g(\rho_o - \rho_w)(h_o^2 - h_{well}^2)}{\mu_o \ln(\frac{r_e}{r_{we}})} \quad \text{..... (4.25)}$$

$$r_{we} = \frac{r_e\left(L/2\right)}{a\left[1+\sqrt{1-\left(L/2a\right)^2}\right]\left[h_o/2r_w\right]^{h_o/L}}$$

Where a = half the major axis of drainage ellipse

L = horizontal well length

Joshi repeats the error that the critical rate is determined when the water touches the bottom of the well, and does not consider that the pressure distribution and flow pattern within the reservoir in horizontal wells are quite different from those of vertical wells. Unlike the water coning in vertical wells, the linear flow is dominant in water cresting toward horizontal wells. Therefore, the critical rate equation developed for radial flow by Meyer and Garder (1954) may

not be applied in horizontal wells. Giger (1984) reported a critical rate equation for horizontal wells under linear flow condition:

$$q_c = \frac{k_o(\rho_w - \rho_o)gh_o^{\,2}}{\mu_o x_e} \quad \text{.....(4.26)}$$

However, Giger (1984) did not include the derivation of the equation in his paper. In Giger's solution, the horizontal well must be at the top of the reservoir. Konieczek (1990) provided a solution for critical rate in horizontal well:

$$q_c = \frac{k_o(\rho_w - \rho_o)g(h_o^{\,2} - h_{well}^2)}{\mu_o x_e} \quad \text{.....(4.27)}$$

This equation takes the well position into account. This critical rate equation appears to be correct, although its derivation appears to be incorrect, as discussed below. In his work, the initial pressure in the oil column is given by:

$$P_i(x,y,z) = P_r + \rho_o g(h_o - z) \quad \text{.....(4.28)}$$

P_r is the reservoir pressure at the initial gas/oil contact, located at $z = h_o$

h_o is the original oil column thickness.

z is the depth coordinate measured positive upward from the base of the oil column.

According to Konieczek, at a later point in time, the GOC will be moved to *h(x,y,t)* then the hydrostatic pressure in the oil zone is:

$$P(x,y,z) = P_r + \rho_o g(h_o - z) + \rho_o g(h_o - h) \quad \text{.....(4.29)}$$

Subtracting Equations 4.29 and 4.28 gives the potential in the oil zone (according to Konieczek 1990):

$$\Phi(x,y,z) = -(\rho_o - \rho_g)g(h_o - h) \quad \text{.....(4.30)}$$

Whereas subtracting Equations 4.29 and 4.28 yields

$$\Phi(x,y,z) = -\rho_o g(h_o - h) \quad \text{.....(4.31)}$$

However, even with this correction, other corrections are needed. The potential difference over time is:

$$\Phi(x,y,z,t)-\Phi(x,y,z,t=0)=-\rho_o g(h_o-h). \quad (4.32)$$

To know the flow rate in the oil zone, the potential gradient over distance must be known, and is not provided in the paper.

In addition, none of these papers listed prove the validity of the Dupuit approach, by investigation of the two errors in approximations:

- The vertical flow component has been neglected. In the vicinity of a well where the flow converges, the vertical flow component may not be negligible.
- At critical condition, the distance between the apex of the crest and the bottom of the well is assumed to be zero, which the more rigorous hodograph solution indicates is incorrect.

One must verify that these two factors do not introduce significant error before applying Dupuit assumptions for horizontal well cresting problems. In the next section, we first derive an expression for critical rate calculation in a water cresting problem for horizontal wells by applying the Dupuit approximation, using the derivation given above. Then the validity will be tested against a hodograph solution we presented earlier, with numerical simulators.

4.2.2 Critical Rate Solution Using Dupuit Approximation

Let us consider the critical crest situation under which the crest reaches the bottom of the well, as shown in Figure 4.18. Because the flow system is symmetric, we only need to analyze the half plane.

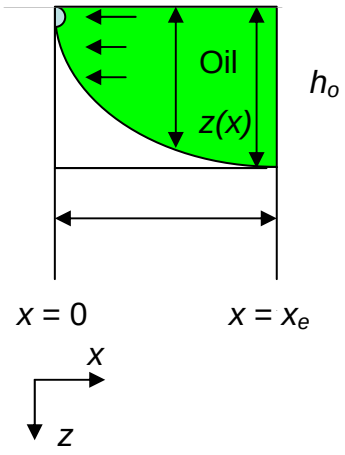

Figure 4.18 The critical water crest condition by the Dupuit approximation

The flow potential in the oil zone is

$$\Phi_o = p_o - \rho_o g z(x) \quad (4.33)$$

Where, p_o is the oil zone pressure at interface.

The flow potential in the water zone is,

$$\Phi_w = p_w - \rho_w g z(x) \quad (4.34)$$

For the interface, where $p_o = p_w$, we obtain,

$$\Phi_o + \rho_o g z(x) = \Phi_w + \rho_w g z(x) \quad (4.35)$$

$$\Phi_o = \Phi_w + (\rho_w - \rho_o) g z(x) \quad (4.36)$$

When applying the Dupuit approximation and using the half well symmetry, the oil flow rate becomes $q_c/2$

$$\frac{q_c}{2} = \frac{k_o}{\mu_o} z(x) \frac{d\Phi_o}{dx} \quad (4.37)$$

Inserting Equation 4.36 into 4.37, we obtain:

$$\frac{q_c}{2} = \frac{k_o}{\mu_o} z(x) \frac{d[\Phi_w + (\rho_w - \rho_o) g z(x)]}{dx} \quad (4.38)$$

Because the water is not flowing, Φ_w is constant, and $\frac{\partial \Phi_w}{\partial x} = 0$. Thus, Equation 4.38 can be rewritten as:

$$\frac{q_c}{2} = \frac{k_o(\rho_w - \rho_o)g}{\mu_o} z(x) \frac{dz(x)}{dx} \quad \text{.....(4.39)}$$

By integrating from $x = 0$ and $z(x) = 0$ to $x = x_e$ and $z(x) = h_o$, we get:

$$\int_{x=0}^{x=x_e} \frac{q_c}{2} dx = \int_{z=0}^{z=h_o} \frac{k_o(\rho_w - \rho_o)g}{\mu_o} z(x)\, dz(x) \quad \text{.....(4.40)}$$

$$\frac{q_c}{2} x_e = \frac{k_o(\rho_w - \rho_o)g}{\mu_o} \frac{h_o^2}{2} \quad \text{.....(4.41)}$$

The critical rate is

$$q_c = \frac{k_o(\rho_w - \rho_o)gh_o^2}{\mu_o x_e} \quad \text{.....(4.42)}$$

Equation (4.42) is identical to the Equation 4.26 given by Giger (1984), and the full derivation for critical rate is included here. Using the same dimensionless group defined in Table 4.1 Equation 4.42 can be rewritten as indicating a inverse relation between the dimensionless critical rate and the dimensionless drainage distance, similar to the results obtained from hodograph method.

$$q_{cD} = \frac{1}{x_{eD}} \quad \text{.....(4.43)}$$

Compared with the solution obtained by using hodograph method in Equations 4.13 and 4.14, the relationship between q_{cD} and x_{eD} in Equation 4.43 is very simple and easily can be computed using hand calculators or simple spreadsheets. In particular, the water-cresting problem has now been treated and solved without applying complex analysis.

4.2.3 Comparison with Hodograph Method

Figure 4.19 shows a comparison between the Dupuit approximation and the hodograph method. The dimensionless critical rate is plotted vs. the dimensionless reservoir extent. The solid line represents the hodograph solution, and the dots are the Dupuit solution. The critical rate from the Dupuit approximation is close to the hodograph solution.

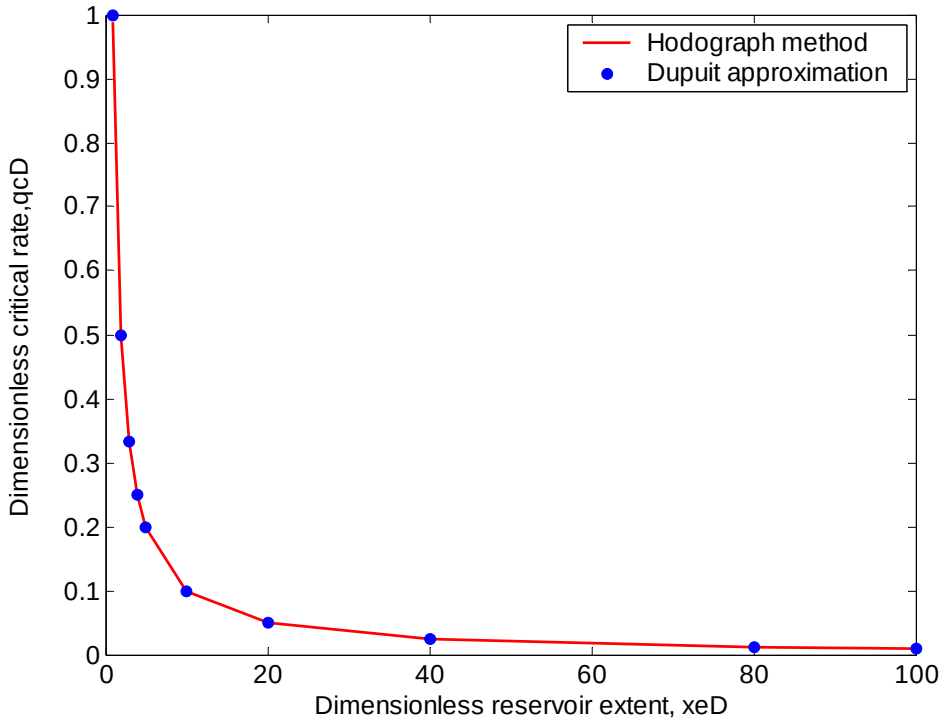

Figure 4.19 Comparison of hodograph vs Dupuit approximation

Figure 4.20 plots the error which is used as an indicator to measure the difference between these two solutions as a function of dimensionless reservoir distance. The approximation is good, within an error of 5 percent for determining the critical rate. The assumption of a purely horizontal flow overestimates the critical rate. On the other hand, assuming the critical crest condition occurs when the crest reaches the well implies that crest shape size is larger than the true size. A larger crest will yield more flow restriction in the oil

zone. This error will underestimate the critical rate. It appears that these two errors approximately balance each other, and thereby give the reasonably accurate answers.

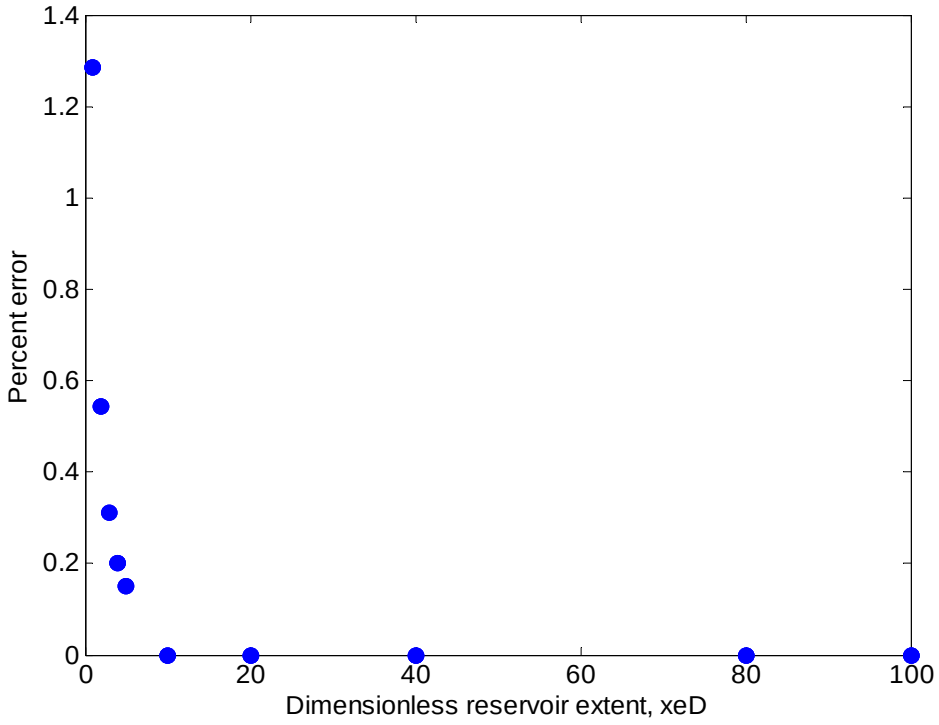

Figure 4.20 Percentage error

As the dimensionless reservoir distance increases, the discrepancy is diminished. That is, when the extent of the reservoir is much larger than the thickness of the oil zone, linear flow dominates the flow domain. As a result, the vertical flow in the vicinity of a well can be neglected.

Figure 4.21 shows the interface shape calculated from the Dupuit approximation, compared with the one obtained by the hodograph method. The discrepancy between the curves predicted by the exact theory of hodograph and by the Dupuit approximation is negligible, except in the vicinity of the well. We can conclude that the solution based on the Dupuit approximation is sufficiently accurate for practical purposes.

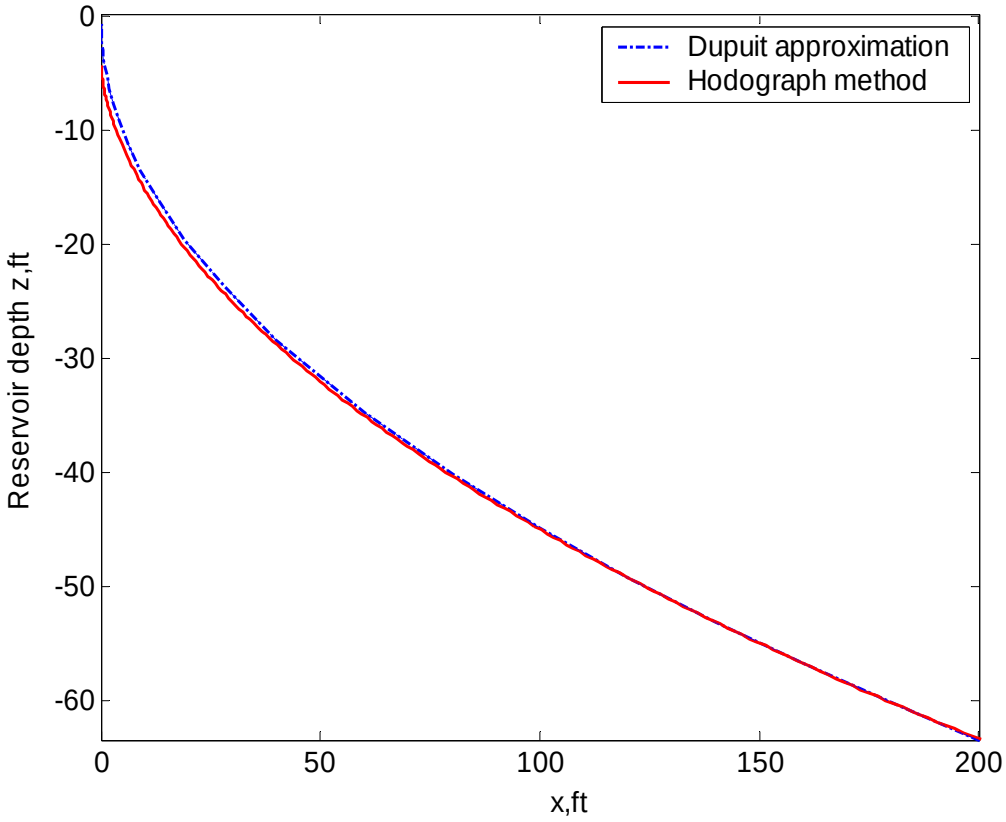

Figure 4.21 Water crest shape comparison

4.2.4 Verification with Numerical Simulation

Figure 4.22 plots the dimensionless critical rate vs. the dimensionless reservoir extent. The solid line plot represents the solution derived from the hodograph method, while the dashed line plot represents the solution from the Dupuit approximation. In Figure 4.22, the result from the Dupuit approximation is close to the result from the hodograph method. Figure 4.23 plots the percentage error, defined as the percentage deviation of the Dupuit analytical solution, from the numerical solution vs. the dimensionless reservoir distance. The difference is less than 10 percent. Again, the percentage error decreases as the dimensionless drainage distance increases.

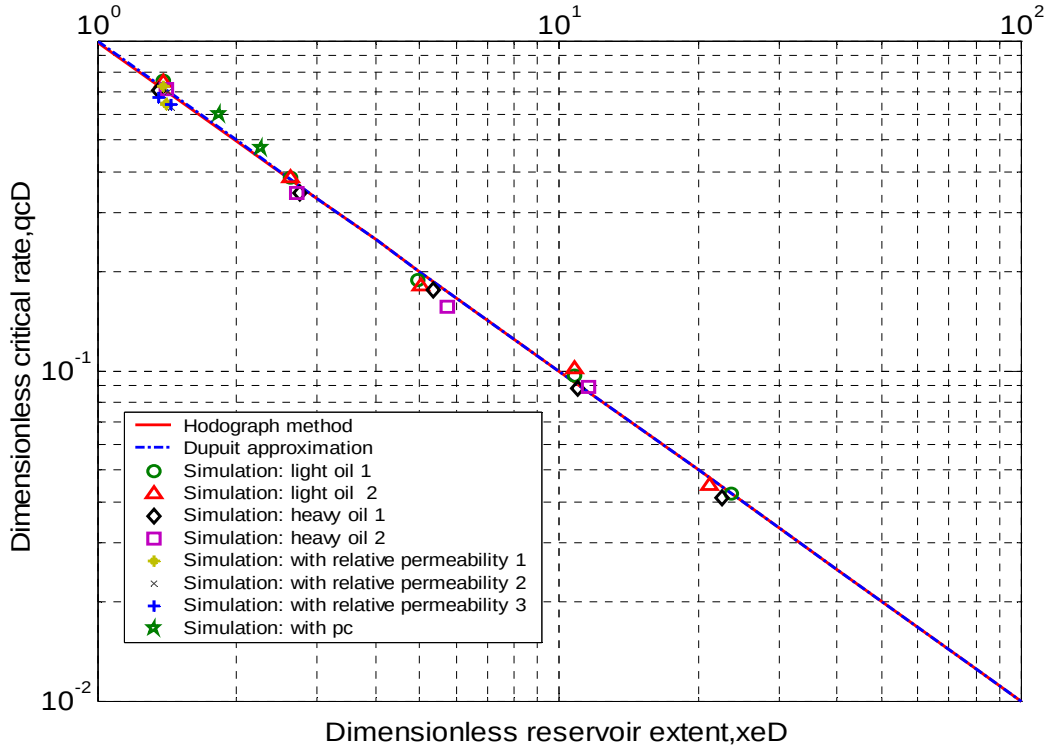

Figure 4.22 Comparison of the analytical solution with the numerical simulation

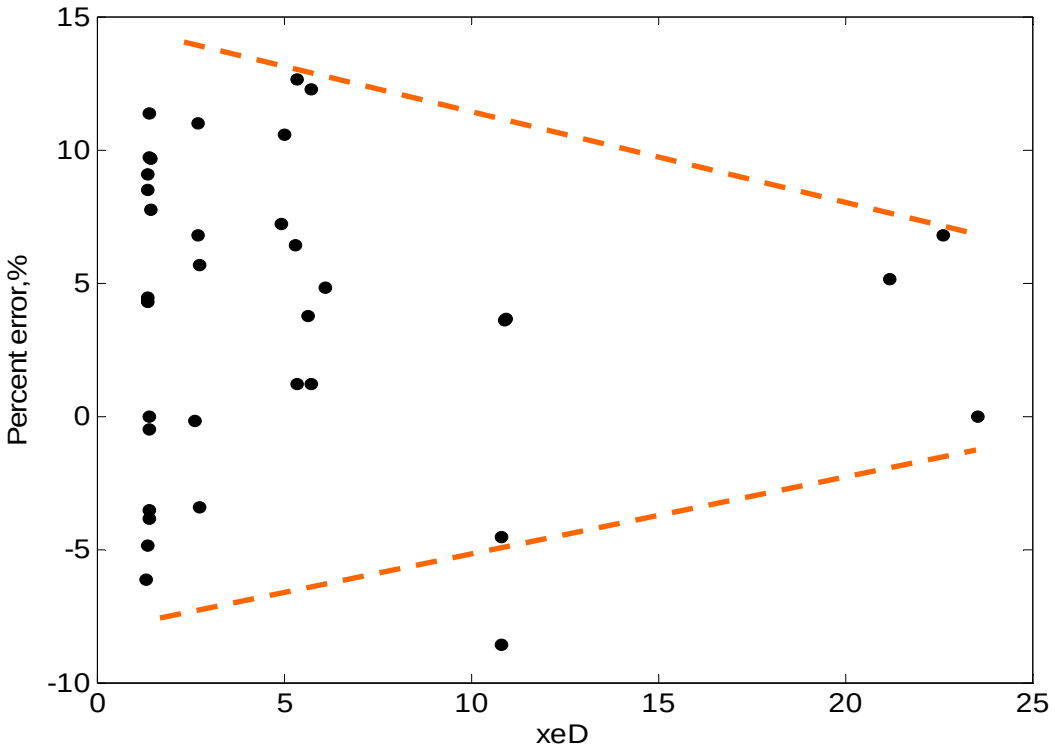

Figure 4.23 Percentage error

4.2.5 Critical Rate for Well below the Reservoir Top

The critical rate model, above, applies to a well located at the top of the oil pay zone. The Dupuit approximation can also be used for horizontal wells located at a distance h_{well} beneath the impermeable boundary, as shown in Figure 4.24.

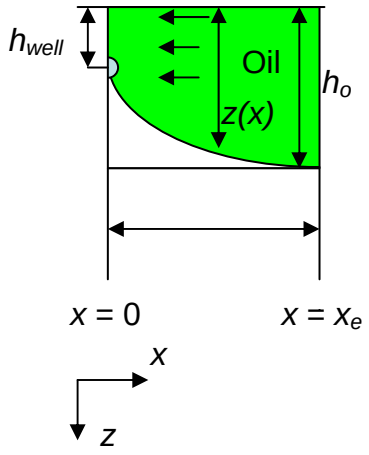

Figure 4.24 Schematic of water cresting in a horizontal well, at any vertical position

We assume, again, that the flow is essentially horizontal and,

for $x = 0$, $h = h_{well}$; $x = x_e$ $h = h_o$

Integrating Equation 4.39 from $x = 0$ *to* $x = x_e$, gives:

$$\int_{x=0}^{x=x_e} \frac{q_c}{2} dx = \int_{z=h_{well}}^{z=h_o} \frac{k_o}{\mu_o} z(\rho_w - \rho_o) g dz \quad \text{(4.44)}$$

$$\frac{q_c}{2} x_e = \frac{k_o}{\mu_o} \frac{1}{2} (h_o^2 - h_{well}^2)(\rho_w - \rho_o) g \quad \text{(4.45)}$$

$$q_c = \frac{k_o}{\mu_o} \frac{1}{x_e} (h_o^2 - h_{well}^2)(\rho_w - \rho_o) g \quad \text{(4.46)}$$

Equation 4.46 can be rewritten in dimensionless form with the same dimensionless group, as in Table 4.1, with the new dimensionless group accounting for the well location.

$$q_{cD} = \frac{1}{x_{eD}} \left[1 - h_{wD}^2 \right] \quad \text{(4.47)}$$

Where $h_{wD} = \frac{h_{well}}{h_o}$

The results are plotted in Figure 4.25 where a dimensionless critical rate is plotted vs. a dimensionless reservoir size for different dimensionless well positions.

$h_{wD} = 0, 0.2, 0.4, 0.6, 0.8$

Where $h_{wD} = 0$ indicates a well at the top of the oil pay zone

The critical rate decreases with an increasing value of h_{wD}. Having determined the values of h_{wD} and x_{eD}, the dimensionless critical rate can be determined using Figure 4.25. These curves are all straight lines on log-log axes with slope of m = -1 and intercepts $\log(1 - h_{wD}^2)$.

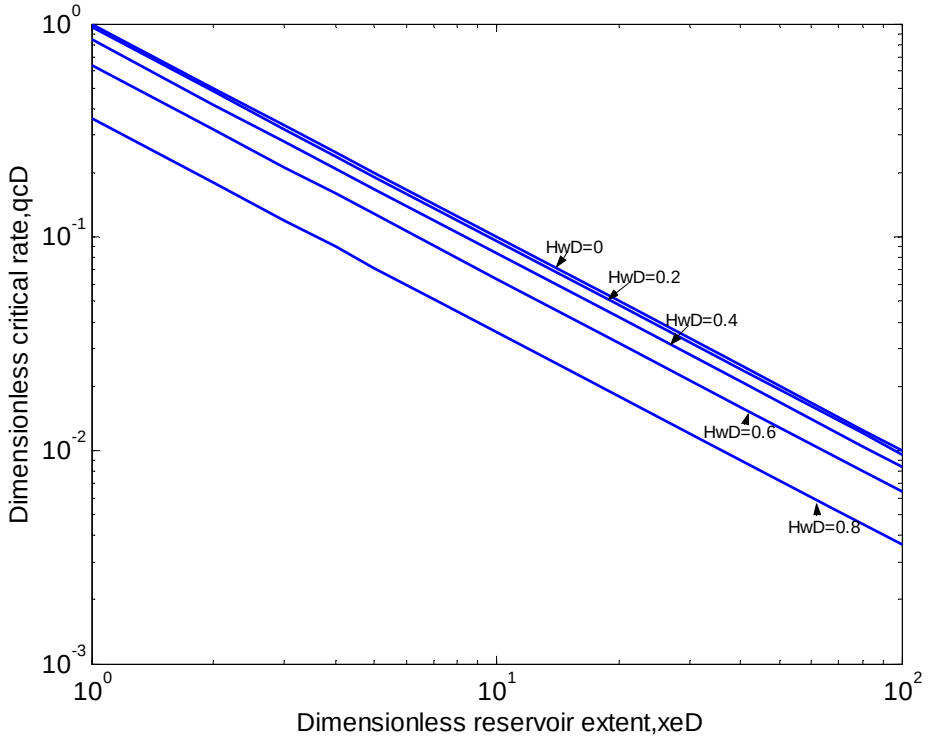

Figure 4.25 Dimensionless critical rate from the Dupuit approximation

Again, the Dupuit approximation assumes that any essentially horizontal flow must be investigated. For h_{wD} = 0, the convergence of the streamlines towards the well have been taken into account by assuming *h (x = 0)* = 0, which implies that all the streamlines intersect at a point

where the well is located. For $h_{wD} \neq 0$, in the region above the well, the streamlines are assumed to be horizontal without meeting each other. The convergences of the streamlines toward the well have been ignored. We may account for the radial flow effects by using the principle presented by Hooghoudt (1937). He divided the flow region between the wells into two parts, linear and radial regions. One flow is a radial flow, located close to the sinks. The second flow is linear flow, located far from the well (Figure 4.26).

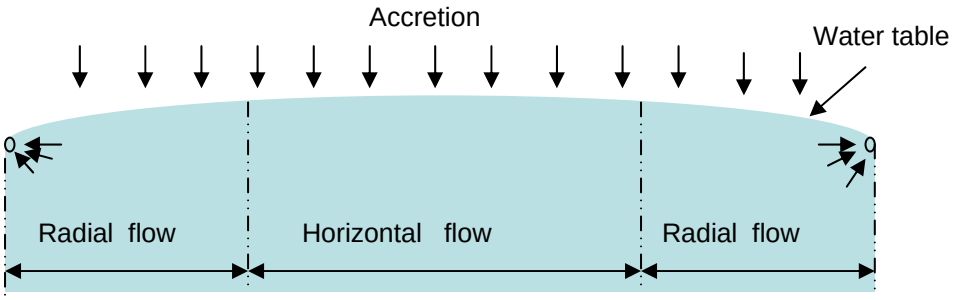

Figure 4.26 Hooghoudt's approach for drainage problems

This study uses the same approach to solve a water cresting problem without accretion such as rain fall or water supply from above. Assume that the reservoir is bounded by two no-flow boundaries. One is a horizontal, impervious top and the initial WOC, taken as another horizontal impervious boundary, is shown in Figure 4.27. The general form of flow potential is derived in Appendix B.

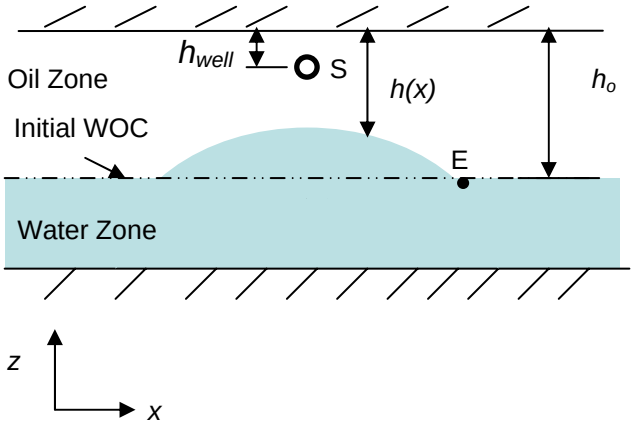

Figure 4.27 Solving the water cresting problem by the Hooghoudt approach

The flow potential at the point located at outer reservoir boundary E is obtained by inserting coordinates (x_e,0) into Equation A-3 in Appendix B:

$$\Phi_{E(x_e,0)} = \frac{q_c \mu_o}{4\pi k_o}\left\{\ln[\cosh\frac{\pi x_e}{h_0} - \cos\frac{\pi(h_o - h_{well})}{h_0}]\times[\cosh\frac{\pi x_e}{h_0} - \cos\frac{\pi(h_o - h_{well})}{h_0}]\right\} + C \quad (4.48)$$

Because $x_e >> h_o$, $\cosh(\pi x_e/h_o) >> \cos\left[\pi\left(h_o - h_{well}\right)/h_o\right]$. The term $\cos\left[\pi\left(h_o - h_{well}\right)/h_o\right]$ in Equation 4.48 can be negligible.

Therefore, Equation 4.48 can be simplified as:

$$\Phi_E = \frac{q_c \mu_o}{2\pi k_o}\ln(\cosh\frac{\pi x_e}{h_0}) + C$$

$$= \frac{q_c \mu_o}{2\pi k_o}\ln[0.5\times\exp(\pi x_e/h_o)] + C \quad (4.49)$$

$$= \frac{q_c \mu_o}{2\pi k_o}\left(\ln 0.5 + \frac{\pi x_e}{h_o}\right) + C$$

Also, the potential at well S can be expressed by Equation A-3 with coordinates (r_w, h_o-h_{well}):

$$\Phi_{S(r_w,h_o-h_{well})} = \frac{q_c \mu_o}{4\pi k_o}\left\{\ln[\cosh\frac{\pi r_w}{h_0} - 1]\times[\cosh\frac{\pi r_w}{h_0} - \cos\frac{2\pi(h_o - h_{well})}{h_0}]\right\} + C \quad (4.50)$$

Because $\cosh(\pi r_w/h_o) \approx 1 + 0.5\left(\pi r_w/h_o\right)^2$

Equation 4.50 can be approximated by:

$$\Phi_S = \frac{q_c \mu_o}{2\pi k_o}\ln\left\{\frac{\pi r_w}{h_0}\times\sin\left[\frac{\pi\left(h_o - h_{well}\right)}{h_o}\right]\right\} + C \quad (4.51)$$

The difference in potential between a point located at outer reservoir boundary E and the well S is given by combining Equations 4.49 and 4.51:

$$\frac{k_o}{\mu_o}(\Phi_E - \Phi_S) = \frac{q_c}{2}\frac{x_e}{h_o} + \frac{q_c}{2\pi}\ln\frac{h_o}{2\pi r_w \sin\frac{\pi(h_o - h_{well})}{h_o}} \quad (4.52)$$

$$\Phi_E - \Phi_S = \frac{\mu_o}{k_o}\left[\frac{q_c}{2}\frac{x_e}{h_o} + \frac{q_c}{2\pi}\ln\frac{h_o}{2\pi r_w \sin\frac{\pi(h_o - h_{well})}{h_o}}\right] \quad \text{.....(4.53)}$$

Applying the Dupuit assumptions, the total flow rate through any vertical line is:

$$\frac{q_c}{2} = \frac{k_o}{\mu_o} h_o \frac{d\Phi}{dx} = \frac{k_o}{\mu_o} h(x)(\rho_w - \rho_o) g \frac{dh(x)}{dx} \quad \text{.....(4.54)}$$

After integrating between from E to S:

$$\int_{\Phi=\Phi_E}^{\Phi=\Phi_S} d\Phi = \int_{h=h_o}^{h=h_{well}} h(x)(\rho_w - \rho_o) g \frac{dh(x)}{h_o} \quad \text{.....(4.55)}$$

$$\Phi_E - \Phi_S = \frac{1}{2}(h_o^2 - h_{well}^2)(\rho_w - \rho_o) g \frac{1}{h_o} \quad \text{.....(4.56)}$$

Inserting Equation 4.53 into 4.56, we obtain:

$$\frac{\mu_o}{k_o}\left[\frac{q_c}{2}\frac{x_e}{h_o} + \frac{q_c}{2\pi}\ln\frac{h_o}{2\pi r_w \sin\frac{\pi(h_o - h_{well})}{h_o}}\right] = \frac{1}{2}\left(h_o^2 - h_{well}^2\right)(\rho_w - \rho_o) g \frac{1}{h_o} \quad \text{.....(4.57)}$$

Showing a combined horizontal and radial flow, the critical rate is obtained by:

$$q_c = \frac{\frac{k_o}{\mu_o}\left(h_o^2 - h_{well}^2\right)(\rho_w - \rho_o) g}{x_e + \frac{h_o}{\pi}\ln\frac{h_o}{2\pi r_w \sin\left[\frac{\pi(h_o - h_{well})}{h_o}\right]}} \quad \text{.....(4.58)}$$

The Equation 4.58 shows that the deviation from linear flow, due to the radial flow close to the wellbore, leads to an additional potential drop.

Let us add to the dimensionless groups, mentioned earlier (q_{cD} , x_{eD} , and h_{wD})- a new dimensionless group, r_{wD}, defined as:

$$r_{wD} = \frac{1}{\pi} \ln \left\{ \frac{h_o}{2\pi r_w \sin\left[\frac{\pi(h_o - h_{well})}{h_o} \right]} \right\} \quad \text{.....(4.59)}$$

Equation 4.58 may be expressed in terms of a dimensionless group as:

$$q_{cD} = \frac{1}{(x_{eD} + r_{wD})}(1 - h_{wD}^2) \quad \text{.....(4.60)}$$

Figure 4.28 plots the dimensionless critical rate as a function of a dimensionless reservoir distance for various dimensionless well locations, with and without taking into account the radial flow around the wellbore.

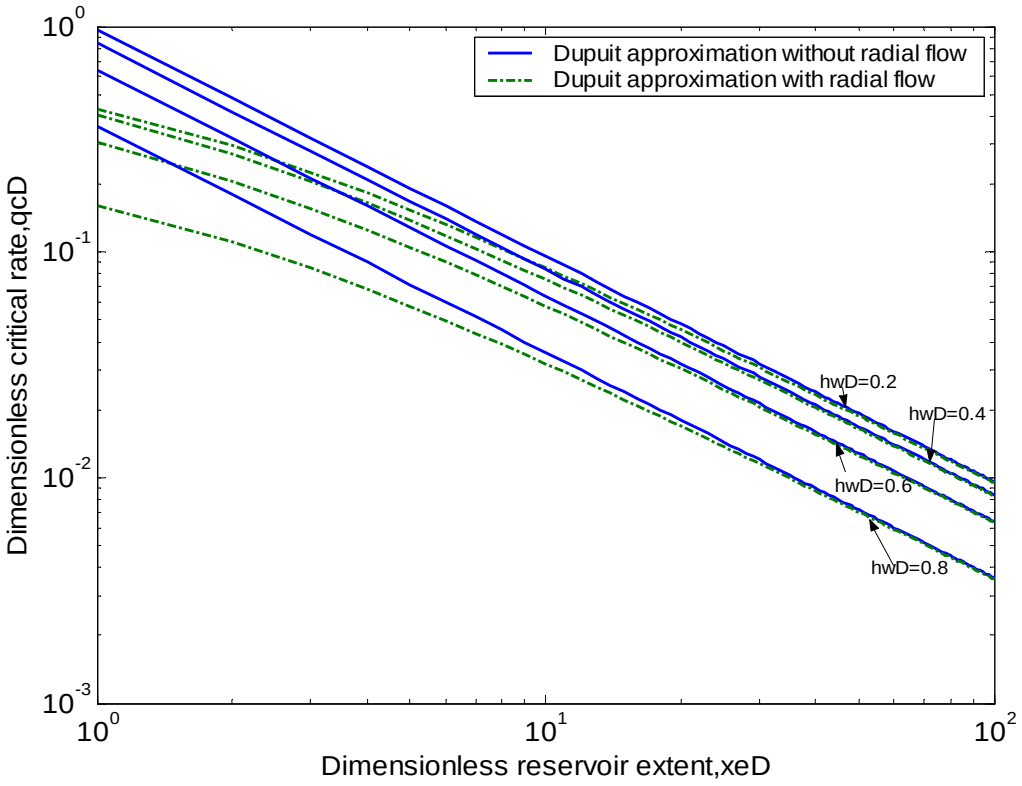

Figure 4.28 Comparison of a dimensionless critical rate, with and without taking into account the radial flow

The dimensionless critical rate is smaller for these cases, in considering the radial flow around the wellbore, when compared to the cases where only horizontal flow is considered. Because the vertical flow component cannot be ignored in the region around the wellbore where

the flow converges, the resistance to the flow increases and the critical rate decreases. As x_{eD} increases, the discrepancy between these two solutions with and without accounting for radial flow decreases. This is because the horizontal flow tends to dominate the reservoir flow and the radial flow effect around the wellbore is negligible compared to the linear flow when the dimensionless reservoir extent is large.

4.2.6 Numerical Verification

Twenty-two cases are considered in this validation study. Also, the dimensionless well vertical placement ranges from 0.01 to 0.9. Figure 4.29 plots the relative error of the two analytical solutions with respect to the simulated results. The relative error is defined as:

$$\text{Percent error} = \frac{\text{Result (analytical) - result (numerical)}}{\text{Result(numerical)}} \times 100$$

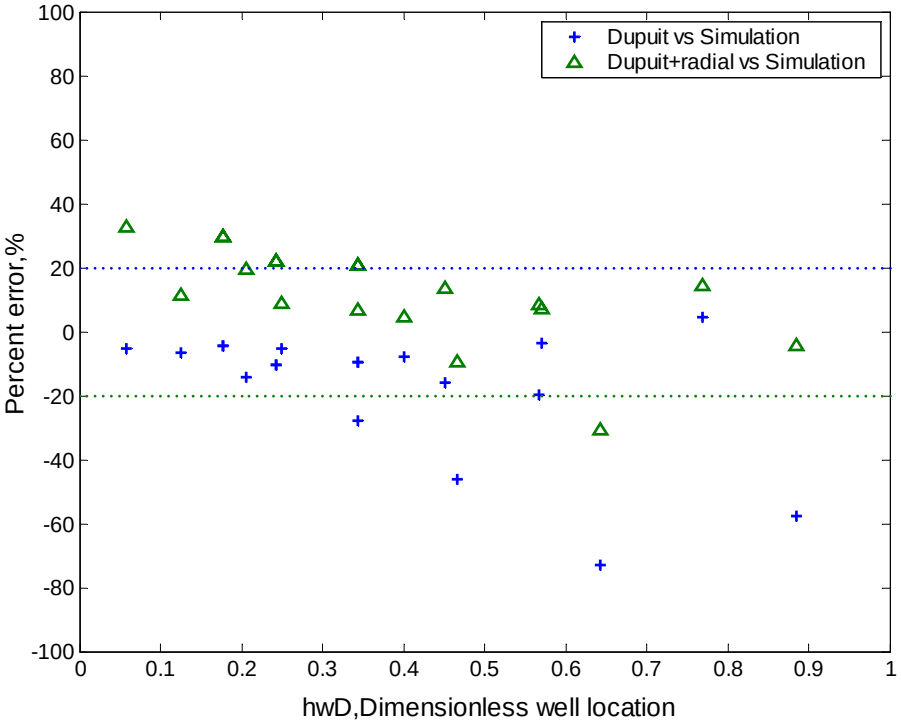

Figure 4.29 Percentage relative error of analytical critical rate compared to simulation

As we mentioned before, the Dupuit approximation regards the flow above the well as horizontal flow. Below the well, Dupuit approximation accounts for the flow convergence towards the well. As h_{wD} increases, flow region above the well becomes larger than that below the well. The more streamlines fall into the horizontal flow category, the less flow convergence has been considered. As a result, the deviation between the Dupuit approximation and the simulation critical rate increases as h_{wD} increases. It shows that the Dupuit approximation without considering a radial flow, when the h_{wD} is less than 0.3, is less than 20 percent deviated from the simulation for a critical rate calculation (Figure 4.29). However, for the case where h_{wD} > 0.3, the Dupuit approximation without considering radial flow at wellbore will give an error larger than 20 percent and reach up to 80 percent for some cases. By taking into account the radial flow around the wellbore, the results are close to the simulation results, with less than a 20 percent deviation.

4.3 Summary

- The new analytical model of critical rate based on the hodograph method is more accurate than the published solutions as it considers the presence of the crest shape.
- The hodograph method –based model of critical rate applies only to cases of horizontal wells at the top of the oil pay zones.
- A critical rate solution, based on the Dupuit approximation, is sufficiently accurate for practical purposes for a well at the top of the oil zone or beneath if h_{wD} is less than 0.3.
- For the cases where h_{wD} > 0.3, the Dupuit approximation alone can't provide an accurate result, because the radial flow around the wellbore must be taken into account.

CHAPTER 5. NEW MODEL OF CRITICAL RATE IN BWS WELLS

It is only after a complete understanding of the physics and water-free production mechanism of BWS wells that one can hope to find the best operational strategy for BWS wells in heavy oil reservoirs with strong bottom water drives. Such an understanding is provided in this chapter through mathematical derivation of the critical rate model for BWS wells. This chapter presents full derivation and verification of the model.

5.1 Basic Assumptions

Many studies have shown that the downhole water sink technology (DWS) can successfully control the water coning and water cresting problem. However, most of the literature is based on numerical simulations. Only a few papers analytically model the dynamic water-coning control mechanism with DWS. Wojtanowicz and Xu (1995) proposed a semi-analytical model using the method of superposition to calculate the water cone shape and critical rate. Shirman and Wojtanowicz (1997) developed a model called the moving spherical sink method to study the relationship between oil production and water drainage rates, and the corresponding cone shapes. Siemek and Stopa (2002) presented a semi-analytical model for determining the critical rate and the dynamic OWC at different oil and water production rates. Ansari (2006) reported an analytical critical rate solution for DWS by accounting for the capillary pressure and relative permeability.

However, these analytical models only pertain to vertical wells and do not apply to the BWS systems. This section presents derivation of the critical rate formula for BWS wells by extending the work for a single well (Chapter 4) to the two-well BWS system.

In addition to the assumptions made for a single well in Chapter 4, the following assumptions are taken for Bilateral Water Sink Wells. The horizontal well system with two

bilaterals completed in the oil and water zones, which produces oil and water independently from their respective zones (Figure 5.1). Also, the oil and water completions are parallel.

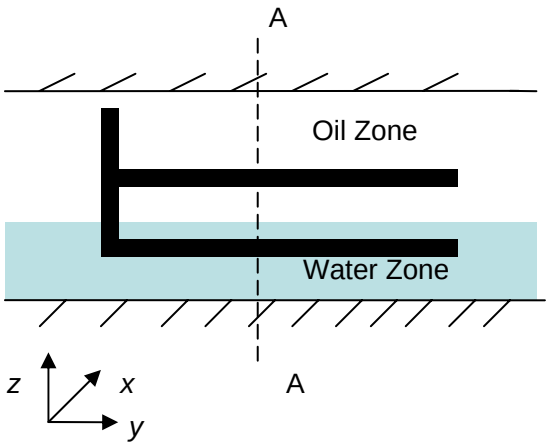

Figure 5.1 The configuration of BWS well system

The wells are assumed to be located within a rectangular drainage area. The wells are modeled as line sources with uniform flux; the end effects are neglected. The flow takes place in the *x*-*z* plane (Figure 5.2). Because the flow is symmetric, we study a half cross-section of the well orthogonal to the well axis (Figure 5.3).

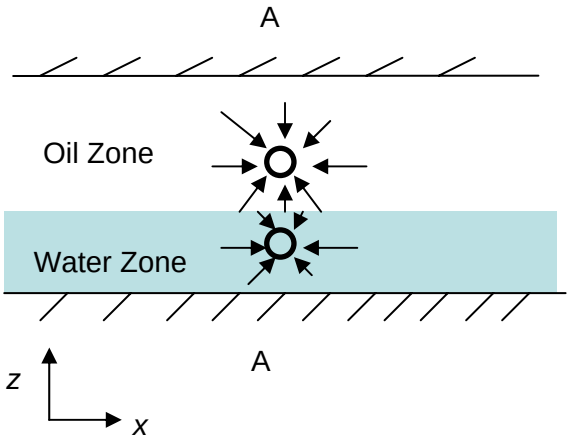

Figure 5.2 Cross-section schematic of BWS wells

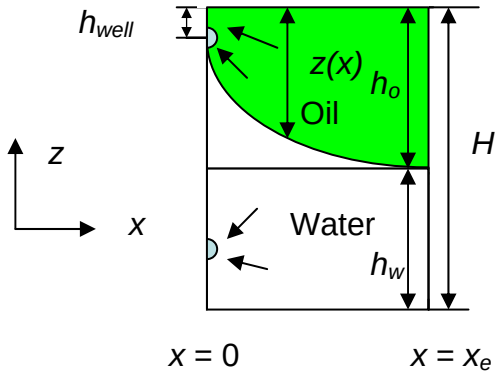

Figure 5.3 Schematic of water cresting in BWS well system

5.2 Critical Rate Solution in BWS Wells

With these assumptions, the potentials for the flow of oil Φ_o and water Φ_w in their respective zones are expressed by:

$$\Phi_o = p_o + \rho_o g z(x) \quad \text{.....(5.1)}$$

$$\Phi_w = p_w + \rho_w g z(x) \quad \text{.....(5.2)}$$

Where ρ_o and ρ_w is the density of oil and water respectively.

The depth of the interface is denoted by *z(x)* (Figure 5.3). Applying the Dupuit approximation to each fluid separately, we may now express q_o and q_w by:

$$\frac{q_o}{2} = \frac{k_o}{\mu_o} z(x) \frac{d\Phi_o}{dx} \quad \text{.....(5.3)}$$

$$\frac{q_w}{2} = \frac{k_w}{\mu_w} (H - z(x)) \frac{d\Phi_w}{dx} \quad \text{.....(5.4)}$$

Inserting Equation 5.1 and 5.2 into Equations 5.3 and 5.4 gives,

$$\frac{q_o}{2} = \frac{k_o}{\mu_o} z(x) \frac{d(p_o + \rho_o g z(x))}{dx} \quad \text{.....(5.5)}$$

$$\frac{q_w}{2} = \frac{k_w}{\mu_w} (H - z(x)) \frac{d(p_w + \rho_w g z(x))}{dx} \quad \text{.....(5.6)}$$

On the interface: $p_o = p_w$

The relationship between the flow rate and the elevation of the interface is obtained by eliminating p from Equations 5.5 and 5.6:

$$\frac{dz(x)}{dx} = \frac{q_w}{2\times\frac{k_w}{\mu_w}(\rho_w-\rho_o)g(H-z(x))} - \frac{q_o}{2\times\frac{k_o}{\mu_o}(\rho_w-\rho_o)gz(x)} \quad \text{.....(5.7)}$$

Rewriting Equation 5.7 as:

$$\frac{dz(x)}{\frac{q_w}{2\times\frac{k_w}{\mu_w}(\rho_w-\rho_o)g(H-z(x))} - \frac{q_o}{2\times\frac{k_o}{\mu_o}(\rho_w-\rho_o)gz(x)}} = dx \quad \text{.....(5.8)}$$

Integrating from $x = x_e$, $z = h_o$ and $x = 0$, $z = h_{well}$

We obtain:

$$\int_{z=h_{well}}^{z=h_o} \frac{dz(x)}{\frac{q_w}{2\times\frac{k_w}{\mu_w}(\rho_w-\rho_o)g(H-z(x))} - \frac{q_o}{2\times\frac{k_o}{\mu_o}(\rho_w-\rho_o)gz(x)}} = \int_0^{x_e} dx \quad \text{.....(5.9)}$$

$$\int_{z=h_{well}}^{z=h_o} \frac{dz(x)}{\frac{q_w}{2\times\frac{k_w}{\mu_w}(\rho_w-\rho_o)g(H-z(x))} - \frac{q_o}{2\times\frac{k_o}{\mu_o}(\rho_w-\rho_o)gz(x)}} - x_e = 0 \quad \text{.....(5.10)}$$

For any given value of q_w, Equation 5.10 yields an implicit equation for q_o. We calculated q_o numerically by using a solver developed by Matlab (Appendix C). Solutions to Equation (5.10) have been expressed in dimensionless terms - dimensionless critical rate (defined in Table 4.1) q_{cD} for various values of x_{eD} and q_{wD}, where q_{wD} is the dimensionless water drainage rate, defined as:

$$q_{wD} = \frac{q_w}{\frac{k_w}{\mu_w}(\rho_w-\rho_o)gh_w} \quad \text{.....(5.11)}$$

Figure 5.4 is a dimensionless plot of critical rate vs. water drainage rate, for x_{eD} = 4, 8, and 16. The dimensionless critical rate increases as the dimensionless water rate increases. If q_{wD} and x_{eD} are known, the corresponding q_{cD} can be obtained from this chart. Note that for $q_{wD} = 0$, q_{cD} is the critical rate value for a single horizontal well, which is extremely small (less than unity) for the three values of x_{eD}. For this scenario, BWS provides an order of magnitude increase of up to $q_{cD} = 30$ in comparison to a single horizontal well. Another finding is that the size of the drainage area affects critical rate only for small values of water drainage rate. The curves for different values of x_{eD} diverge for dimensionless $q_{wD} < 1.5$ (Figure 5.5).

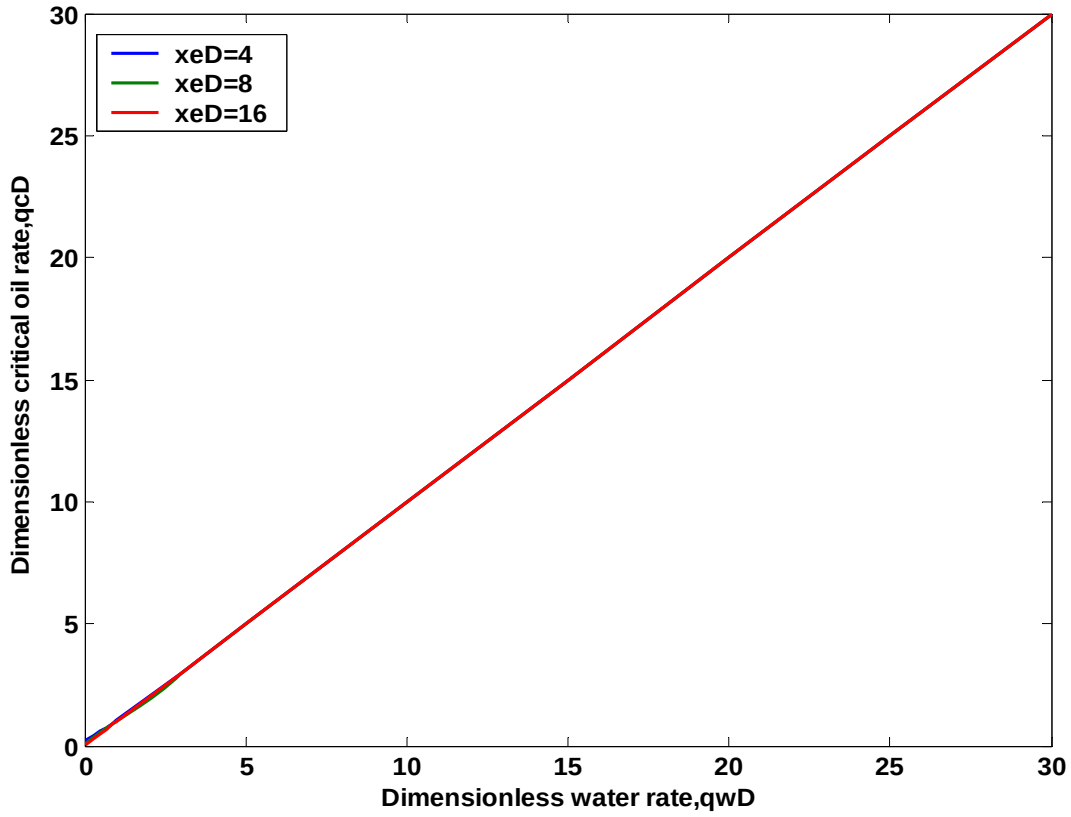

Figure 5.4 Dimensionless plot of BWS critical oil rate vs. water drainage rate

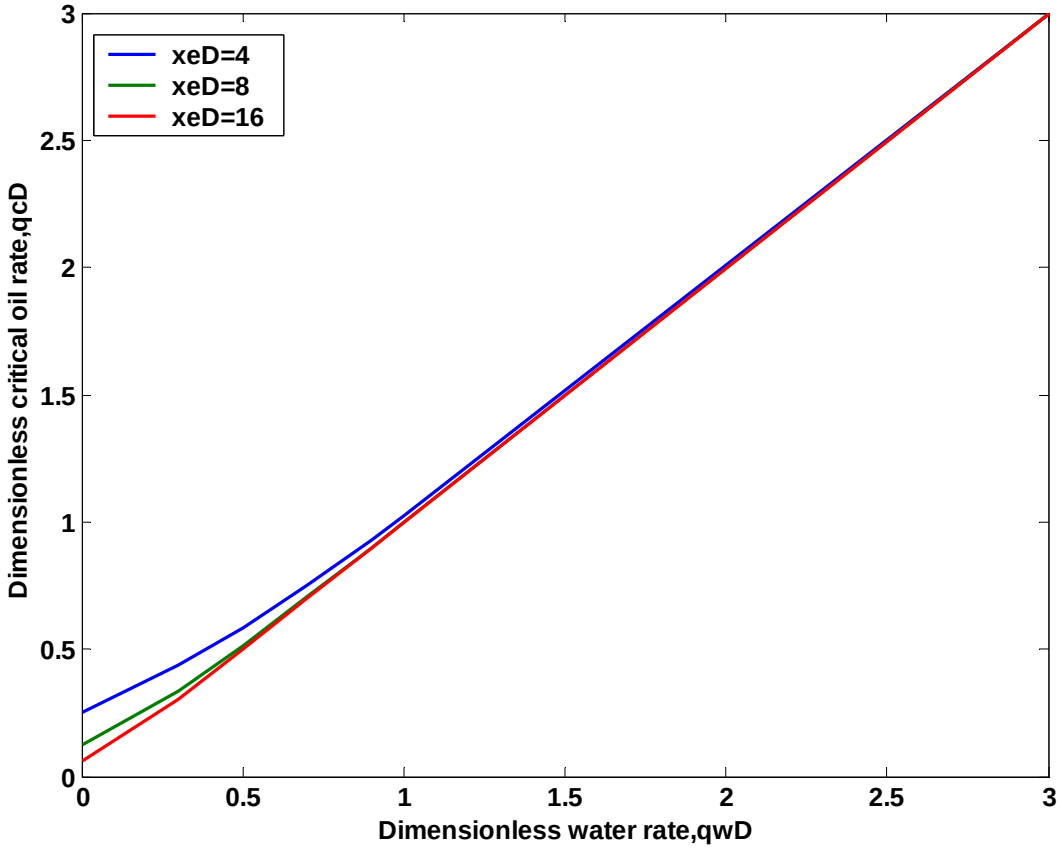

Figure 5.5 Effect of drainage size diminishes for $q_{wD} > 1.5$

As q_{wD} increases, the discrepancy diminishes, and the dimensionless critical oil rate q_{cD} becomes a strictly linear relationship with dimensionless water drainage rate q_{wD}, with slope m = 1, which indicates that at larger value of q_{wD}, the dimensionless critical rate can be calculated as $q_{cD} = q_{wD}$. This can be expressed as

$$\frac{q_o}{\frac{k_o}{\mu_o}(\rho_w - \rho_o)gh_o} = \frac{q_w}{\frac{k_w}{\mu_w}(\rho_w - \rho_o)gh_w} \quad \text{(5.12)}$$

The consequences of this finding are explained in the following section.

5.3 "No Water Crest" Solution in BWS Wells

It can be noticed that Equation 5.12 describes the condition when the OWC doesn't deform upwards, i.e. no water crest is formed, or $z\,(x) = h_o$ for any value of z in Equation 5.7,

$$\frac{q_w}{2\times\frac{k_w}{\mu_w}(\rho_w-\rho_o)gh_w}-\frac{q_o}{2\times\frac{k_o}{\mu_o}(\rho_w-\rho_o)gh_o}=\frac{dz(x)}{dx}=0 \quad \text{.....(5.13)}$$

When $z(x)$ is independent of x, $\frac{dz(x)}{dx}=0$

Equation 5.13 can be also written as,

$$\frac{q_w}{q_o}=\frac{\frac{k_w}{\mu_w}h_w}{\frac{k_o}{\mu_o}h_o} \quad \text{.....(5.14)}$$

Equations 5.12 through 5.14 represent the "no water crest" inflow condition (Figure 5.6), where the OWC remains in the original horizontal position without forming a water crest. This situation can only be created with BWS, because as for a single well, water cresting is inevitable - the well's pressure drawdown in the reservoir causes upwards deformation of the OWC to form a crest. In BWS wells, however, by controlling q_o and q_w according to Equation 5.14, one can ensure the OWC does not rise to cause a water crest (Figure 5.6).

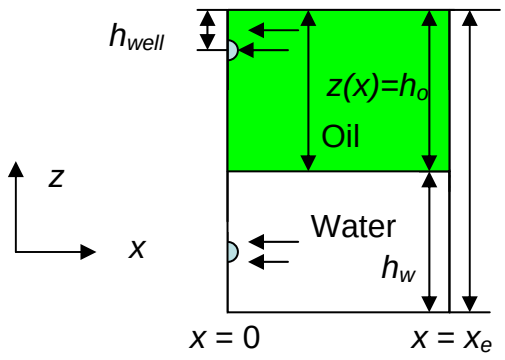

Figure 5.6 "No water crest" scenario

Figures 5.7 and 5.8 demonstrate the difference between the "no water crest" and critical rate solutions. It shows that the difference is practically meaningless for most of the practically possible sizes of drainage areas.

The solution of "no water crest" (dashed line, Figures 5.7 and 5.8) passes through the origin with slope $m = 1$ and the solutions nearly overlay for $q_{wD} > 3$ along with the critical rate solution represented by solid lines. At small values of q_{wD} ($q_{wD} < 1.5$, Figure 5.8), the critical rate solutions deviate from the "no water crest" solution. However, the deviation becomes smaller as q_{wD} increases and eventually coincides with the "no water crest" line. The interpretation of this will be described in 5.4.3 in conjunction with numerical simulations.

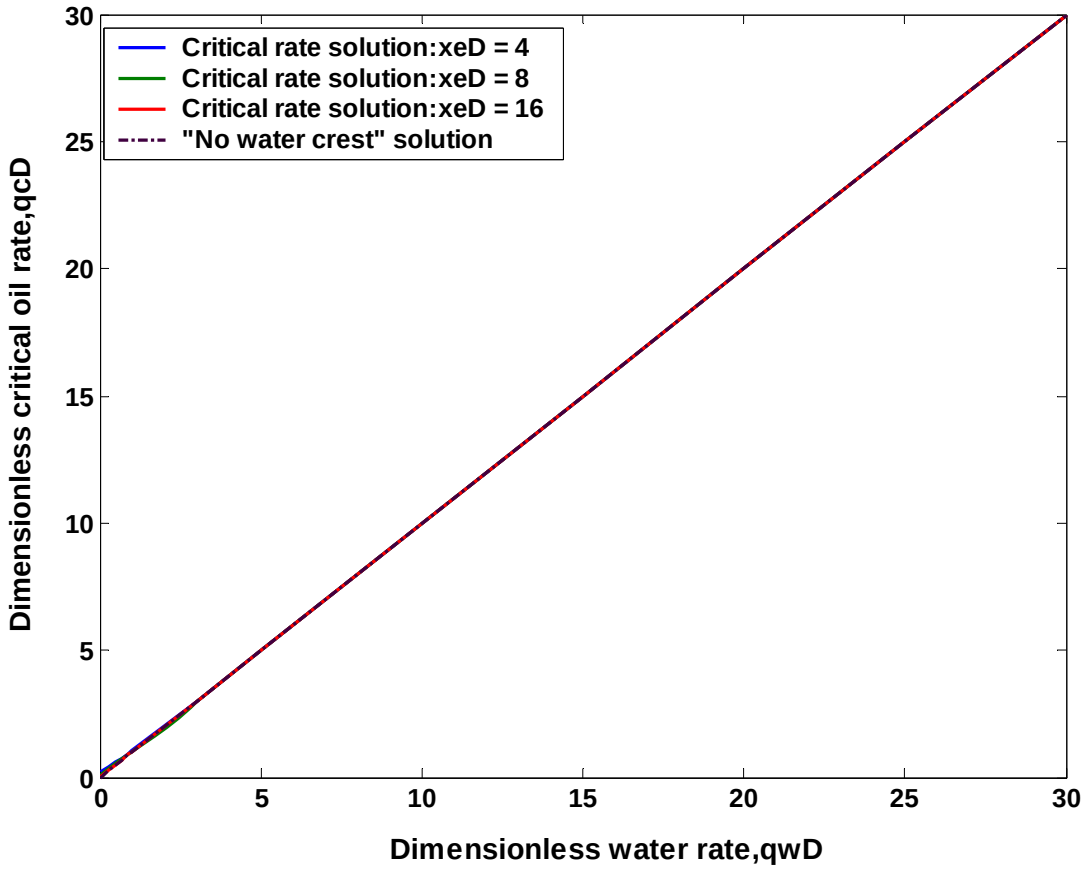

Figure 5.7 "No water crest" solution vs. critical rate solution

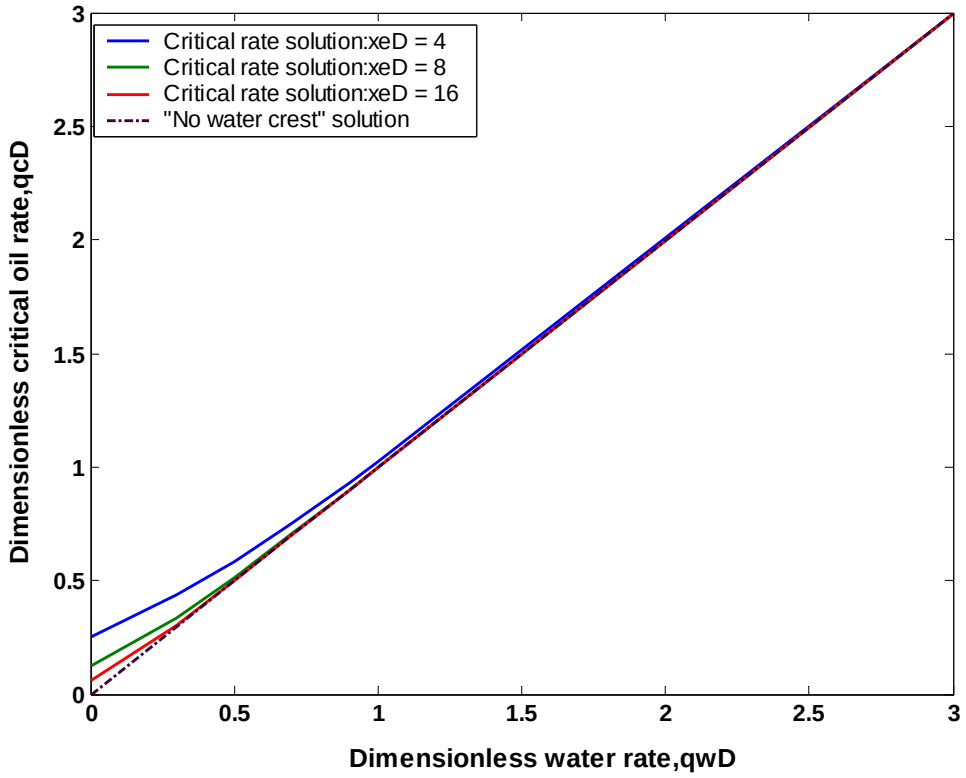

Figure 5.8 "No water crest" solution vs. critical rate solution for $q_{wD} < 3$

5.4 Verification Using Numerical Simulation

5.4.1 Model Description

The numerical simulation model was built to test the validity of the analytical model by using a commercial simulator IMEX developed by CMG group.

As we discussed earlier, a grid block size is fixed at 0.5 ft, in the z direction. In the horizontal direction, the fine grids around the wellbore D_x = 0.5 ft and a coarse grid away from the wellbore were used to provide reliable results. As shown in Figure 5.9, in the x-z 2D cross-section model, a horizontal well is perforated at the top of the oil zone, while another well is perforated in the bottom of the water zone. Two injection wells are used to create the constant potential boundary at x_e by re-injecting the produced fluids into the oil and water zone,

respectively. Rock and fluid properties were chosen from the cases presented in Chapter 3. The cases considered in modeling BWS are listed in Table 5.1.

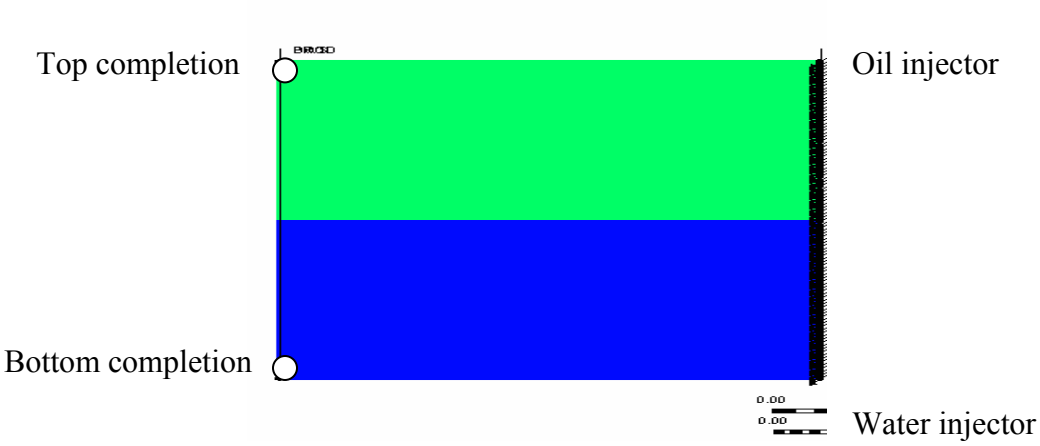

Figure 5.9 The reservoir geometry

Table 5.1 Summary of selected cases for numerical simulation

Case number	Oil Type	k(md)	μ(cp)	Φ(%)	API	x_{eD}	q_{wD}
1	Light oil 2	200	2	20	26	1.8000	1.0786
2		200	2	20	26	4.0000	3.8831
3		200	2	20	26	4.0000	7.7662
4		200	2	20	26	4.0000	15.5324
5		200	2	20	26	4.0000	31.0648
6		200	2	20	26	8.0000	1.3203
7		200	2	20	26	8.0000	2.6405
8		200	2	20	26	8.0000	5.2801
9		200	2	20	26	8.0000	10.5620
10		200	2	20	26	8.0000	13.2025
11		200	2	20	26	8.0000	21.1241
12	Heavy oil 1	870	20	30	20	1.8000	1.0306
13		870	20	30	20	4.0000	1.8139
14		870	20	30	20	4.0000	3.6278
15		870	20	30	20	4.0000	7.2556
16		870	20	30	20	4.0000	14.5112
17		870	20	30	20	4.0000	29.0224
18	Heavy oil 2	5000	65	30	14	1.8000	1.0287
19		5000	65	30	14	4.0000	1.8516
20		5000	65	30	14	4.0000	3.7033
21		5000	65	30	14	4.0000	5.5549
22		5000	65	30	14	4.0000	9.2581
23		5000	65	30	14	4.0000	18.5163

5.4.2 Critical Rate Verification

In the simulation runs, q_{wD} is given to seek the critical rate q_{cD} of the upper lateral of BWS well, by a trial and error approach in numerical simulations through a series of oil rates until the critical oil rate is found. Then, the simulated critical rate values were compared to those values computed from Equation 5.10.

Figure 5.10 and Figure 5.11 show the dimensionless critical rate estimated from the analytical solution and the simulation results as the function of a dimensionless water drainage rate; the solid lines are for the analytical solutions of critical rate (Equation 5.10) and the points are the numerical simulation results, and the "no water crest" solution (Equation 5.14) is again plotted as a dashed line. Figure 5.12 plots the percentage error between the critical rate analytical model and numerical simulation approaches, with the percentage of error defined as:

$$\text{Percent error} = \frac{\text{Result (analytical) - result (numerical)}}{\text{Result(numerical)}} \times 100$$

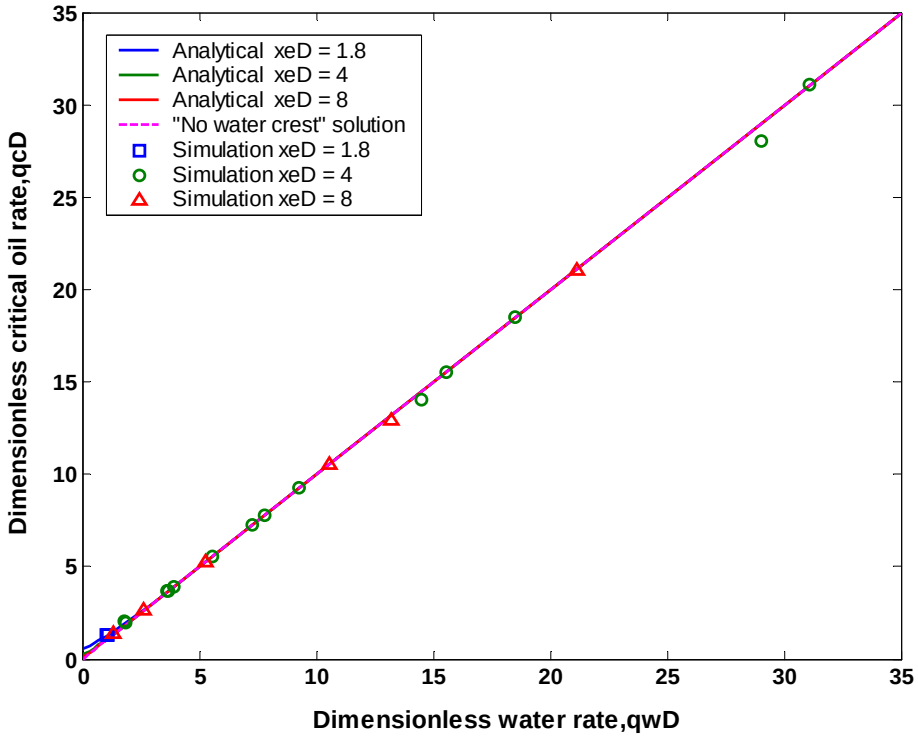

Figure 5.10 Critical rate comparison in BWS wells

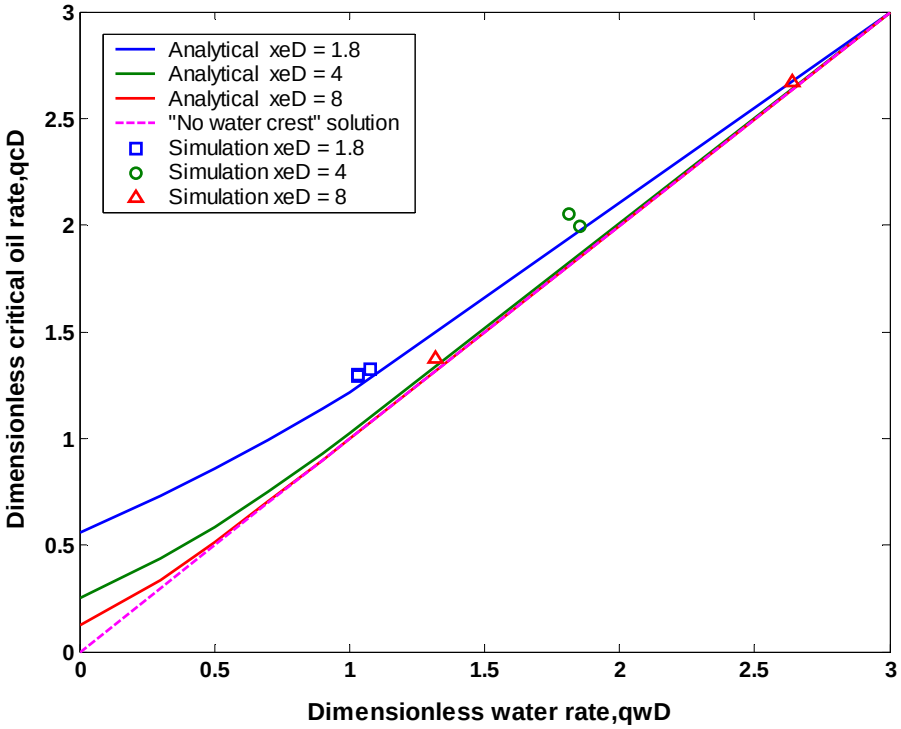

Figure 5.11 Critical rate comparison in BWS wells for $q_{wD} < 3$

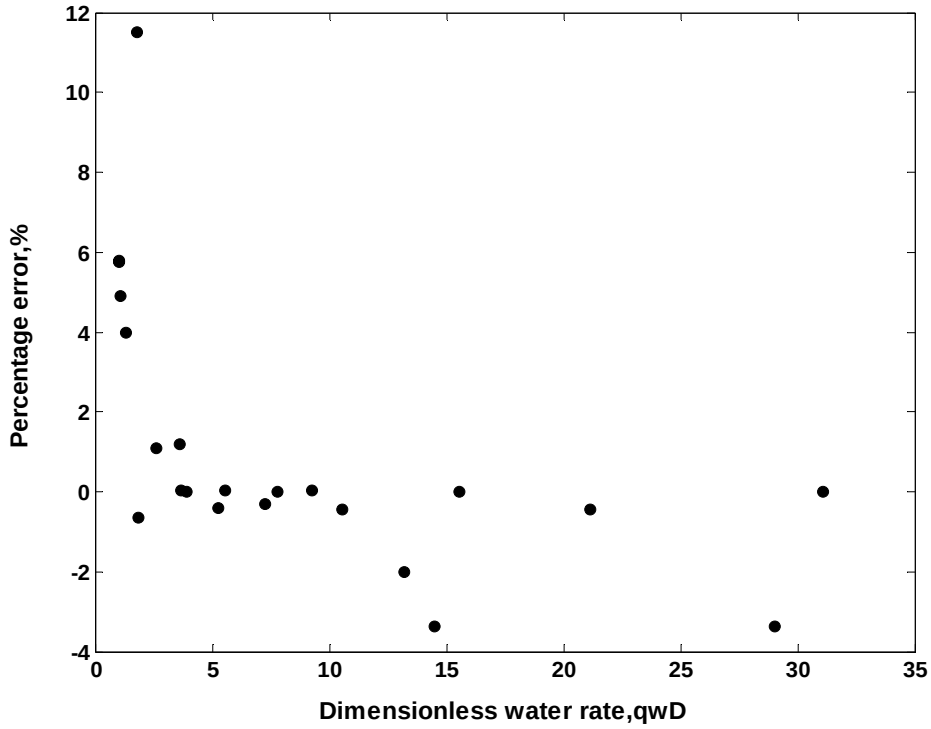

Figure 5.12 Critical rate percentage error, %

As shown in Figures 5.10 and 5.11, the analytical results are in good agreement with the numerical simulations, with an average error of less than 5 percent (Figure 5.12). The results also validate "no water crest" model of critical rate in BWS wells, as the two solutions are practically identical and they very slightly diverge for $q_{wD} < 3$.

The "no water crest" model (Equation 5.14) predicts the ratio of oil and water rates in BWS wells to avoid water bypassing oil and assure water-free oil production. The simple linear form of the "no water crest" formulation (Equation 5.14) allows easier design compared to the implicit equation of the critical rate (Equation 5.10). In practical applications, the "no water crest" formulation could be used to determine the economic critical oil rate. The approach would be valid for $q_{wD} > 3$.

5.4.3 "No Water Crest" Verification

Figure 5.13 compares the location of the water oil interface at the critical crest condition from the simulation for cases 19 and 23 (Table 5.1).

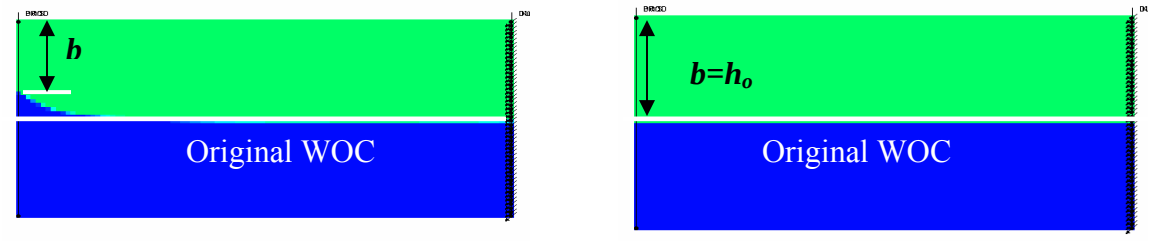

(A) Critical crest in case 19 ($q_{wD} = 1.8516$) (B) Critical crest in case 23 ($q_{wD} = 18.5163$)

Figure 5.13 Water saturation profile for case 19 and 23 after 33 years of production

Muskat and Wyckoff's (1935) experimental results show that critical crest remains at a certain distance *b* away from the wellbore (Figure 5.13). In the case 19 where $q_{wD} = 1.8516$, the simulation results of the water saturation profile shows the consistency with their experiment's

findings (Figure 5.13 A). However, the distance *b* between the apex of the crest to the wellbore increases as q_{wD} increases. As shown in Figure 5.13 B in case 23, q_{wD} = 18.5163, $b = h_o$ the crest maintains as a stable crest only at its original flat interface condition. Any infinitesimal increase of oil rate will cause the interface to lose its stability and rise to the well. At this condition, the critical crest condition becomes the "no water crest" condition. The OWC in the simulation maintained horizontal throughout production life (Equation 5.14 applied to case 23; $q_{wD} > 3$). This verifies that the "no water crest" condition provides useful critical rates.

5.5 Summary

In this chapter, the critical rate solution for BWS is being sought under a steady-state condition with an open outer boundary. The effect of BWS on critical rate improvement over the single horizontal well has been demonstrated quantitatively. Although the critical rate solution is an implicit equation, it can be approximated using the "no water crest" solution for $q_{wD} > 3$. The explicit nature of the "no water crest" solution allows the easy calculation of critical rates in BWS wells with an error less than 5 percent in comparison to the numerical simulation.

CHAPTER 6. DESIGN OF BWS WELL PRODUCTION STRATEGY AND APPLICATION

To this point, a mathematical BWS model has been constructed and matched to the numerical simulations. The assumption of a constant - potential outer boundary makes the model applicable to reservoirs with strong bottom water drives, and water-flood systems with a constant - potential boundary between producers and injectors. This assumption is equivalent to one that assumes the reservoir has a completely open outer boundary, where fluid withdrawal can be exactly balanced by fluid entry across the boundary. For other cases with spaced horizontal wells where each well drains from its own bounded reservoir, modifications must be made to calculate critical rates in those cases.

More importantly, the recovery factor can be determined in a no-flow boundary case. The effect of BWS on enhancing oil recovery by enabling high values of critical rate and avoiding the water breakthrough will be studied in this chapter.

6.1 Single Horizontal Well Operation Strategies for Water Cresting Control

Even though the well is placed in a bounded reservoir, the encroachment of water from the bottom aquifer helps to maintain the reservoir potential. As a result, the reservoir potential does not vary with time and the boundary potential remains constant during the project life. Moreover, as shown in Chapter 3, through numerical simulation, the water cresting stabilization time in heavy oil is so short that it could be ignored. Thus, the flow system can be regarded as a steady-state flow system so that the critical rate solution derived in Chapter 4 can be applied.

However, critical rate solution of a constant potential boundary reservoir cannot be used without further analysis. In particular, the *influence* distance x_i is different from the expected drainage distance x_e, which is based on well spacing. To apply the critical rate solution for the

bounded reservoir case (with constant-potential water influx at the boundary), an adjustment must be made to determine the actual drainage distance x_i.

6.1.1 Determination of Drainage Distance x_i

The determination of x_i requires examining the drive mechanism for bottom water drive reservoirs. Here, we investigate the flow mechanics of a bottom water drive reservoir mathematically. In the open boundary cases discussed in Chapters 4 and 5, only oil is in motion while the bottom water is stationary, with a stationary interface between the water and oil. This situation occurs when side water "drives" the oil laterally towards the well while the bottom water advancement is negligible. In contrast, the OWC would become a moving (upwards) interface in the case of a well draining from a finite reservoir with no water invasion at the boundary.

Kuchuk (1991) and Ozkan (1990) treated the original OWC as a constant potential boundary to provide a pressure support that is similar to a water flood from below in such reservoirs. Kuchuk derived a potential distribution solution for a laterally infinite reservoir in the Laplace domain and Ozkan presents a similar solution for a well, drained in a rectangular drainage region, using Green's functional product method.

Although Green's functional product method provides a general solution of potential distribution in bottom water drive reservoirs as a function of time, the solution is difficult to evaluate and therefore difficult to use in design. We will demonstrate that the oil potential distribution solution and drainage distance x_i may be obtained alternatively in a straightforward manner using the method of images.

Except for the boundary condition, the assumptions made in deriving the critical rate equation in Chapter 4 are retained. Because the steady-state condition has been verified in Chapter 3, Laplace's equation can be taken as the governing equation for describing the flow

behavior of steady-state flow system. A 3D (Figure 6.1 A) solution may be obtained by a sum of all the 2D planes along the well shown in Figure 6.1(B), and the problem can be solved in 2D.

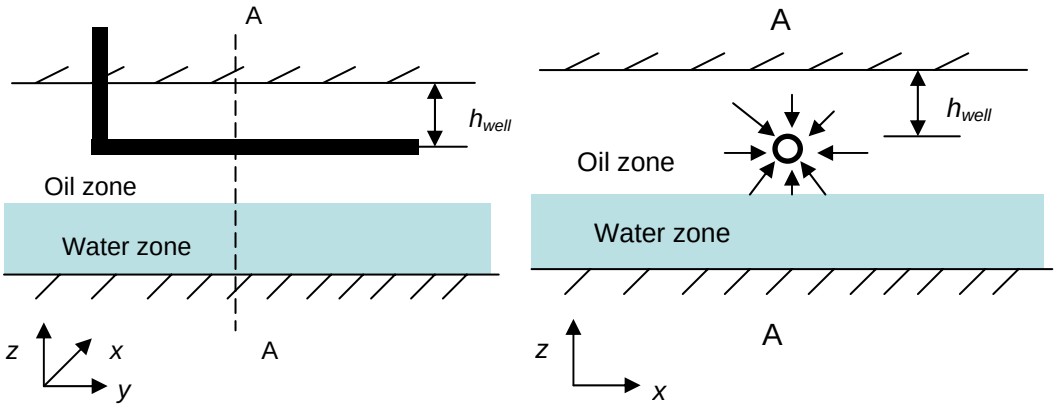

(A) (B)

Figure 6.1 Schematic of boundary condition

The reservoir boundary at the top of the formation is assumed to be no-flow boundary and a constant potential boundary at the original OWC. The horizontal well in such a reservoir may be modeled as an infinite set of image wells (Figure 6.2). The resultant potential at any point of the reservoir is the superposed effect created by all sinks,

$$\Phi_{(x,z)} = \frac{q_0 \mu_o}{2\pi\, k_o} \sum_{-\infty}^{\infty} \ln \sqrt{[x^2 + (z - h_0 - h_{well} - 4nh_0)^2] \times [x^2 + (z - 4nh_0 - h_o + h_{well})^2]}$$

$$- \frac{q_0 \mu_o}{2\pi\, k_o} \sum_{-\infty}^{\infty} \ln \sqrt{[x^2 + (z - 3h_0 + h_{well} - 4nh_0)^2] \times [x^2 + (z - 4nh_0 + h_o - h_{well})^2]} \quad \text{.....(6.1)}$$

$$+C$$

Based on Muskat (1937):

$$\sum_{-\infty}^{+\infty} \ln[(\xi - h)^2 + (na - \eta)^2] = \ln[\cosh[2\pi(\xi - h)/a] - \cos(2\pi\eta/a)] \quad \text{.....(6.2)}$$

Equation 6.1 can be simplified as follows:

$$\Phi_{(x,z)} = \frac{q_o \mu_o}{4\pi k_o}\left[\ln \frac{\cosh\frac{\pi x}{2h_0} - \cos\frac{\pi(z-h_o+h_{well})}{2h_0}}{\cosh\frac{\pi x}{2h_0} + \cos\frac{\pi(z-h_o+h_{well})}{2h_0}} \times \frac{\cosh\frac{\pi x}{2h_0} + \cos\frac{\pi(z+h_o-h_{well})}{2h_0}}{\cosh\frac{\pi x}{2h_0} - \cos\frac{\pi(z+h_o-h_{well})}{2h_0}}\right]$$

$$+\Phi_e \qquad \text{... (6.3)}$$

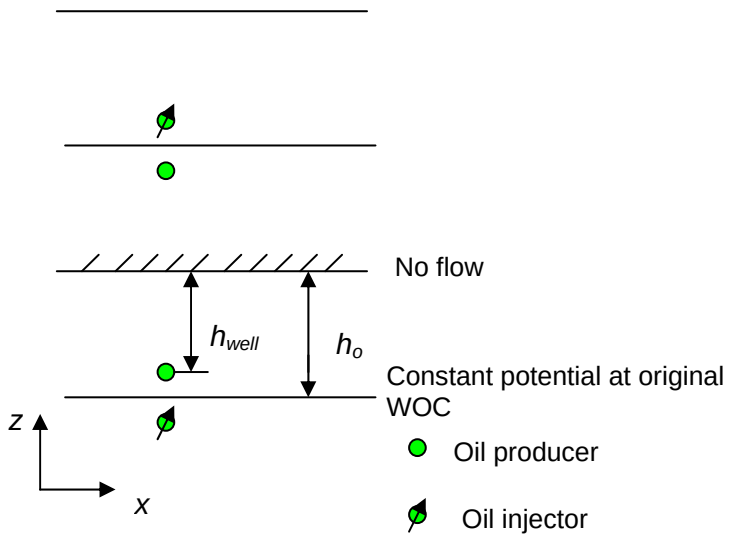

Figure 6.2 Transformation of boundary condition

The flow potential distribution plots in Figure 6.3 compare the analytical flow potential with numerical simulations. In all these figures, the dashed lines represent the analytical solution from Equation 6.3, and the solid lines represent simulation results at stabilized flow conditions. The oil and rock properties are listed as Table 3.1 and Table 3.2 in Chapter 3.

It can be seen that as the oil approaches heavy oil properties, the discrepancy between the analytical solution and numerical simulations become negligible; therefore the analytical solution is valid for heavy oil.

The conclusion drawn from this analytical study based on Equation 6.3 is that for the heavy oil underlying a strong aquifer, the flow system is dominated by a constant potential boundary at the original OWC, and the lateral no-flow boundary of the reservoir has only a

negligible effect. In other words, a constant-potential boundary occurs at $x = x_i$ independent of the physical no-flow boundary at x_e, even at later time. Therefore, oil is being produced only in the small region $x < x_i$, while the oil outside this region, does not feel the pressure response in the well– hence, not being recovered.

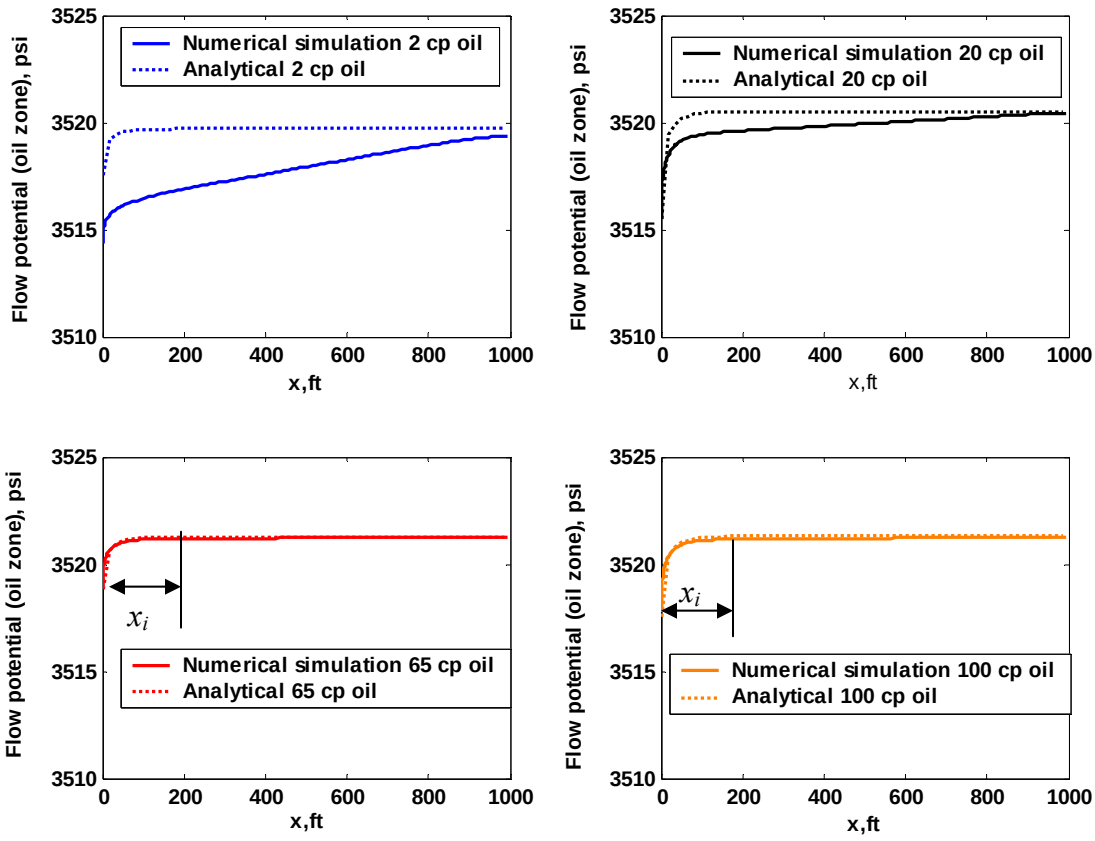

Figure 6.3 Numerical verification of analytical solution shows good match for heavy oils

A particular advantage of this analysis is that x_i can be determined graphically (Figure 6.3) or by setting the potential gradient equal to zero (Equation 6.4) and solving the Equation 6.4 numerically with Newton's method for x_i.

$$\frac{\partial P_{(x,z)}}{\partial x} = \frac{q_l \mu_o}{4\pi k_o} \sinh\left(\frac{\pi x_i}{2h_o}\right) \left\{\left[\cosh\left(\frac{\pi x_i}{2h_o}\right)\right]^2 - 1\right\}^{(-1)} \cong 0 \qquad (6.4)$$

6.1.2 Time-dependent Critical Rate in Single Horizontal Well

A discussed above, a single horizontal well produces oil only from small region $x < x_i$ with practically constant potential at $x = x_i$. Critical rate for that region can be predicted by substituting x_i obtained from Equation 6.4 into x_e, in Equation 4.42.

$$q_c = \frac{k_o(\rho_w - \rho_o)gh_o^2}{\mu_o x_e} \quad \text{.....(4.42)}$$

As more oil is produced, the oil column in the actual drainage area ($x < x_i$) decreases as a function of time. As a result, the critical rate would also decrease with time. The procedure presented here calculates the critical rate over a series of certain time steps - such as one month, for example. The procedure is described as follows:

- First, calculate x_i, numerically, using Equation 6.4
- Second, the critical rate is calculated from Equation 4.42 by using the original oil thickness h_o
- Then, set the well to produce at this rate for Δt, with a new oil thickness calculated at the end of the time period by using a material balance, which is:

$$h = h_o - \frac{q_c \Delta t B_o}{\varphi(1 - S_{wc} - S_{or})A} \quad \text{.....(6.5)}$$

- Insert this new oil thickness in the Equation 4.42, thus calculating a new value of q_c, corresponding to production time t.
- Again, the new q_c was held constant for a period of time Δt, reworking the material balance to give the new h_o and q_c.

As an example, time-dependent critical rate curves are plotted in Figure 6.4 for the oil properties of Case 3, listed in Table 3.1 for a x_e = 500 ft lateral length reservoir with calculated x_i approximately 100 ft. Assuming the well length is equal to 3000 ft, it can be seen that the

required critical rate for water-free oil production is too small to make the project profitable (less than 20 stb/d).

To ensure the critical rate solution derived for constant potential outer boundary is applicable to the finite reservoir case, the flow potential at calculated boundary x_i = 100 ft is plotted in Figure 6.5, in which the boundary potential is not varying as a function of time and the constant potential outer boundary is valid in the bounded reservoir.

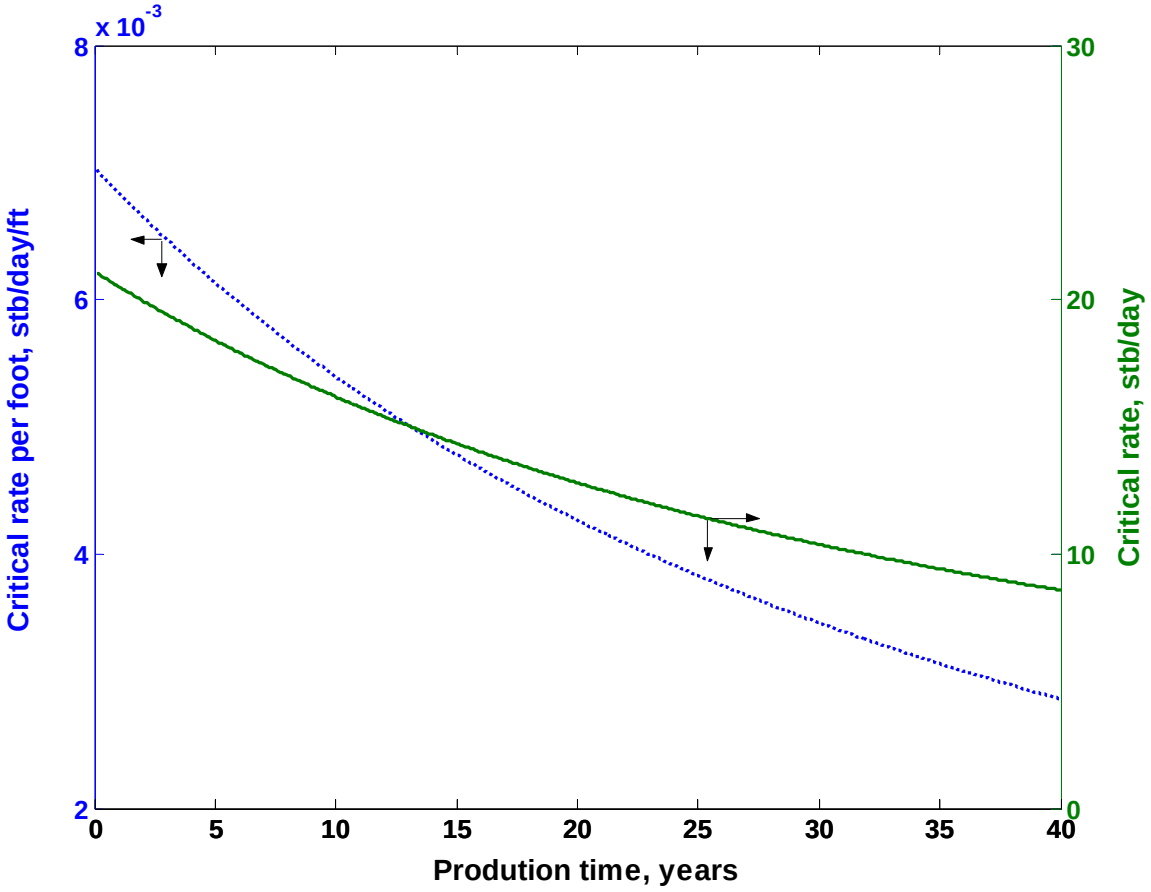

Figure 6.4 Time dependent critical rate for single horizontal well in heavy oil

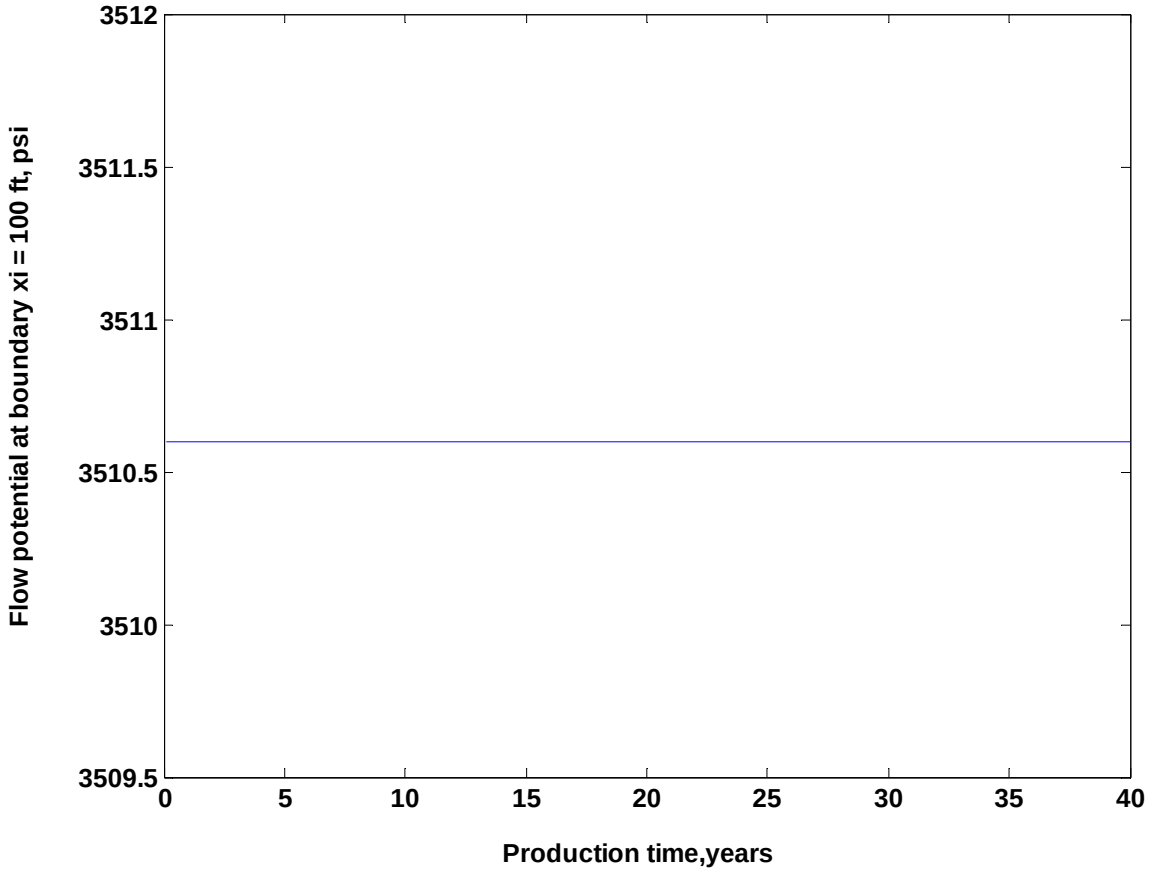

Figure 6.5 Simulation result of the flow potential at calculated boundary (x_i = 100 ft)

6.1.3 Comparison of Water-free and Water Cut Production for Single Well

Figure 6.6 shows the simulation results in terms of water cut and recovery factor as a function of time, by producing well above or at critical rate. Time-dependent critical rate production (Figure 6.4) is a comparison to the case of producing oil above critical rate in the same reservoir for a constant liquid rate q_l = 0.12 stb/d/ft (q_l = 360 stb/d for 3000 ft long well). By operating the well at the critical rate, the oil could be produced water-free for 30 years. However, in terms of a recovery factor, operating the well at critical rate would be deficient in comparison to producing oil with water at rates much exceeding critical rate. Clearly, a water-

free production strategy would not work for a single well because critical rate is too small and mobile oil recovery is too slow (less than 5 percent over 30 years).

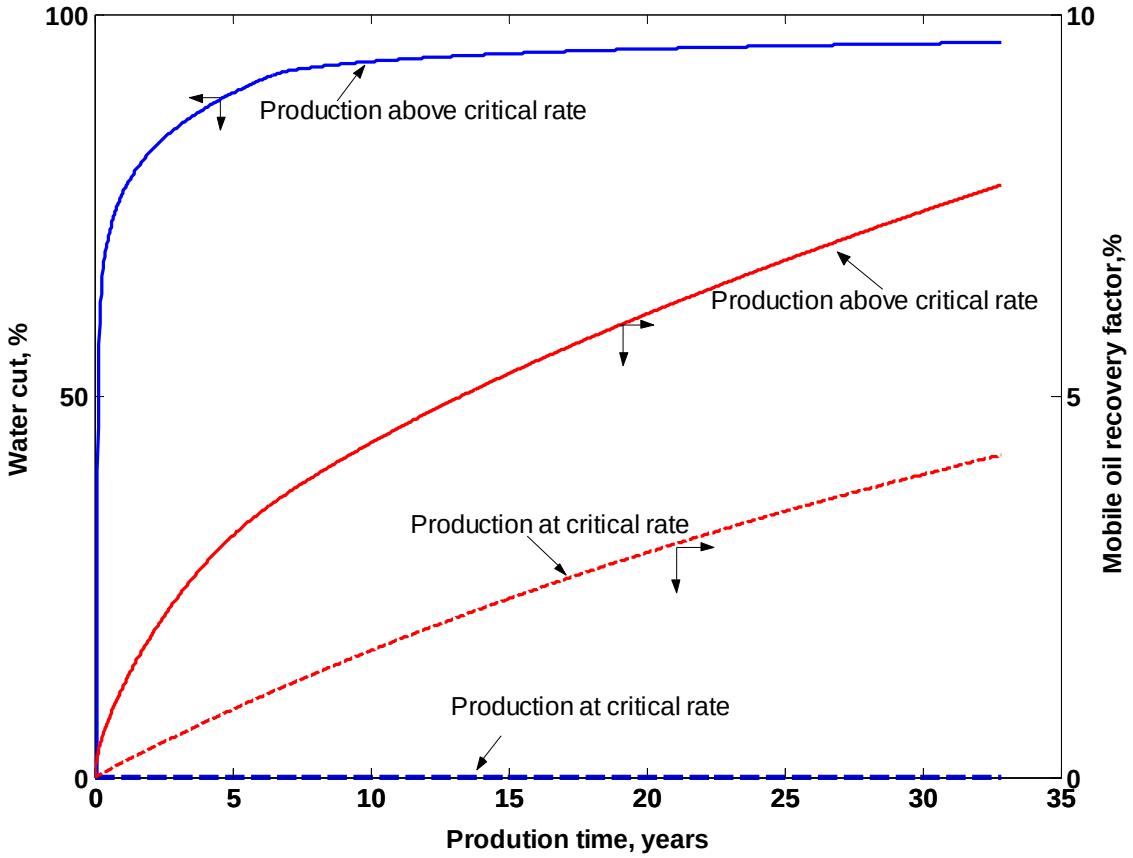

Figure 6.6 Simulation results of water cut development comparison

In addition, Figure 6.7 shows the comparison of water cresting performance at the end of production life t = 30 years in these two cases. Green represents oil and blue represents water.

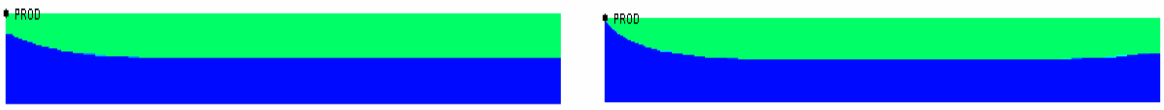

At critical rate Above critical rate

Figure 6.7 Simulation results of water saturation profile comparison

The negative aspect of the small drainage distance in a single horizontal production has not been offset by operating at critical rate (Figure 6.7 and 6.8). In conclusion, for a single

horizontal well, the water-free production strategy is ineffective for achieving high oil recovery from bottom-water heavy oil reservoirs.

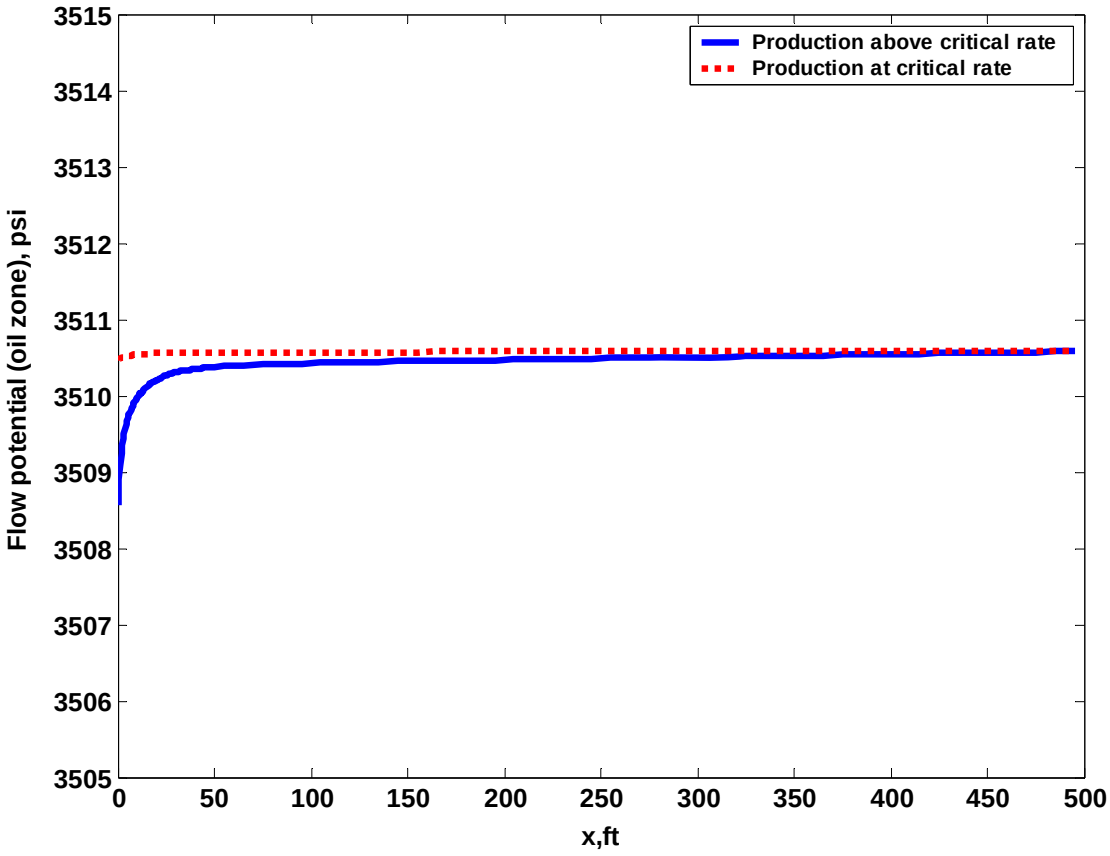

Figure 6.8 Simulation results of oil potential distribution

6.2 Application of BWS with "No Water Crest" Model to Recovery Design

The effect of the BWS to raise the critical oil rate has been analyzed in Chapter 5, using the Dupuit approximation. In this section we assess the practical application of BWS on improving oil recovery. The application requires considering a certain reservoir volume to be recovered – the drainage volume limited by no-flow boundaries between producing wells and practical limits of maximum water cut for the commingled production of water and oil. Therefore, this first step is to verify - with numerical simulation - whether the analytical solution

(Equation 5.14) derived for constant-potential outer boundary would apply to real field cases with a well draining from a bounded reservoir.

In this chapter, we use a reservoir simulator to predict recovery from the same reservoir system with either BWS or a single horizontal well. The simulation models provide comparisons with fewer assumptions than analytical solutions and use widely-verified commercial numerical models.

The horizontal well is completed at the top of the oil zone to produce oil from a bounded oil reservoir, while another (BWS) well is at the bottom of the water zone and drains water from the aquifer. The geometry of the bottom water reservoir is shown in Figure 6.9 A, and it can be approximated with the simulation model (Figure 6.9 B) with rectangular shape. The oil zone has a no flow outer boundary. In the water zone, an infinite aquifer was attached to the outer boundary to allow strong natural water flux. Rock and fluid properties are chosen from the cases presented in Table 3.1 and Table 3.2. In all these runs, the top completion is produced at 0.12 stb/d/ft liquid rate. The water drainage rate at bottom completion is determined by the application of the "no water crest" solution (Equation 5.14) to avoid water breakthrough at the top completion. The calculated water drainage rates for different cases are listed in Table 6.1.

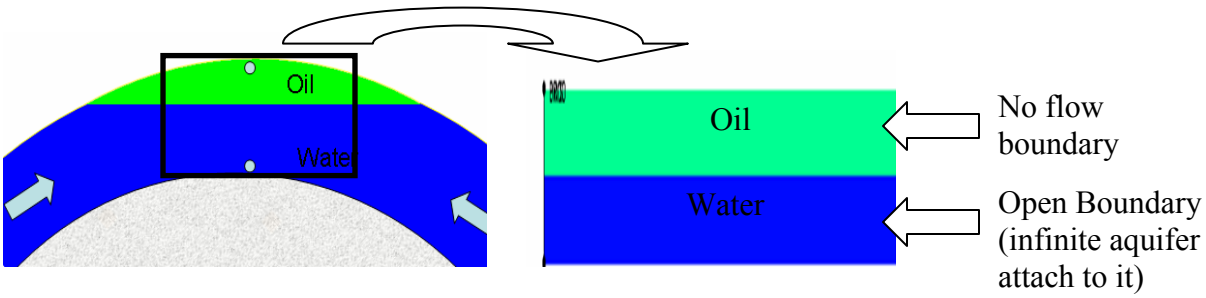

(A) Schematic of bottom water drive reservoir (B) Reservoir simulation model

Figure 6.9 Reservoir model represents the bottom water drive reservoir

Table 6.1 Input data for recovery mechanism study

Oil type		Case Number	API	μ (cp)	k (md)	Φ (%)	Production rate -top completion stb/d/ft	Production rate - bottom completion (Equ 5.14) stb/d/ft
Conventional oil	Single well	1	26	2	200	20	0.12	0
Heavy oil 1		2	20	20	870	30	0.12	0
Heavy oil 2		3	14	65	5000	30	0.12	0
Heavy oil 3		4	14	100	5000	30	0.12	0
Conventional oil	BWS wells	5	26	2	200	20	0.12	0.25
Heavy oil 1		6	20	20	870	30	0.12	2.5
Heavy oil 2		7	14	65	5000	30	0.12	8.125
Heavy oil 3		8	14	100	5000	30	0.12	12.5

As mentioned above, the use of Equation 5.14 needs to be justified because the formula has been derived for a constant potential outer boundary but is being used here for a case where the reservoir is bounded. The verification is performed using numerical simulation. Figure 6.10 plots the flow potential obtained from numerical simulation at the boundary where x_e = 1000 ft. Because the potential decline is relatively small (less than 0.05 psi/y) for the heavy oil cases (case 6, 7, 8 in Table 6.1), we conclude that the use of Equation 5.14 is justified for heavy oil reservoirs. That is, the bounded and constant-potential cases will have similar cresting behavior.

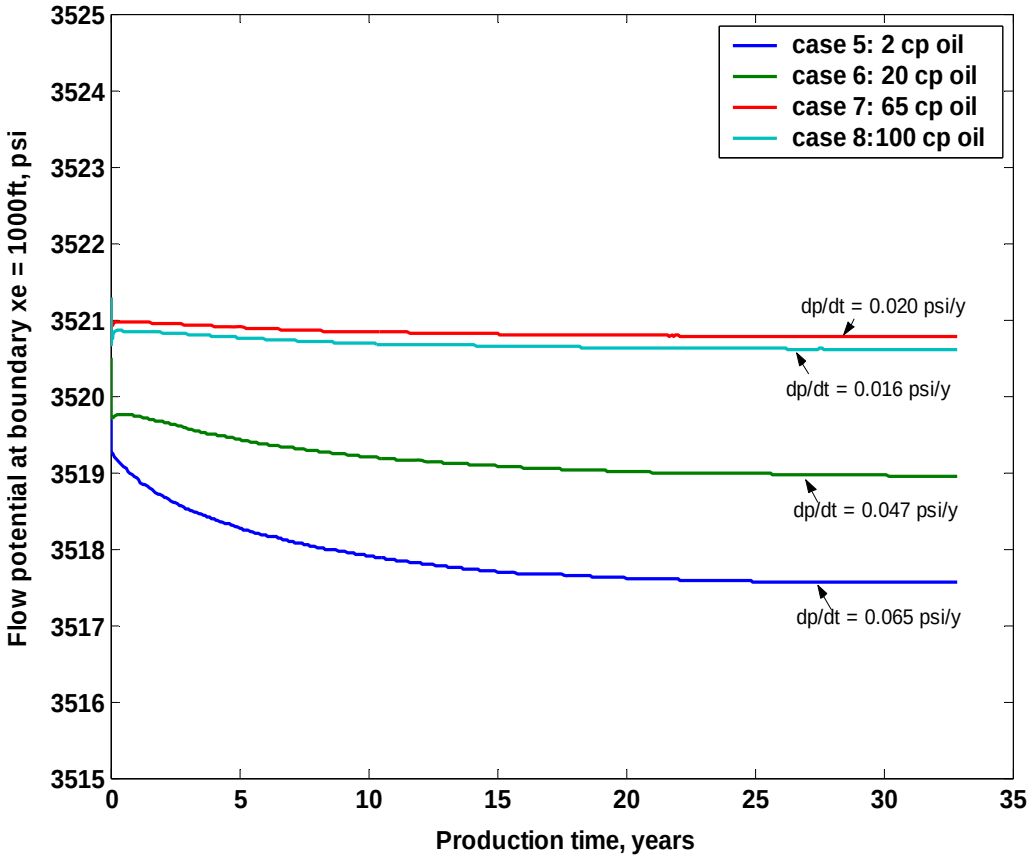

Figure 6.10 Simulation results of flow potential at boundary where x_e = 1000 ft

6.2.1 Recovery Design Using "No Water Crest" Model

Simulation results of water cut and recovery factor are plotted in Figure 6.11 for these cases presented in Table 6.1. The results show that - except in the conventional oil case - application of BWS in heavy oils leads to complete avoidance of water breakthrough to the production well at pay zone more than 30 years, if the oil and water rates are selected using the "no water crest" relation (Equation 5.14). Without water breakthrough, mobile oil recovery linearly increases with time (Figure 6.11) and can be simply calculated from Equation 6.6.

$$\text{Mobile oil recovery factor } \% = 100 \times \frac{N_p}{N(1 - S_{or} - S_{wc})} \quad \text{.....(6.6)}$$

Since the N_p, N, S_{or} and S_{wc} values are the same in cases 6, 7, and 8, the recovery plots in Figure 6.11 for BWS overlay, regardless the different rock and fluid properties in those cases. Table 6.2 gives the results for heavy oils recovery showing a drastic, almost 40-percent, improvement in oil recovery after 30 years of production by using BWS.

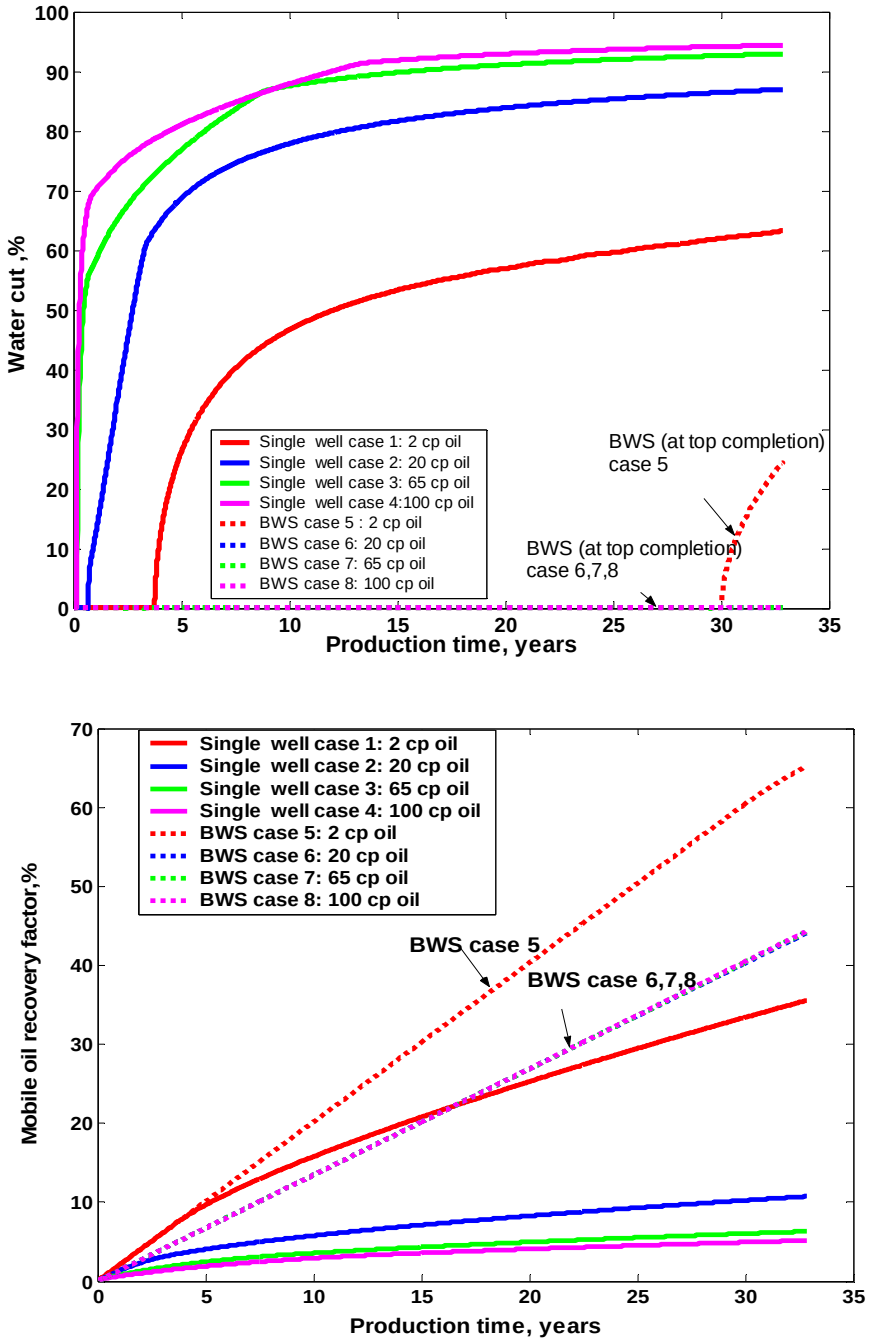

Figure 6.11 Simulation results of water cut and oil recovery

Table 6.2 Recovery factor comparison

Single horizontal well Mobile oil recovery factor %	BWS Mobile oil recovery factor %	Percent increase %
11 (case 2 Table 6.1)	44 (case 6 Table 6.1)	33
6 (case 3 Table 6.1)	44 (case 7 Table 6.1)	38
5 (case 4 Table 6.1)	44 (case 8 Table 6.1)	39

Simulation results of the water saturation distributions at the end of 30 years of the production life provides an interesting insight into the recovery mechanism with the two production methods – as shown in Figure 6.12.

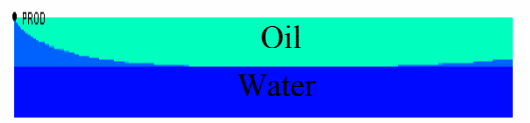

Case 2 (20 cp oil) single well

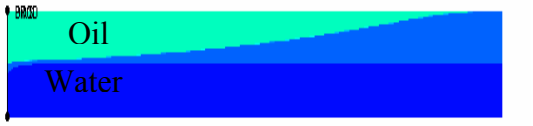

Case 6 (20 cp oil) BWS well

Case 3 (65 cp oil) single well

Case 7 (65 cp oil) BWS well

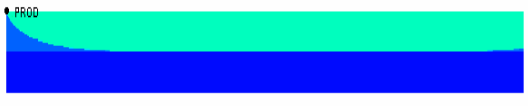

Case 4 (100 cp oil) single well

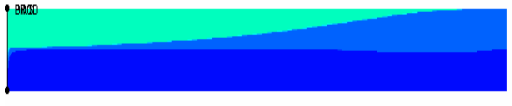

Case 8 (100 cp oil) BWS well

(A)

(B)

Figure 6.12 Simulation results of water advancement for single horizontal and BWS wells

The water cresting is a natural phenomenon that happens in a reservoir when the well is being produced. Water cresting is inevitable in single-well systems, irrespective how small the rates are (Figure 6.12 A). It causes the water to by-pass the oil, rendering the water drive mechanism inefficient. On the other hand, the simulation results of oil/water saturation distribution in BWS show that water cresting can be prevented (Figure 6.12 B). The results also imply that the "no water crest" relationship in Equation 5.14 for an open boundary case could be used for the designing BWS operation for a finite (closed) well drainage volume.

The simulation results also reveal that the water drive mechanism with BWS. The water crest is suppressed by simultaneously producing oil and water (no water crest solution), allowing the water to enter the oil pay zone at the edges of the drainage area and to displace oil towards the producing well. Thus, by converting the water by-passing oil situation in a single horizontal well to more favorable water drive condition, high oil recovery can be obtained (Table 6.2).

6.2.2 Comparison Recovery for BWS and Single Well - Analytical Analysis

In the proceeding section, recovery with BWS is compared to a single well by assuming that the oil-only rate from the top BWS lateral is the same as the liquid (oil + water) rate at the single well.

Unlike the flow behavior in a single horizontal well, in which the water-oil interface is moving vertically towards the well. The water-oil interface has kept its original horizontal position in the BWS flow system, while the interface acts as a streamline where only the components of velocity that are tangent to the interface are possible, while the normal components are zero. Thus, the interface can be considered as a no-flow boundary (Figure 6.13) and the flow potential distribution of a well draining between two no-flow boundaries is given in Appendix B.

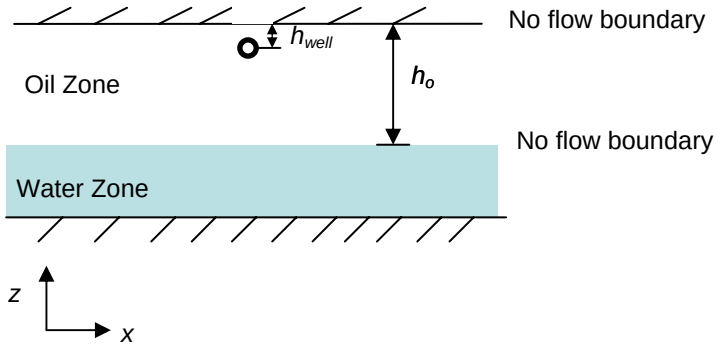

Figure 6.13 Boundary condition in BWS wells

The flow potential equation can be written as follows:

$$\Phi_{(x,z)} = \frac{q_l \mu_o}{4\pi k_o}\left[\ln(\cosh\frac{\pi x}{h_0} - \cos\frac{\pi(z-h_o+h_{well})}{h_0}) \times (\cosh\frac{\pi x}{h_0} - \cos\frac{\pi(z+h_o-h_{well})}{h_0})\right] + C \quad \text{..... (6.7)}$$

The new form of potential distribution can be used to determine how the reservoir potential drops for given selected rates in BWS. Knowledge of this potential drop will assist in reservoir development. Another important feature of Equation 6.7 is that the well productivity, which can be obtained as:

$$p_e - p_{wf} = q_l \frac{\mu_o}{k_o}\left[\frac{x_e}{2h_o} + \frac{1}{2\pi}\ln\frac{h_o}{2\pi r_w \sin\frac{\pi(h_o - h_{well})}{h_o}}\right]$$

$$J = \frac{q_l}{p_e - p_{wf}} = \frac{k_o}{\mu_o\left[\frac{x_e}{2h_o} + \frac{1}{2\pi}\ln\frac{h_o}{2\pi r_w \sin\frac{\pi(h_o - h_{well})}{h_o}}\right]} \quad \text{..... (6.8)}$$

The validity of the analytical potential solution is confirmed by numerical simulations for the cases 6, 7, and 8 presented Table 6.1. The analytical solutions are shown by circles, while the

solid lines represent the numerical simulation results (Figure 6.14). Again, the simulation results are obtained after a stabilized flow condition prevails in a reservoir. The results from these two approaches are very close, indicating a good agreement between analytical solutions and numerical simulations.

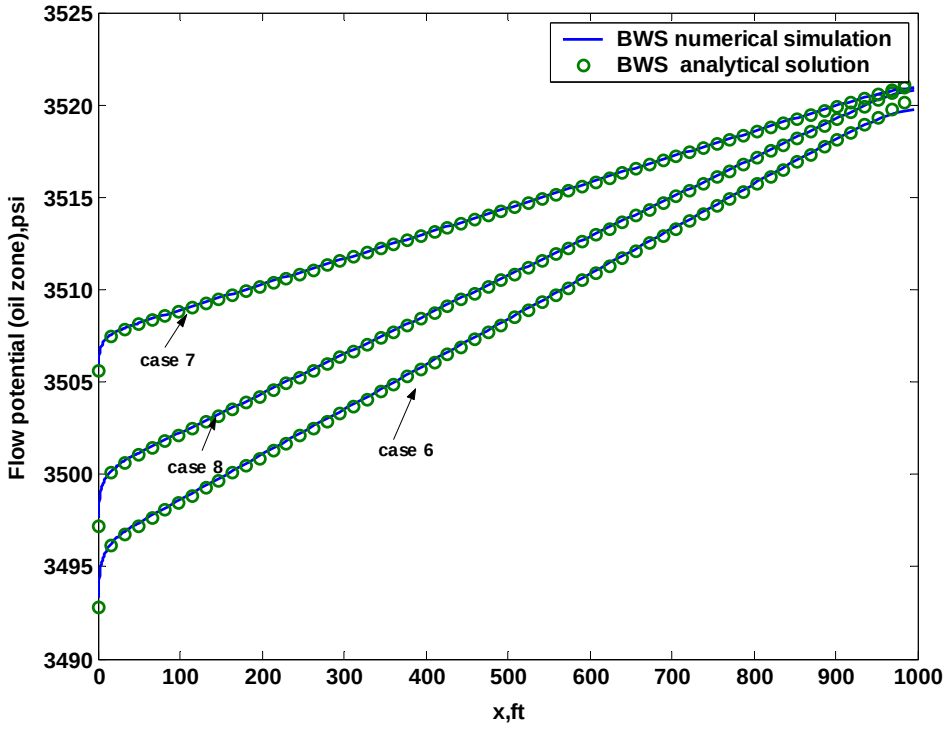

Figure 6.14 Oil flow potential distribution for analytical model and numerical simulation

Once the analytical BWS potential distribution model has been obtained, it is used to compare the BWS upper well performance to the performance of a single horizontal well by Equation 6.3.

Figure 6.15 plots oil potential distribution for the BWS flow system (case 7 in Table 6.1), in comparison to a single horizontal well flow system for case 3 in Table 6.1.

As discussed earlier Chapter 6.1.1, in a single horizontal well flow system the potential drop is concentrated close to the well within $x < x_i$. Beyond the distance x_i, the potential gradient is negligible compared with the gradient near the well. As a result, little oil moves and is therefore recovered from beyond this distance. In contrast, the potential drop in the BWS system

extends from the no-flow outer boundary to the wellbore. This study finds that the potential drop away from the wellbore is larger than the one in the vicinity of the well.

In Equation 6.8, the term $x_e/(2h_o)$ describes the linear flow far from the well and term $\ln\{h_o / [2\pi r_w \sin(\pi(h_o - h_{well}) / h_o)]\}/2\pi$ describes the radial flow near the well. Because the $x_e >> h_o$, the linear flow potential drop dominates the radial flow potential drop. In the linear flow system, for a well producing at constant liquid rate, the potential drop is directly proportional to the drainage distance (Equation 6.8). Because BWS enables the drainage distance extend from x_i ($x_i << x_e$) in a single well case to x_e at the outer boundary. As a result, the potential drop is much larger than that of a single horizontal well case (Figure 6.15). This finding is consistent with the simulation results of water and oil saturation distribution (Figure 6.12), which show that for the BWS the aquifer contributes in producing the whole reservoir by displacing the oil from the edges of the reservoir. BWS increases oil recovery compared to a single horizontal well because the drainage area has been increased and by-passed oil is reduced.

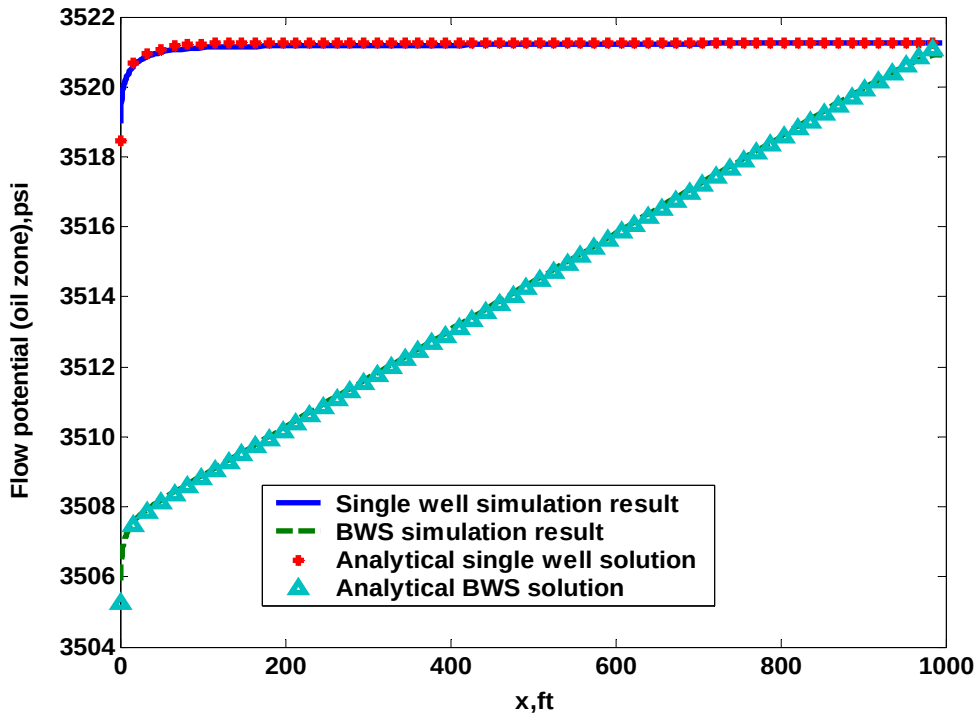

Figure 6.15 Oil potential profile comparison between single horizontal well and BWS

6.2.3 Allowance for the Effect of Capillary Transition Zone

The "no water crest" solution Equation 5.14 is derived for the case in which the effect of capillary transition zone is negligible and the oil and water are completely segregated. This assumption can be justified if the capillary transition zone h_{pc} is very thin in comparison to the reservoir thickness h_o. On the other hand, if the capillary transition zone is of the same order of magnitude as the reservoir thickness ($h_o \approx h_{pc}$), allowance must to be made to take the capillary transition zone effect into account.

The main assumption still pertains: the flow is under vertical equilibrium condition. Average relative permeability need to be generated to reducing the flow description to one dimension. Mathematically, the thickness averaged relative permeabilities are expressed as (Dake 1978):

$$\overline{k_{rw}}(\overline{S_w}) = \frac{\int_0^{h_w+h_{pc}} k_{rw}(S_w(z))dz}{h_w + h_{pc}} \quad \text{..... (6.9)}$$

$$\overline{k_{ro}}(\overline{S_o}) = \frac{\int_0^{h_o-h_{pc}} k_{ro}(S_w(z))dz}{h_o - h_{pc}} \quad \text{..... (6.10)}$$

Using the averaged permeability, the Dupuit Approximation representing the average flow along the centre line still can be used for selecting rates in BWS wells. The absolute permeability k_o and k_w in Equation 5.14 will be replaced by the thickness average permeability $k_o\overline{k_{ro}}$ and $k_w\overline{k_{rw}}$ respectively (Equations 6.9 and 6.10). Also the oil zone and water zone thickness h_o and h_w in Equation 5.14 will be replaced by $h_o - h_{pc}$ and $h_w + h_{pc}$ respectively. The verification was done by using numerical simulations.

The case considered is the same as presented in Table 6.1 case 8. Here, the only difference is that the rock relative permeability and capillary pressure are included (Figure 6.16).

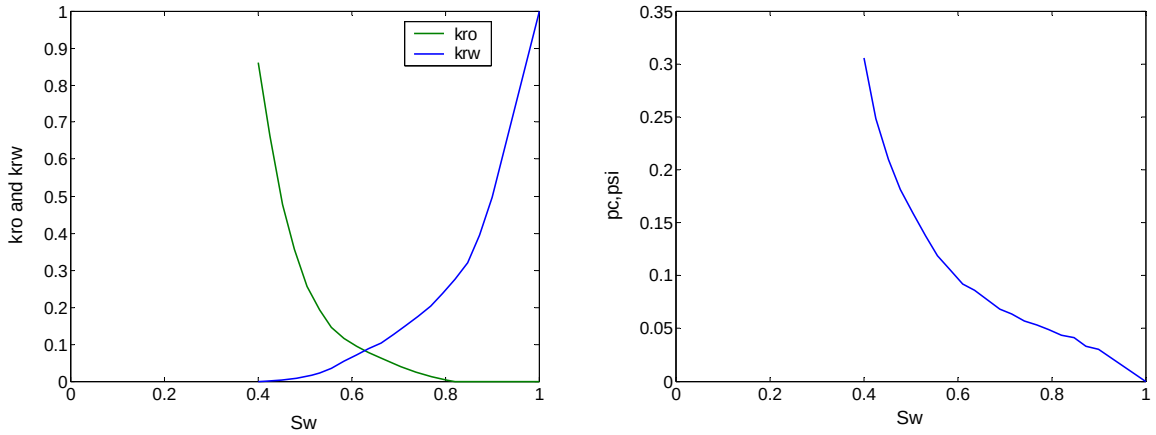

Figure 6.16 The input relative permeability and capillary pressure curve

The corresponding values of thickness averaged oil and water relative permeability can be solved by numerically integration of Equation 6.9 and 6.10 through a simple computer programming. The calculated results are $\overline{k_{ro}} = 0.8597$, $\overline{k_{rw}} = 0.899$.

Using the value of thickness average permeabilities and their corresponding oil zone thickness $h_o - h_{pc}$ and water zone thickness $h_w + h_{pc}$ in Equation 5.14, for the given oil rate $q_o = 0.12$ stb/d/ft, the new computed water rate becomes $q_w = 16.98$ stb/d/ft. The simulation results of oil and water saturation distribution at different production time are shown in Figure 6.17. It indicates that the water crest has been suppressed and laterally water displacement occurs similar to the results presented in Figure 6.12 (B) for BWS well without the capillary transition zone. With the averaged permeability the "no water crest" solution can be applied to the case when the capillary transition effect can not be ignored.

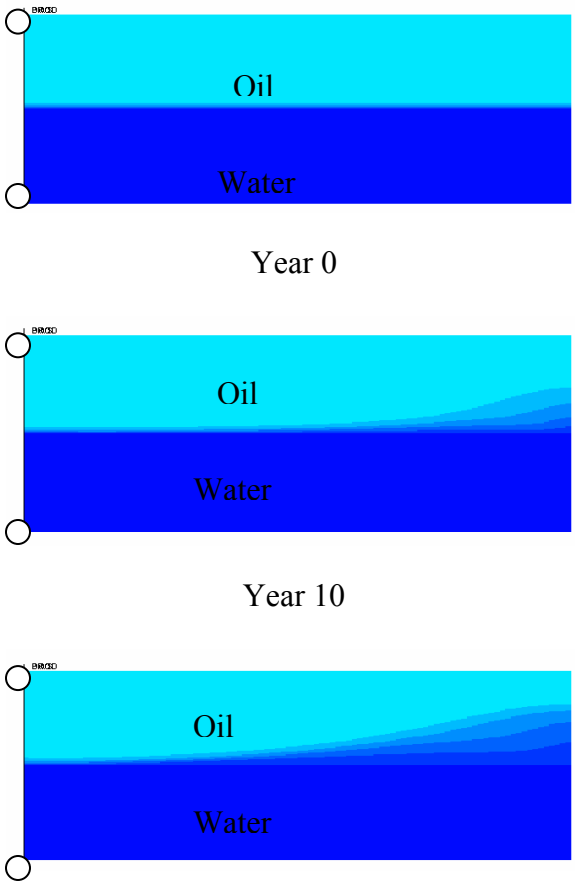

Figure 6.17 Simulation results of oil and water saturation distribution for BWS with capillary pressure considered

6.2.4 Procedure for Designing BWS Operation

So far, all the mathematical tools necessary to guide a heavy oil reservoir with bottom water drive developments have already been presented. They are summarized in Figure 6.18. The starting point in this flow chart is the decision whether to use a single horizontal well or BWS wells. If the calculated critical rate in single horizontal well is too small to be economically viable, one should consider BWS to increase primary oil recovery and reduce water contamination of oil. The sequence of the analytical design of the BWS operation is shown in Figure 6.18. Analytical estimation of bilateral water sink well rates assumes a sharp interface between oil and water, i.e., that flow is segregated. The calculated rates are used as input for the

numerical simulations. After the numerical simulation is matched with the predicted displacement process in BWS systems, it means water cresting has been prevented. One can use the numerical simulation to estimate water cut and the recovery factor or calculate it analytically (Equation 6.6). Alternatively, if the numerical simulation does not match with the analytical solution (Equation 5.14), meaning the effect of capillary transition zone can't be ignored, then the relative permeability curve and capillary transition zone may be taken into account. Because the reservoir is homogeneous and the flow is governed by vertical equilibrium, the saturation is distributed in accordance with the saturation-capillary rise function. Using the thickness averaged water and oil permeability (Equations 6.9 and 6.10) as an input into Equation 5.14 to recalculate the rates in the BWS operation scheme, a good match should be obtained by comparison with numerical simulation.

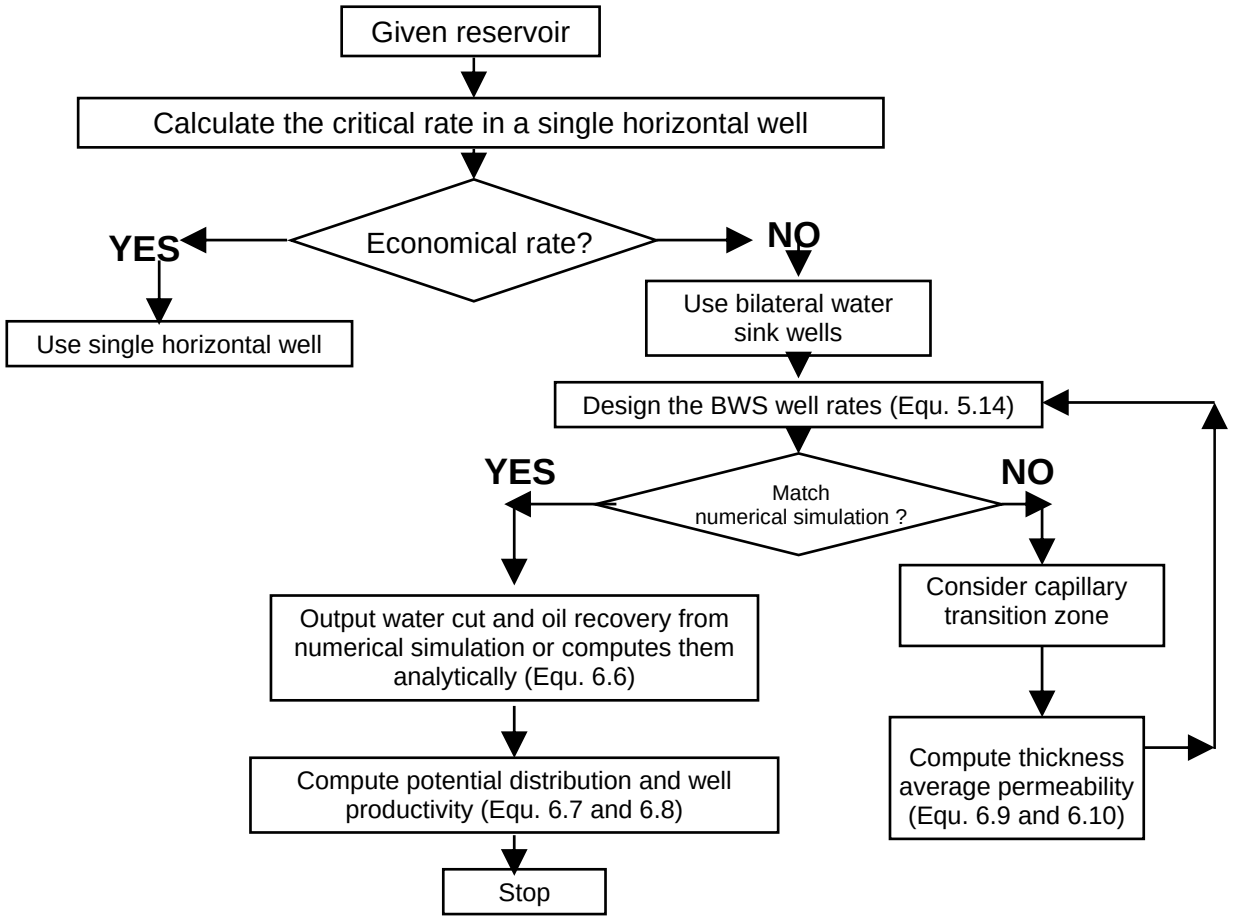

Figure 6.18 Flow chart of BWS operation procedure

6.2.5 Discussion of Recovery Mechanism

All the above comparisons between the single horizontal well and BWS are constrained with the top completion rate is the same. Another basis for comparison is to set the single well liquid rate equal to the sum of the top completion rate and bottom completion rate in BWS. Figure 6.19 shows the recovery comparison and water cut for case 8 (BWS with top rate equal to 0.12 stb/d/ft and bottom water drainage rate equal to 12.5 stb/d/ft) with single horizontal well producing at total rate q_l = 12.5 + 0.12 = 12.62 stb/d/ft, almost 100 times the BWS top rate. Higher fluid production rates for a single horizontal well would result in an increasing water-oil ratio, and immediate water production, with water cut rapidly increasing to 90 percent after 15 days. If we assume that a water cut of 95 percent is the economic limit, the well would have to be abandoned after only 42 days and the ultimate oil recovery is only 1.5 percent. However, allowing a single horizontal well to produce at a water cut above 95 percent will increase oil recovery (oil recovery for BWS equals 44 percent and oil recovery for single horizontal well is 48 percent) compared with that of BWS wells at the end of production life. The water saturation profile at different times is shown in Figure 6.20. Again, blue represents water and green represents oil. In a single horizontal well with high production rate, water breakthrough and water cresting is quickly established in less than 1 year with water cut at 99 percent. The oil recovery at breakthrough is very small. As the oil is being produced water flows across the outer boundary to displace some of the oil. The saturation profile at the end of production life demonstrates high oil recovery can be obtained through a high production rate if a high water cut (> 99 percent) can be tolerated.

Producing the horizontal well at a very high water cut may be impractical, especially for the offshore environment; at the economic limit the cost of the water lifting, treating and disposal

is equal to the profit from the oil. Producing a well with water cut above the economic limits will result in negative cash flow. At this point, the well would have to be abandoned.

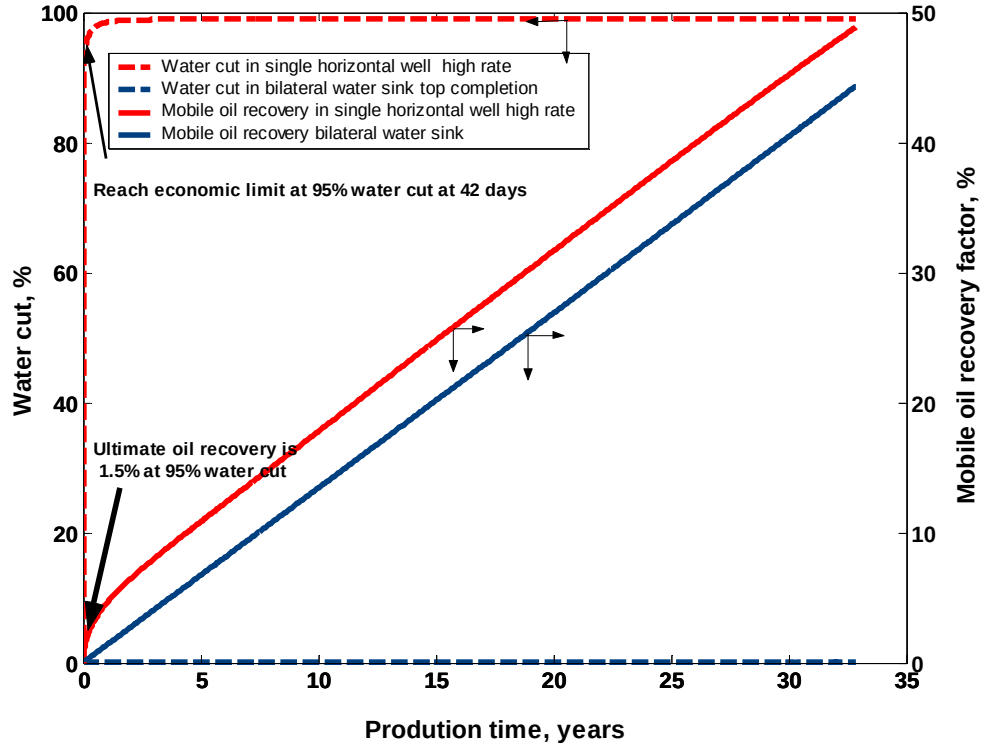

Figure 6.19 Water cut and mobile oil recovery in BWS compared with single horizontal well at high rate

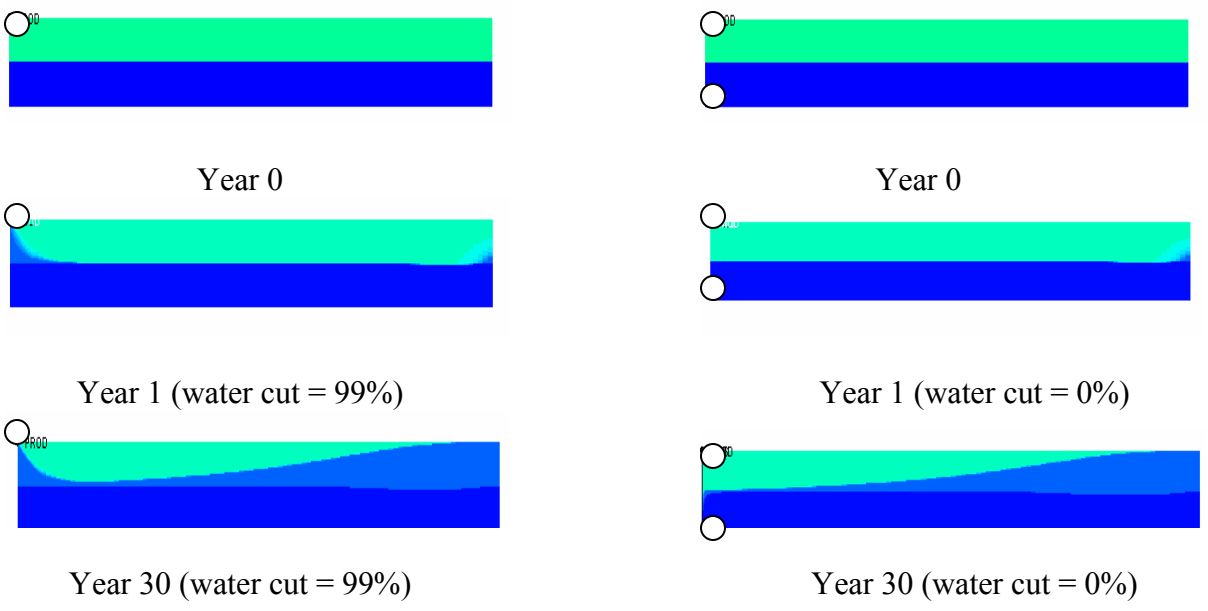

Single horizontal well (q_l=12.62 stb/d/ft) BWS (q_{top} = 0.12 stb/d/ft, q_{bottom} = 12.5 stb/d/ft)

Figure 6.20 Water saturation profile comparison (single well with high rate vs BWS)

Based on the literature (Aziz and Flores 1974; Miller and Rogers 1973), the ultimate recovery is determined this maximum water cut. For instance, for an offshore Louisiana light oil reservoir, the water cut economic limit at 1000 stb/d gross liquid rate is 94.4 percent (Miller and Rogers 1973), and in North Sea, the horizontal well GA-03 was shut down when the water cut reach 95 percent (Barratt et al. 2010). Another factor limiting the water cut arises from the difficulties in oil-water separation. The small density difference between oil and water results in emulsion of the heavy oil with water (Visser 1989). Emulsions present in production operations reduce oil/water separation efficiency, according to the Marlin field test (Euphemio et al. 2007), "even with the injection of de-emulsifier just upstream of the choke valve, only about ten percent of original water cut could be removed at the separator, operating with a retention time up to 20 minutes." Assuming the 95 percent water cut as an economic limit is a more optimistic value for heavy oil offshore due to the emulsion problem and the limited size of the production facilities.

In contrast, the BWS produces water-free oil at the top completion and clean water at the bottom completion. This avoids the oil-water separation and water treatment problems. In addition, even after 30 years oil is still being produced and the recovery factor is 44 percent (Figure 6.19). The reservoir can continue to produce oil until the water cut reaches its economic limits. But if the oil-water separation is available for very high water cuts (circa 99 percent), single horizontal well with high production rate achieve higher oil recovery compared with BWS.

6.3 BWS Application – Field Example

In this section, we use a field example to demonstrate the application of the BWS design procedure in Figure 6.18.

The example is an oil field in Bohai Bay, offshore China. Heavy oils account for 70 percent of the total oil resources in Bohai Bay. Figure 6.21 shows the locations of heavy oil fields under production phase.

Figure 6.21 Location of heavy oil fields in Bohai Bay

The oil field we are investigating is the NB35-2. It is located in the centeral area of Bohai Bay in a water depth of about 36 ft. It is a large offshore heavy oil field with an in-situ oil viscosity range from 43-260 cp. The oil field is geographically divided into 2 blocks: south and north. The oil is mainly produced from the Minghua (*Nm*) formation. The *Nm* formation is a fluvial reservoir with meandering channels, multiple sand body systems, and is subject to a strong bottom water drive. The development facilities include two platforms. The field commenced production in 2005. The field was originally developed with deviated wells. The primary reservoir development issue is to control the premature water breakthrough and reduce water cut. Horizontal wells have been used for delaying water breakthrough and improving well productivity in this field. Typically, the lateral section length of the wells would range from 800 ft to 1970 ft, with the average production rate 220 stb/d. Operating the horizontal well at minimum pressure drawdown (less than 72 psi) and placing the well at the top of the formation were considered to be effective ways to control water cresting. Separation of oil and water is also a problem in this field, as the well is considered to be a water out well at a water cut equal to 95 percent.

In spite of theoretical expectations, some wells in this field still show premature water breakthrough and rapid water rising. For example, the 1000-foot long horizontal well A, shown in Figure 6.22, started to produce on Feb, 2005 at constant liquid rate (85 stb/d).

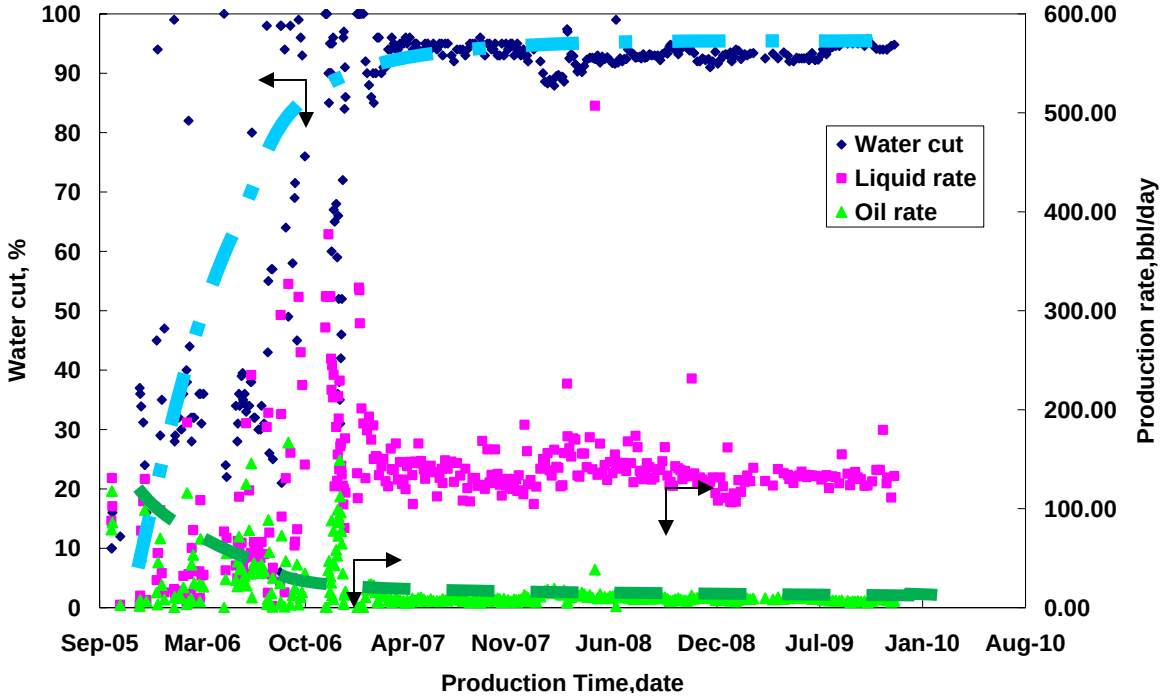

Figure 6.22 Performance of horizontal well A in Bohai Bay oilfield

The water breakthrough occurred almost immediately and the water cut increased to nearly 90 percent in two years. In April 2007, the operator increased the liquid rate to approximately 150 stb/d, and the water cut quickly jumped to 90 percent with a very low oil rate (14 stb/d). The operator attributed the ineffectiveness of the horizontal well in water cresting control to lacking a "flow barrier." Until 2010, the average water cut in the field was 72 percent, and 16 wells have been shut down because of high water cut, such as well B with 98 percent water cut, well C with 99 percent water cut and 100 percent water cut in well D.

We consider the BWS well technology to be a potential solution to the water problem in the Bohai Bay oilfield. The potential BWS advantage is the production of water-free oil above the economic rate without premature water breakthrough. The NB35-3 field example is used to

demonstrate how BWS would improve the well's productivity and oil recovery compared to a single horizontal well. We follow the production design procedure described in Figure 6.18. In the computations, we use input reservoir and fluid properties provided by the operator (Table 6.3).

Table 6.3 Input reservoir and fluids properties for Bohai Bay oilfield

Oil zone thickness	85 ft
Water zone thickness	44 ft
Reservoir Pressure	1540 psi
Bubble point pressure	788 psi
Horizontal permeability	986 md
Vertical permeability	986 md
Porosity	33 %
Oil density	56.49 lb/ft3
Water density	62.14 lb/ft3
Oil viscosity	44 cp
Water viscosity	0.96 cp
Oil compressibility	5×10^{-6} /psi
Water compressibility	3×10^{-6} /psi
Rock compressibility	4×10^{-6} /psi
Connate water saturation	0.34
Residual oil saturation	0.2
Oil relative permeability exponent	1
Water relative permeability exponent	1
Reservoir lateral extent	1000 ft
Well length	1528 ft

Step 1: Calculate the Critical Rate in a Single Horizontal Well and Make Decision

The first step for calculating the critical rate in a single horizontal well is to compute the actual drainage distance x_i using Equation 6.4. The potential distribution is presented in Figure 6.23, for a well producing at 220 stb/d (current average production rate in this field).

The effective drainage distance can be approximated as 200 ft. Then, the time-dependent critical rate is calculated by following procedure from 6.1.2, shown in Figure 6.24. It can be seen that the critical rate is very small – at a maximum 55 stb/d, thus justifying the use of BWS for economic development of this reservoir.

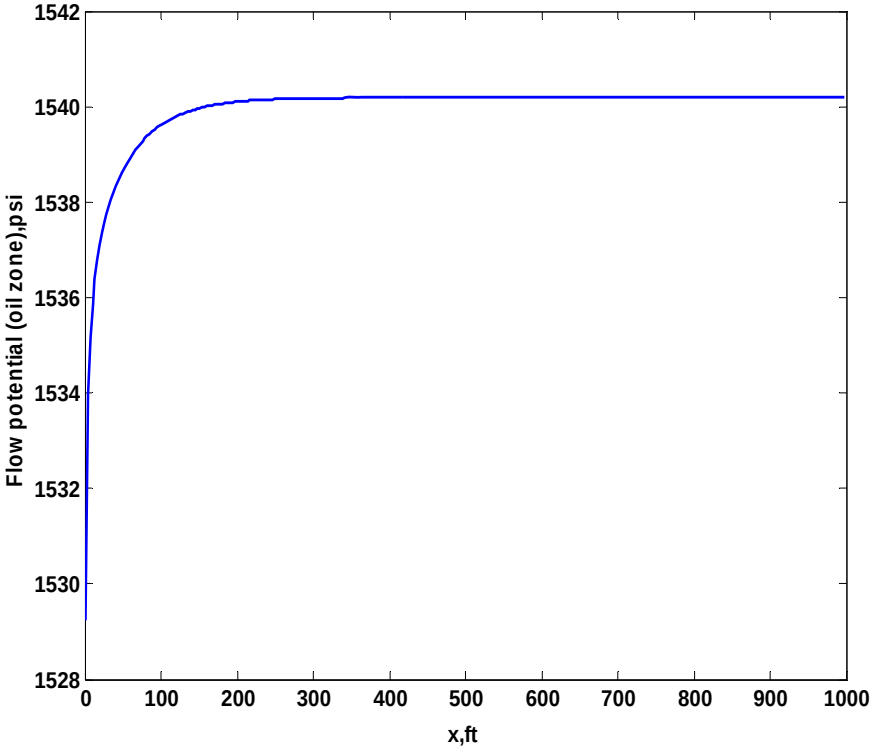

Figure 6.23 Flow potential computed using Equation 6.3

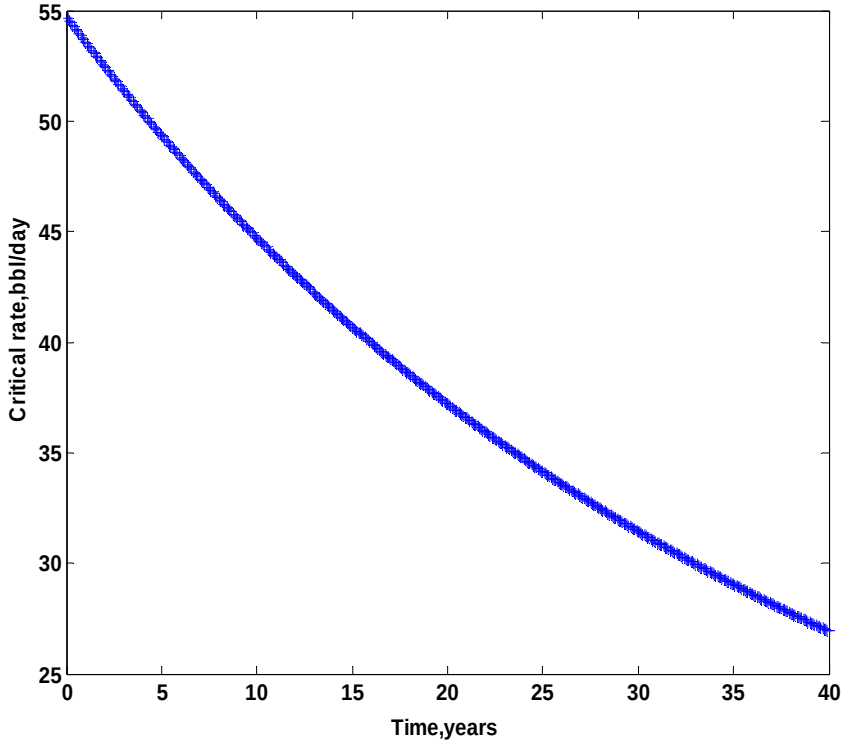

Figure 6.24 Time-dependent critical production rate for well A from Equation 4.42

Step 2: Design BWS Well Rates

Finding production rates for a BWS well is an optimization problem. As shown above, the recovery mechanism with BWS involves an initial long period when the thickness of the oil pay zone is practically constant and water invasion and oil displacement occurs laterally at the periphery of the reservoir. During that period, the oil production and water drainage rates are also constant. Later, the displacement becomes vertical with the OWC moving upwards, which requires a variable rate approach. In this example, we use a simplified approach by searching for a constant-rate strategy and considering only two cases. Each case compares BWS with a single well operation at the same rate of production from the oil pay zone. Water production is not considered in the procedure, as it is aimed strictly at comparing the recovery rather than the economics.

Four cases are considered. To understand the typical production characteristics of a horizontal well in this field, case 1 represents the current production condition where a well producing at a constant liquid rate ($q_l = 220$ stb/d) in a l528 ft long horizontal section, which is equivalent to 0.144 stb/d/ft. Case 2 is defined as the case where production rate is increased by 2 fold, to test the idea of a well producing at a high rate for high ultimate oil recovery. Case 3 and case 4 are for BWS application, corresponding to case 1 and case 2 respectively. The production rates and their corresponding water rate computed from Equation 5.14 in those cases are summarized in Table 6.4.

Table 6.4 Input production rate for simulation runs

	Liquid production rate (Top completion) stb/d/ft	Water drainage rate (Bottom completion) stb/d/ft
Case 1 (single well)	0.144	0
Case 2 (single well)	0.288	0
Case 3 (BWS)	0.144	3.4
Case 4 (BWS)	0.288	6.8

The reservoir simulation model is the same as presented in Figure 6.9. The straight-line relative permeability curve is used since we assume the oil and water are segregated with a sharp interface. Capillary pressure has been ignored. If relative permeability and capillary pressure effects need to be taken into account, then replace the end point permeability in Equation 5.14 by average permeability with respect to thickness for calculating the rates. In all of those cases, the reservoir is considered to be homogeneous, which is the least favorable condition for a bottom water drive reservoir. This is because the flow barriers would generally have some effect on delaying the water breakthrough.

Step 3: Compute Recovery Factor

Simulation results of water cut and recovery factors are shown in Figure 6.25 and Figure 6.26 respectively. Figure 6.25 demonstrates the ineffectiveness of horizontal wells for mitigating water cresting problems. For case 1 in Table 6.4, water breakthrough occurred after 3 years of production and the water cut quickly climbed to over 50 percent. This contaminated oil production with a large quantity of water production not only causes the problem of oil-water separation on the rig, but also the oil recovery is limited by excessive water production. Only 15 percent oil has been recovered after 30 years of production. Case 2 (Table 6.4) aims at achieving a profitable oil rate and accelerating recovery by producing at higher rate. However, high pressure drawdown is needed for a high rate, resulting in a more severe water cresting problem. Water breakthrough happened in less than a year and a high value of water cut (above 80 percent) remains for over 25 years. Even though the oil is produced at rates two times larger than that of case 1, the recovery factor (16 percent) stays nearly the same as that in case 1 (Figure 6.26). That implies that the high production does not facilitate a high percentage oil recovery in a shorter time period due to the water cresting problem. To maintain a sufficiently high production

rate to justify development, BWS is applied for this field as a potential solution for economic development of offshore heavy oils.

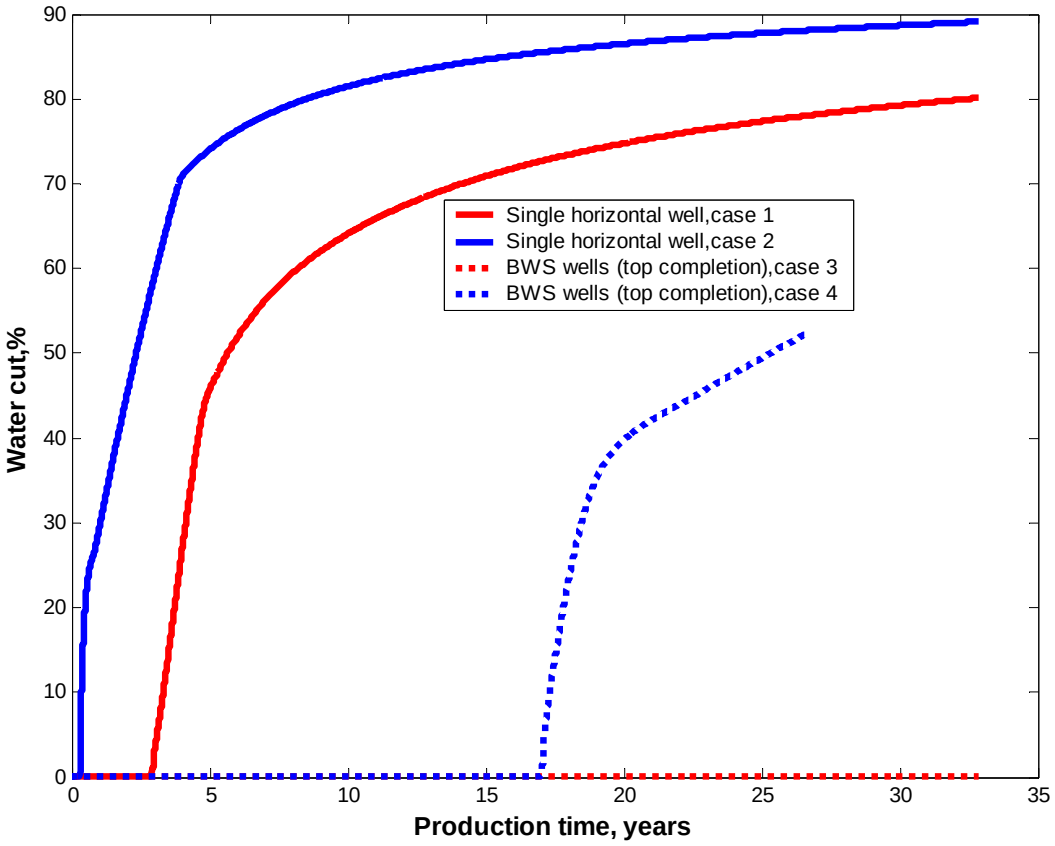

Figure 6.25 Comparison of water cut for BWS and single wells (field cases)

The plots in Figure 6.25 also show that the use of BWS could lead to successful avoidance of water breakthrough at top completion for the entire production life (case 3,Table 6.4) and more than 15 years of water free production (case 4, Table 6.4). In terms of recovery factor (Figure 6.26), case 3 achieves a 40 percent recovery factor at 30 years of production duration and case 4 obtains almost the same recovery factor of 40 percent in a shorter time period (15 years) at the water breakthrough time. Compared with a single horizontal well in

which recovery is 15 percent, BWS allows more oil to be recovered and less water being produced. The straight line recovery line is equal to the value calculated using Equation 6.6.

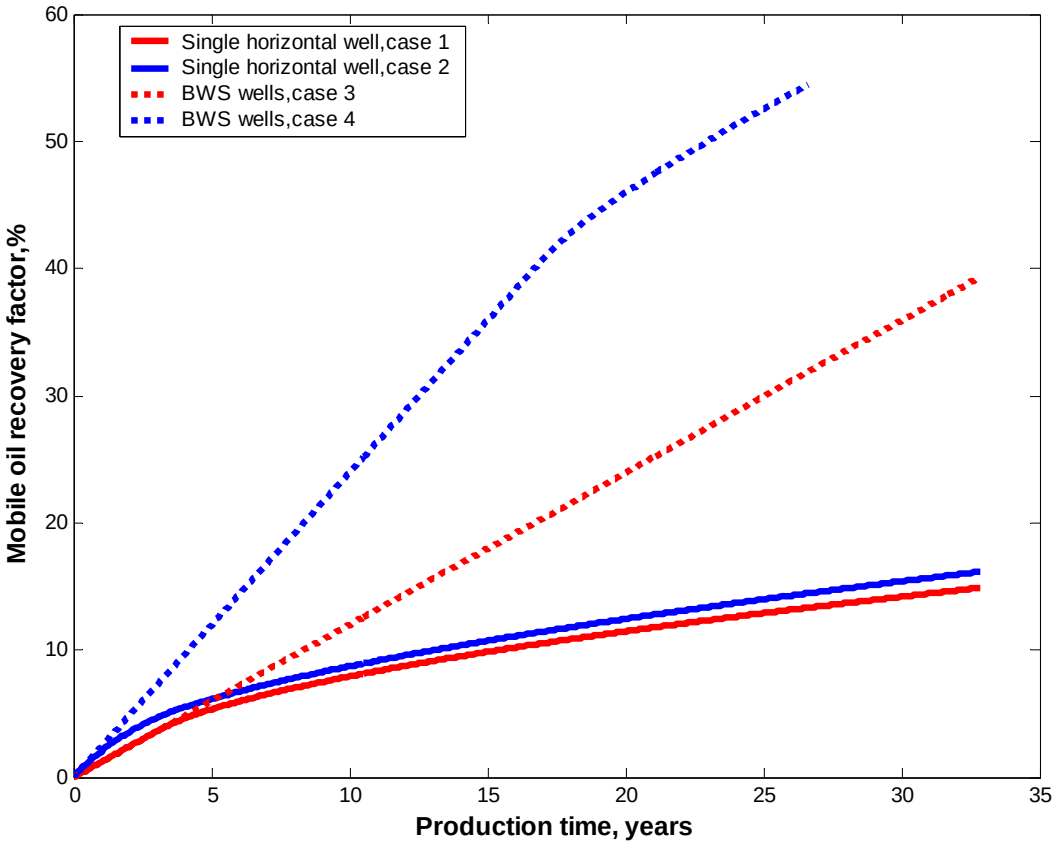

Figure 6.26 Comparison simulation results of recovery factors for BWS and single well (field case)

Step 4: Compute Potential Drawdown and Productivity Index

Potential drawdown at the well and productivity index are an operational parameters of interest to the operator. The flow potential in the oil zone is computed using Equation 6.7, and matched with numerical simulations (Figure 6.27). The well index can be calculated using Equation 6.8 J = 220 (stb/d) / (1540-1498) psi = 5.23 stb/d/psi, which is a direct measure of well performance. The flow potential in the oil shows that BWS extends the drainage area and imposing larger potential drawdown for oil production from the whole reservoir.

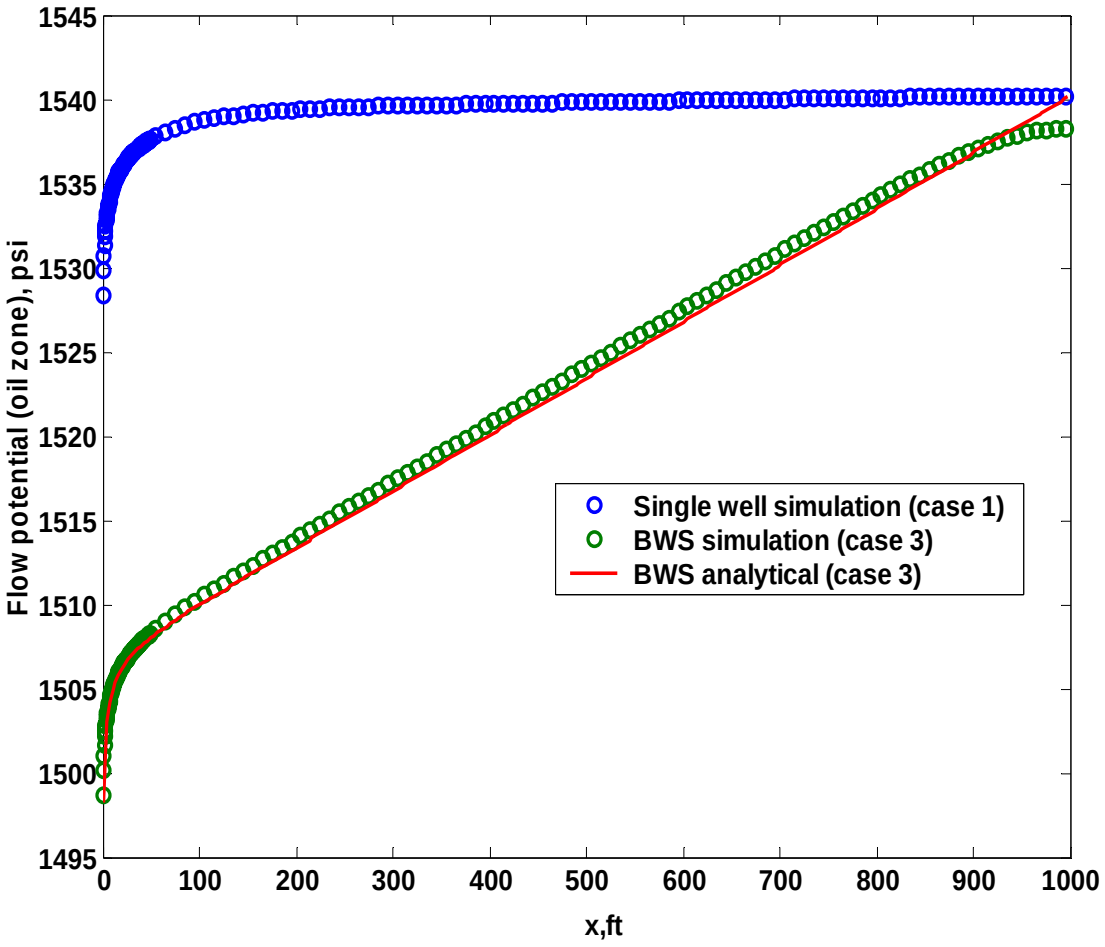

Figure 6.27 Flow potential in the oil zone: analytical (Equation 6.7) vs. numerical simulations

As discussed above, BWS would converts the water-bypassing oil through water cresting to an edge water drive system (Figure 6.28). With the BWS well, water cresting is totally suppressed, so that higher sweep efficiency and high oil recovery are obtained. Water breakthrough in case 4 (shown in Figure 6.28) is due to the high mobility ratio. Water under-runs the oil in the form of a water tongue and eventually breaks into the well, which is typical in the edge water drive system (Dake 1978). If water cresting is eliminated, a high oil production rate can lead to more oil recovery in a relatively shorter time span. In this application, operator would use a high-volume artificial lift method to increase water-free oil production rates and accelerate oil recovery.

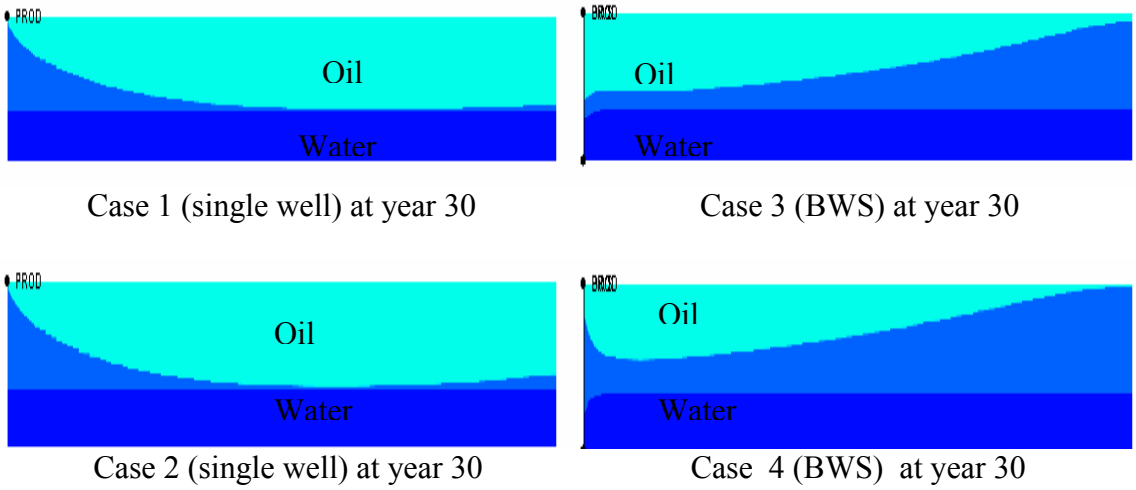

Figure 6.28 Comparison of water invasion to oil pay zone for BWS and single wells after 33 years of production

6.4 High Rate Production with Single Horizontal Well in Bohai Bay Field

This section presents a possible alternative to BWS when a single horizontal well produces at the total rate equal to the sum of the top and bottom rates of BWS for case 3 in Table 6.4. As presented before one can improve oil recovery by producing a single well at high rate; here we consider the case when the single well produces at the rate (q_l = 3.544 stb/d/ft) equal to the sum of the top (q_{top} = 0.144 stb/d/ft) and bottom BWS rates (q_{bottom} = 3.4 stb/d/ft). The water cut and mobile oil recovery are shown in Figure 6.29. It shows the high production rate strategy causes water cut to quickly approach economic limits in less than 5 years and shorten the well life. Ultimate oil recovery is only 9 percent by producing the well at such a high production rate. On the other hand, BWS allows a big improvement in oil recovery by reducing the water cut at top completion from over 90 percent (single horizontal well) to zero.

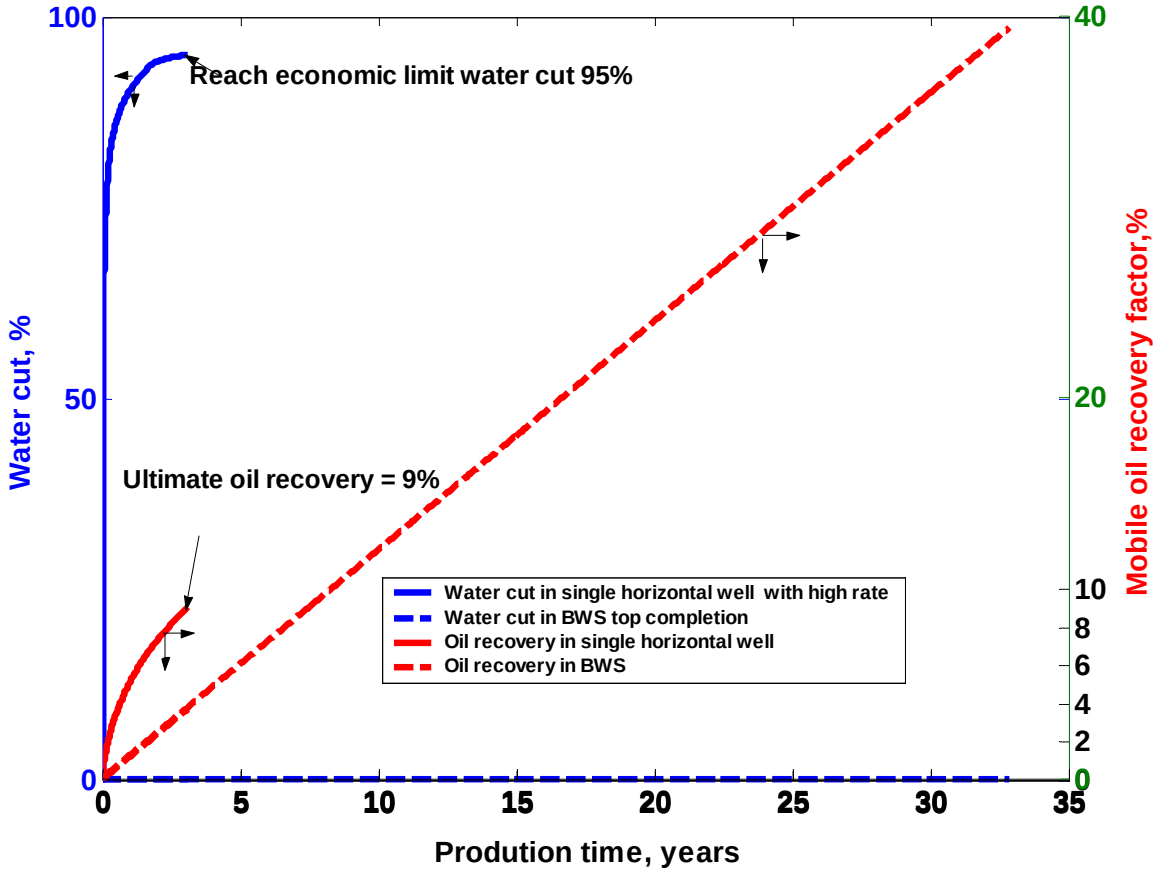

Figure 6.29 Simulation results of water cut and mobile oil recovery comparison (field case)

6.5 Summary

This chapter has shown the application of critical rate models for single and BWS wells to recover heavy oil from actual (bounded) reservoirs with bottom water. It has demonstrated that the BWS analytical model for "no water crest" design can be used in the bounded drainage areas with certain well spacing as long as constant potential at the boundaries between the wells is maintained by a strong bottom aquifer.

The chapter also presents a comparison of the oil recovery process with BWS and single wells using simulations of water invasion to the oil pay zone and distributions of flow potential calculated analytically from a new model. Together with the evidence from numerical simulation, the analytical models reveal that BWS allows high oil recovery through complete

suppression of water cresting. Only through that, can the water by-passing oil due to water cresting be prevented. Also water provides an effective displacement from the edge of the reservoir. High oil recovery is obtained because the by-passed oil is largely reduced.

The BWS design procedure and a flowchart has been provided. The procedure helps to determine the BWS well rates for a required value of the water-free oil production rate from the oil pay zone. The desired oil rate for BWS accelerates recovery and improves asset value. The rate could be optimized, but that was not done in this study. The presented field example describes BWS application and indicates its potential success in the development of heavy oil with bottom water in the Bohai Bay oilfield. For this reservoir, with a severe water problem (current water cut of 72 percent, and expected recovery of 15 percent), BWS might increase oil recovery to over 40 percent without water breakthrough.

The study also shows the inability of the current single-well technology to produce at high fluid rates comparable with the total (oil + water) rate of the BWS wells. Although theoretical recovery at those high rates would slightly exceed that with BWS (by 5 percent in the case presented), the water cut value would exceed the maximum water cut of circa 95 percent for economic profitability and effective separation of oil from water.

CHAPTER 7. CONCLUSIONS AND RECOMMENDATIONS

7.1 Conclusions

1. Early water breakthrough, rapid water cut increase after breakthrough, and a small displaced oil region are the main causes of poor recovery of heavy oil in reservoirs underlain by strong water drives.
2. Operating wells at or below the critical rate can avoid early water breakthrough, but it fails to improve the ultimate oil recovery because the displaced oil region still comprises a small fraction of the well pattern.
3. Existing analytical models for critical rate prediction either oversimplify the boundary condition or misrepresent the boundary, leading to misestimation of the critical rate in single horizontal wells.
4. A new analytical model using the hodograph method yields improved estimates of critical rates. However, it is too complex to use in design calculations. Nonetheless, it provides a useful validation method for further approximations.
5. The Dupuit approximation provides a simple, efficient, and accurate method to predict critical rate. However, previous forms of the Dupuit approximation only apply to the cases where the well is within the top one-third of the reservoir.
6. An analytical model derived in this study combined the Dupuit approximation with a model for convergence of flow near the wellbore. This model gives a more general and accurate solution for critical rate determination for a single horizontal well at any position in the reservoir (not restricted to the top one-third).

7. The new critical rate model shows that the BWS can significantly increase the critical rate. Subject to the water drainage rate, critical rate in BWS can show increases as large as several fold compared with that in a single horizontal well.
8. An analytic "no water crest" solution is derived to provide guidelines to select the appropriate oil and water rates to maximize oil recovery.
9. The "no water crest" solution can design BWS systems with water free oil production at top completion and high oil recovery factor. The principal mechanism is enlargement of the displaced region (compared with single well cases). This allows the water drive to displace oil to the horizontal oil completion.

7.2 Recommendations

1. There is a need to study and evaluate the well placement with the BWS performance, to find the optimum well placement for BWS.
2. A study on the application of BWS with thermal methods should be performed, in which aquifers impact the steam flood operations negatively resulting in higher than desired steam chest pressures. BWS can lower the steam chest pressure, making more latent heat available.
3. An economic study should be conducted to determine the economic limits for BWS production and the profit margin.

REFERENCES

Alboudwarej, H., Felix, J., et al. 2006. Highlighting Heavy Oil. Oilfield review 18(2): 34-53.

Ali, S. M. F. 1974. Heavy Oil Recovery - Principles, Practicality, Potential and Problems. Paper SPE 4935, the Rocky Mountain Regional Meeting of the Society of Petroleum Engineers of AIME, Billings, Mont. May 15-16.

Ali, S. M. F. 1986. Prospects Of EOR Techniques In Saskatchewan Oil Reservoirs. The Journal of Canadian Petroleum Technology 25(2): 64-67.

Ali, S. M. F., Jones, J.A., Meldau, R. F. 1997. Practical Heavy Oil Recovery, University of Alberta, Edmonton, Alberta, Canada.

Ansari, R. Z. 2006. Superposition of Analytical Coning Solutions, The university of Texas at Austin. Master.

Aziz, K., Govier, G.W. and Fogarasi, M. 1972. Pressure Drop in Wells Producing Oil and Gas. Journal of Canadian Petroleum Technology 11(3): 38-47.

Aziz, K., and Flores, J. 1974. Influence of Production Rate and Oil Viscosity on Water Coning. 25th Ann. Tech. Meeting of the Petroleum Sciety of CIM, Calgary, Alberta. May7-10.

Barratt, T., Goldsworthy, B., et al. 2010. A Case History: The Installation of a Damaged Control Line Replacement Safety Valve System in a North Sea Well. Paper SPE 134500, SPE Annual Technical Conference and Exhibition, Italy, Florence, September 19-22.

Bear, J. 1972. Dynamics of fluids in porous media. New York, American Elsevier.

Bear, J. and Dagan, G. 1964. Some Exact Solutions of Interface Problems by Means of the Hodograph Method. J. Geophys. Res. 69(8): 1563-1572.

Bezerra, M. F. C., Jr, C. P., et al. 2004. The Appraisal and Development Plan for the Heavy Oil Jubarte Field, Deepwater Campos Basin, Brazil. Paper SPE 16301-MS, Offshore Technology Conference, Houston, Texas, U.S.A. May 3-6.

Butler, R. M. and Mokry, I. J. 1993. Closed-Loop Propane Extraction Method For The Recovery Of Heavy Oils And Bitumens Underlain By Aquifers: The Vapex Process. Paper SPE SS-93-35, Technical Meeting / Petroleum Conference Of The South Saskatchewan Section, Regina, October 18-20.

Bunton, M. A. 1999. Vacuum Jacketed Tubing: Past, Present, and Future. Paper SPE 55994, SPE Western Regional Meeting. Anchorage, Alaska. May 26-28.

Chaperon, I. 1986. Theoretical Study of Coning Toward Horizontal and Vertical Wells in Anisotropic Formations: Subcritical and Critical Rates.Paper SPE 15377, SPE Annual Technical Conference and Exhibition, New Orleans, Louisiana, October 5-8.

Chen, H.-K. 1993. Performance of Horizontal Wells, Safah Field, Oman. Paper SPE 25568, Middle East Oil Show, Bahrain, April 3-5.

Coats, K.H., Dempsey, J.R., Henderson, J.H. 1971. The Use of Vertical Equilibrium in Two Dimensional Simulation of Three Dimensional Reservoir Performance. Soc. Pet. Eng. J. 11(1):63-71.

Coats, K.H., Nielsen, R.L., et al. 1967. Simulation of Three Dimensional, Two Phase Flow in Oil and Gas Reservoirs. Soc. Pet. Eng. J. 7(4):377-388.

Curtis, C., Kopper, R., et al. 2002. Heavy-Oil Reservoirs. Oilfield review 14(3): 30-51.

Dake, L. P. 1978. Fundamentals of Reservoir Engineering, Elsevier.

Diaz, B. M., Tremblay, B., et al. 2002. Optimizing Sand Production Through Horizontal Well Slots in Primary Production ™. Paper SPE 2002-192, Canadian International Petroleum Conference, Calgary, Alberta, June 11-13.

Dietrich, J. K. 1990. Steamflooding in a Waterdrive Reservoir: Upper Tulare Sands, South Belridge Field. SPE Reservoir Engineering 5(3): 275-284.

Dikken, B. J. 1990. Pressure Drop in Horizontal Wells and Its Effect on Production Performance. SPE Journal of Petroleum Technology 42(11): 1426-1433.

Dupuit, J. 1863. Theoretical and Practical studies on underground water movement. Pairs.

Dusseault, M. B. 2006. Sequencing Technologies to Maximize Recovery. Paper SPE 2006-135, Canadian International Petroleum Conference, Calgary, Alberta, June 13-15.

Efros, D. A. 1963. Study of multiphase flows in porous media. Gastoptexizda, Leningrad.

Euphemio, M., Oliveira, R., et al. 2007. Subsea Oil/Water Separation of Heavy Oil: Overview of the Main Challenges for the Marlim Field--- Campos Basin. Offshore Technology Conference, Houston Texas, U.S.A. 30 April-3 May.

Fram, J. H. and Palermo, R. M. 1996. "Closing the Flood Gates" - History of the South Belridge Field Steam Drive Aquifer Project. Paper SPE 35660, SPE Western Regional Meeting, Anchorage, Alaska, May 22-24.

Geilikman, M. B., Dusseault, M. B., et al. 1994. Fluid Production Enhancement by Exploiting Sand Production. Paper SPE 27797, SPE/DOE Improved Oil Recovery Symposium, Tulsa, Oklahoma, April 17-20.

Giger, F. M. 1989. Analytic Two-Dimensional Models of Water Cresting Before Breakthrough for Horizontal Wells. SPE Reservoir Engineering 4(4): 409-416.

Giger, F. M., Reiss, L. H., et al. 1984. The Reservoir Engineering Aspects of Horizontal Drilling. Paper SPE 13024, SPE Annual Technical Conference and Exhibition, Houston, Texas, September 16-19.

Guo, B. and Lee, R. L. 1992. Determination of Maximum Water-Free Production Rate of a Horizontal Well with Water/Oil/Interface Cresting. Paper SPE 24324, SPE Rocky Mountain Regional Meeting, Casper, Wyoming, May 18-21.

Gupta, V., Barrio, C. and Mahrooqi, A. K. 2008. Lessons Learnt and Experiences Gained in Developing Heavy Viscous Oil Field Using Pattern Waterflood: Case History if a Field in South Oman. Paper IPTC 12159, International Petroleum Technology Conference, Kuala Lumpur, Malaysia, December 3-5.

Hamel, G. 1934. Über Grundwasserströmung. (Abhandlungen zur Hydrodynamik II.). ZAMM - Journal of Applied Mathematics and Mechanics / Zeitschrift für Angewandte Mathematik und Mechanik 14(3): 129-157.

Henry, H. 1959. Salt Intrusion into Fresh-Water Aquifers. J. Geophys. Res. 64(11): 1911-1919.

Hooghoudt, S. B. 1973. Bijdragen tot de kennis van eenige natuurkundige grootheden van de grond, 6 Bepaling van de doorlatenheid in gronden van de tweede soort; theorie en toepassing van de kwantitative strooming van het water in ondiep gelegen grondlagen vooral in verband met ontwaterings- en infiltratievraagstuken. Versl. Landbouwk 43: 461-676.

Houpeurt, A. 1975. Elements of fluid mechanics in porous media. Paris.

Huang, B. S., Marcum, B.E., et al. 1997. Cold Production of Heavy Oil from Horizontal Wells in the Frog Lake Field. Paper SPE 37545, SPE International Thermal Operations & Heavy Oil Symposium, Bakersfield, California, February 10-12.

Inikori, S. O. and Wojtanowicz, A. K. 2002. New Concepts of Dual-Completion for Water Cresting Control and Improved Oil Recovery in Horizontal Wells. Paper SPE 77416, SPE Annual Technical Conference and Exhibition, San Antonio, Texas, September 29-October 2.

Jayasekera, A. J. and Goodyear, S. G. 2000. The Development of Heavy Oil Fields in the United Kingdom Continental Shelf: Past, Present, and Future. SPE Reservoir Evaluation & Engineering 3(5): 371-379.

Jespersen, P. J. 1989. Horizontal well application at the Tangleflags North Steam Flood Pilot Project The Petroleum Society Heavy Oil Special Interest Group, Calgary, April 20.

Jespersen, P. J. and Fontaine, T. J. 1991. The Tangleflags North Pilot A Horizontal Well Steamflood. Paper SPE SS-92-4, Technical Meeting / Petroleum Conference Of The South Saskatchewan Section, Regina, October 7-9.

Joshi, S. D. 1988. Augmentation of Well Productivity With Slant and Horizontal Wells (includes associated papers 24547 and 25308). SPE Journal of Petroleum Technology 40(6): 729-739, 942-943.

Joshi, S. D. 1991. Thermal Oil Recovery With Horizontal Wells (includes associated papers 24403 and 24957). SPE Journal of Petroleum Technology 43(11): 1302-1304.

Joshi, S.A. 1991. Horizontal Well Technology, PennWell Books, Tulsa, OK.

Joshi, S. D. 1994. Horizontal Wells: Sucesses and Failures. Journal of Canadian Petroleum Technology 33(3):15-17.

Jr, B. D., Siqueira, C. A. M., et al. 2007. Jubarte Field-Development Strategy. Paper SPE 19088-, Offshore Technology Conference, Houston, Texas, April 30-May 3.

Ju, B., Dai, S., et al. 2005. An Effective Method to Improve Recovery of Heavy Oil Reservoir with Bottom Water Drive. Paper SPE 10521-MS, International Petroleum Technology Conference, Doha, Qatar, November 21-23.

Karmaker, K. and Maini, B. B. 2003. Applicability of Vapor Extraction Process to Problematic Viscous Oil Reservoirs. Paper SPE 84034, SPE Annual Technical Conference and Exhibition, Denver, Colorado, October 5-8.

Kasraie, M. and Ali, S. M. F. 1987. Steamflooding Bottom Water Reservoirs. Paper SPE SS-87-5, Technical Meeting / Petroleum Conference Of The South Saskatchewan Section, Regina, October 6-8.

Kidder, R. E. 1956. Flow of Immiscible Fluids in Porous Media: Exact Solution of a Free Boundary Problem. Journal of Applied Physics 27(8): 867-869.

Konieczek, J. 1990. The Concept of Critical Rate in Gas Coning and Its Use in Production Forecasting. Paper SPE 20722, SPE Annual Technical Conference and Exhibition, New Orleans, Louisiana, September 23-26.

Kuchuk, F. J., Goode, P. A., et al. 1991. Pressure-Transient Behavior of Horizontal Wells With and Without Gas Cap or Aquifer. SPE Formation Evaluation 6(1): 86-94.

Kuo, M. C. T. 1983. A Simplified Method for Water Coning Predictions. Paper SPE 12067, SPE Annual Technical Conference and Exhibition, San Francisco, California, October 5-8.

Kuo, M. C. T. 1989. Correlations rapidly analyze water coning. Oil and Gas Journal: 77-80.

Lillie, W. H. E. and Springer, F. P. 1981. Status of the Steam Drive Pilot in the Georgsdorf Field, Federal Republic of Germany. SPE Journal of Petroleum Technology 33(1): 173-180.

Liu, Y., Yang, H., et al. 2010. Improve Offshore Heavy Oil Recovery by Compound Stimulation Technology Involved Thermal, Gas and Chemical Methods. Paper SPE 20907, Offshore Technology Conference, Houston, Texas, May 3-6.

Marcio, F.C., et al. 2004. The appraisal and development plan for the heavy oil Jubarte field, Deepwater Campos Basin, Brazil. Paper SPE 16301, Offshore Technology Conference, Houston, Texas, May 3-6.

Mattax, C. C. and Dalton, R. L. 1990. Reservoir simulation, Monograph Vol.13, Society of Petroleum.

McCarthy, J. F. 1993. Improved model of water cresting. The ANZIAM Journal 35(02): 207-222.

Meyer, H. I. and Garder, A. O. 1954. Mechanics of Two Immiscible Fluids in Porous Media. Journal of Applied Physics 25(11): 1400-1406.

Miller, R.T., and Rogers. W. L. 1973. Performance of Oil Wells in Bottom Water Drive Reservoirs: Paper SPE 4633, 48th Ann. Fall Meeting, Soc. of Petroleum Engineers, AIME, Las Vegas, Nev. September 30-October 3.

Murphy, P. J. 1990. Performance of Horizontal Wells in the Helder Field. SPE Journal of Petroleum Technology 42(6): 792-800.

Muskat, M. 1937. Flow of Homogeneous Fluids Through Porous Media, McGraw-Hill Book Co., New York.

Muskat, M. 1947. The Performance of Bottom Water-drive Reservoirs. Trans. AIME 170: 81-111.

Muskat, M. and Wycokoff, R. D. 1935. An Approximate Theory of Water-coning in Oil Production. Trans. AIME 114: 144-163.

Ozkan, E. and Raghavan, R. 1990. Performance of Horizontal Wells Subject to Bottomwater Drive. SPE Reservoir Engineering 5(3): 375-383.

Penmatcha, V. R. and Aziz, K. 1998. A Comprehensive Reservoir/Wellbore Model for Horizontal Wells. Paper SPE 39521, SPE India Oil and Gas Conference and Exhibition, New Delhi, India, February 17-19.

Pinto, A. C. C., Branco, C. C. M., et al. 2003. Offshore Heavy Oil in Campos Basin: The Petrobras Experience. Paper SPE 15283-MS, Offshore Technology Conference, Houston, Texas, May 5-8.

Proyer, G., Chaziteodorou, G., et al. 1985. Results of a Steamdrive Pilot Project in the Ruehlertwist Field, Federal Republic of Germany. SPE Journal of Petroleum Technology 37(2): 284-294.

Qin, W. and Wojtanowicz, A. K. 2007. Well Performance Analysis for Heavy Oil With Water Coning.2007-162, Canadian International Petroleum Conference, Calgary, Alberta, June 12-14.

Saskoil, S. S. and Butler, R. M. 1990. The Production Of Conventional Heavy Oil Reservoirs With Bottom Water Using Steam-Assisted Gravity Drainage. The Journal of Canadian Petroleum Technology 29(2): 78-86.

Satter, A., Iqbal ,G.M. and Buchwalter, J.L. 2007. Practical Enhanced Reservoir Engineering. Pennwell, Tulsa, Oklahoma.

Shecaira, F. S., Branco, C. C. M., et al. 2002. IOR: The Brazilian Perspective.SPE paper 75170, SPE/DOE Improved Oil Recovery Symposium, Tulsa, Oklahoma, April 13-17.

Sherrard, D. W., Brice, B. W., et al. 1987. Application of Horizontal Wells at Prudhoe Bay. SPE Journal of Petroleum Technology 39(11): 1417-1425.

Shirman, E. I. and Wojtanowicz, A. K. 1997. Water Cone Hysteresis and Reversal for Well Completions Using the Moving Spherical Sink Method. Paper SPE 37467, SPE Production Operations Symposium, Oklahoma City, Oklahoma, March 9-11.

Siddiqi, S. 2001. A Study of Bottom Water Drive Reservoir Using a Scaled Physical Model and a Numerical Simulator. Louisiana State University. Master Thesis.

Siemek, J. and Stopa, J. 2002. A Simplified Semi-Analytical Model for Water-Coning Control in Oil Wells With Dual Completions System. Journal of Energy Resources Technology 124(4): 246-252.

Stokes, D. D., Brew, J. R., et al. 1978. Steam Drive as a Supplemental Recovery Process In an Intermediate-Viscosity Reservoir, Mount Poso Field, California. SPE Journal of Petroleum Technology 30(1): 125-131.

Targac, G. W., Redman, R. S. , et al. 2005. Unlocking the Value in West Sak Heavy Oil. Paper SPE 97856, SPE/PS-CIM/CHOA International Thermal Operations and Heavy Oil Symposium, Calgary, Alberta, Canada. November 1-3.

Target, P. L. 1992. The Haven Oil Field: Development of a Tiny Marginal Field With Horizontal Wells. SPE Journal of Petroleum Technology 44(4): 496-501.

Trindade, W. L. and Branco, C. C. M. 2005. The Offshore Heavy Oil Development Challenges in Brazil. Paper SPE 97381, SPE Latin American and Caribbean Petroleum Engineering Conference, Rio de Janeiro, Brazil, June 20-23.

Visser, R. C. 1989. Offshore Production of Heavy Oil. SPE Journal of Petroleum Technology 41(1): 67-70.

Wehunt, C. D., Burke, N. E., et al. 2003. Technical Challenges for Offshore Heavy Oil Field Developments. Paper SPE 15281.Offshore Technology Conference, Houston, Texas, May 5-8.

Wojtanowicz, A. K. and Armenta, M. 2004. Assessment of Down-Hole Water Sink Technology for Controlling Water Inflow at Petroleum Wells. Journal of Energy Resources Technology 126(4): 334-341.

Wojtanowicz, A. K. and Xu, H. 1995. Downhole Water Loop-A New Completion Method to Minimize Oil Well Production Watercut in Bottom-water-drive Reservoirs. Journal of Canadian Petroleum Technology 33 (8):56-62.

Zhou, W., J. Zhang, et al. 2008. Key Technologies of Polymer Flooding in Offshore Oilfield of Bohai Bay. Paper SPE 115240, SPE Asia Pacific Oil and Gas Conference and Exhibition. Perth, Australia, October 20-22.

APPENDIX A

MATLAB PROGRAM FOR CRITICAL RATE CALCULATION USING HODOGRAPH METHOD FOR SINGLE HORIZONTAL WELL

```
clc
clear all
close all

global do dw ko muo ho hw  ...
%%%%%%%%%%% Input reservoir properties%%%%%%%%%%%%%%

prompt{1}  = 'oil density,m^3/kg            '      ;
prompt{2}  = 'water density,m^3/kg'      ;
prompt{3}  = 'reservoir permeability, md'      ;
prompt{4}  = 'oil viscosity,cp'      ;
prompt{5}  = 'oil thickness,ft'   ;
prompt{6}  = 'well distance to top reservoirft'   ;
title      = 'INPUT DATA set single well '  ;


do=995*0.85;
dw=995;
ko=10;
muo=1.5;
h=32.5%63.5ft
hw=0 %m 10ft

default_ans = {num2str(do),num2str(dw),num2str(ko),num2str(muo),num2str(h),num2str(hw),};
answer      = inputdlg(prompt,title,1,default_ans);

maduro = size(answer);
[maduroA,maduroB]=size(answer);
for maduroC = 1:maduroA;
   answerD(maduroC) = str2num(answer{maduroC});
end
save backupDD answerD
do=answerD(1); %wellbore radius,ft
dw=answerD(2); %drainage radius,ft
ko=answerD(3)*0.987*10^(-15); % reservoir thickness, ft
muo=answerD(4)*10^(-3); %horizontal pemeability ,md
h=answerD(5)*0.3048;
hw=answerD(6)*0.3048;
clear prompt



K=(ko/muo)*(dw-do)*9.81
```

```
% need change with different xe
%%%%%%%%%%%%Solve t for given xe%%%%%%%%

function F=myfun(t)
 Xe=42 %%%%%%%% input reservoir distance
 H=8.5 %%%%%%%%%%%% input reservoir thickness
F=Xe-H*3.14*2*(0.5005*t^2-0.0203*t-0.2527+0.2527)/(3.14*3.14)/(log(2)+log(cosh(t)))

t0=2
t = fsolve(@myfun,t0)
%%%%%%%%%%%%%%% Output critical rate and crest shape%%%%%%%%

a=0.2206/K+log(cosh(t))/(3.14*K)
Q1=h/a  % critical rate for well at the top

H=@ff;% unconfined reservoir
H2=@L;
H3=@Ly;
yc=-log(cosh(t))/3.14*Q1/K
for t=0:0.05:t
I=2*quad(H,0,t)/(3.14*3.14)
O=-log(cosh(t))/3.14
A=I*Q1/K
B=O*Q1/K % crest height
yy=-(h+yc)
a1=0.2206*Q1/K
plot(A/0.3048,(B+yy)/0.3048,'-.') % plot crest shape
hold on
end

function y=ff(t)
y=t.*tanh(t);

function y=L(t)
y=t.*tanh(t)./(1+cosh(t).^2/100).^0.5

function y=Ly(t)
y=tanh(t)./(1+cosh(t).^2/100).^0.5
```

APPENDIX B

DERIVATION OF POTENTIAL DISTRIBUTION FOR HORIZONTAL WELL LOCATED BETWEEN TWO NO-FLOW BOUNDARIES

A 2-D model of a horizontal well located at a distance h_{well} from the reservoir top can be described in Figure A-1:

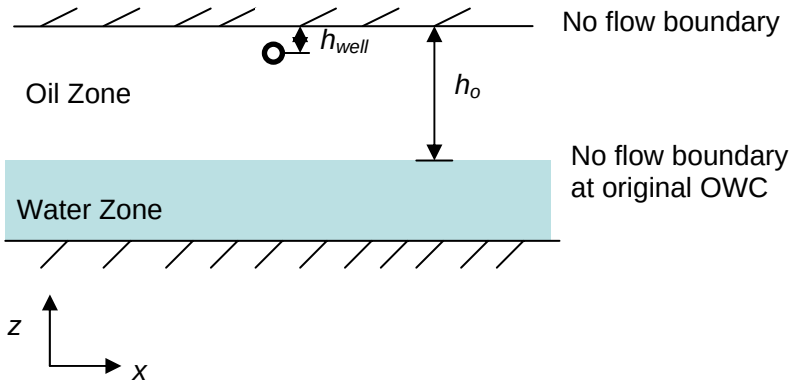

Figure A-1 A well between two no-flow boundary

A general equation of flow potential can be derived for steady-state condition as follows by solving the Laplace equation:

$$\frac{\partial^2 \Phi}{\partial x^2} + \frac{\partial^2 \Phi}{\partial z^2} = 0 \quad \text{.....(A-1)}$$

At boundary conditions: $\frac{\partial \Phi}{\partial z} = 0$ for $z = h_o$ and at $z = 0$

After a superposition in place, as shown in Figure A-2.

The flow system in Figure A-2 can be represented by an infinite row of wells in an infinite reservoir without imposed boundary. The general form of flow potential in such a reservoir may be expressed as follows:

$$\Phi_{(x,z)} = \frac{q_l \mu_o}{2\pi k_o} \sum_{-\infty}^{\infty} \ln \sqrt{[x^2 + (z - 2nh_o - h_o + h_{well})^2] \times [x^2 + (z - 2nh_o + h_o - h_{well})^2]} \quad \text{.....(A-2)}$$

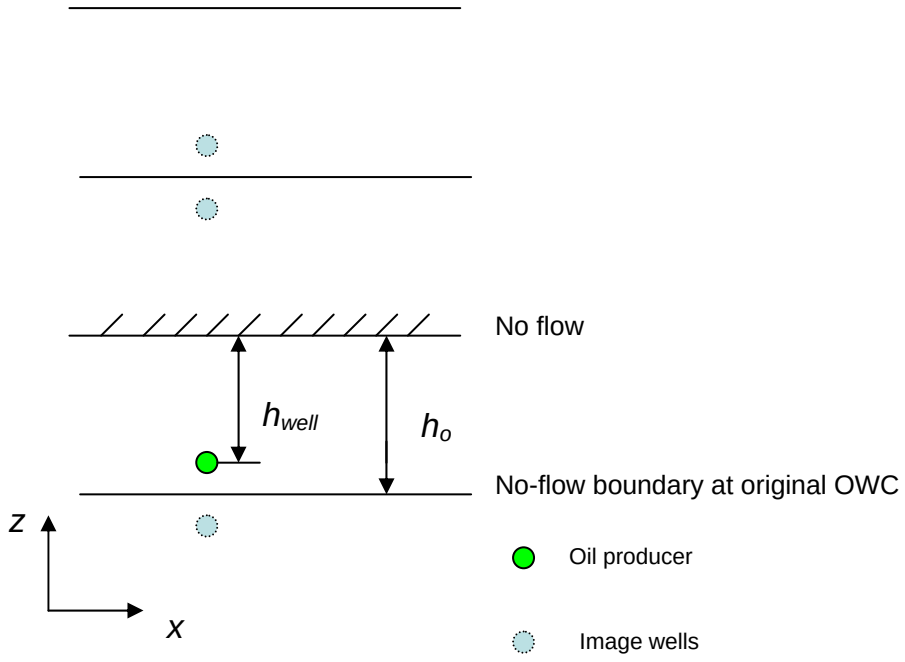

Figure A-2 Transformation of boundary conditions

The above equation can be simplified as follows:

$$\Phi_{(x,z)} = \frac{q_l \mu_o}{4\pi k_o}\left\{\ln[\cosh\frac{\pi x}{h_0} - \cos\frac{\pi(z - h_o + h_{well})}{h_0}] \times [\cosh\frac{\pi x}{h_0} - \cos\frac{\pi(z + h_o - h_{well})}{h_0}]\right\} + C \quad \text{(A-3)}$$

For well located at $h_{well} = h_o$ (at the bottom of the reservoir), A-3 yield the expression as A-4, which is identical to the expression given by (Houpeurt 1975)

$$\Phi_{(x,z)} = \frac{q_l \mu_o}{2\pi k_o}\ln[\cosh\frac{\pi x}{h_0} - \cos\frac{\pi z}{h_0}] + C \quad \text{(A-4)}$$

APPENDIX C

MATLAB PROGRAM FOR CRITICAL RATE CALCULATION USING DUPUIT APPROXIMATION FOR BWS WELLS

```
clc

clear all

close all

global do dw ko muo muw ho hw  ...

%%%%%%%%%%Input dataset%%%%%%%%%%%%%%%%%%%%


prompt{1}  = 'oil density,m^3/kg            '      ;

prompt{2}  = 'water density,m^3/kg'       ;

prompt{3}  = 'reservoir permeability, md'       ;

prompt{4}  = 'water zone permeability, md'       ;

prompt{5}  = 'oil viscosity,cp'       ;

prompt{6}  = 'water viscosity,cp'       ;

prompt{7}  = 'oil thickness,ft'   ;

prompt{8}  = 'water thickness,ft'   ;

prompt{9}  = 'reservoir radius,ft'   ;

prompt{10}  = 'water rate,bbl/day/ft'   ;

title      = 'INPUT DATA set  DWS wells'  ;


do=995*0.85;

dw=995;

ko=10;
```

```
kw=10;
muo=1.5;
muw=0.96;
ho=(100-50)*0.5;
hw=50-ho;
L=(100-50)*0.5*1.8;
Qw=(5.7355e-008)*(24*60*60*0.3048/1.0/0.1589)*1.2;

default_ans =
{num2str(do),num2str(dw),num2str(ko),num2str(kw),num2str(muo),num2str(muw),num2str(
ho),num2str(hw),num2str(L),num2str(Qw),};
answer      = inputdlg(prompt,title,1,default_ans);

maduro = size(answer);
[maduroA,maduroB]=size(answer);
for maduroC = 1:maduroA;
   answerD(maduroC) = str2num(answer{maduroC});
end
save backupDD answerD
do=answerD(1);
dw=answerD(2);
ko=answerD(3)*0.987*10^(-15);
kw=answerD(4)*0.987*10^(-15);
muo=answerD(5)*10^(-3);
```

```
muw=answerD(6)*10^(-3);
ho=answerD(7)*0.3048;
hw=answerD(8)*0.3048;
L=answerD(9)*0.3048;
Qw=answerD(10)/(24*60*60*0.3048/1.0/0.1589);
clear prompt
M=(ko/muo)/(kw/muw)
%%%%%%%%Solve Equation 5.10 using MATLAB function solve%%%%%%%%%
syms Qo  C D h hh hhw
H=hw+ho;
A=(1-dw/do)*do*Ko*Kw*H;
B=(1-dw/do)*do*Ko*Kw;
C=Qw*dw*Ko+Qo*do*Kw;
D=Qo*do*Kw*H;
f=-(A*h-B*h^2)/(C*H-D);
h=0
hh=1/C^2*h*D*B-1/C*A*h+1/2/C*B*h^2-D/C^2*log(-C*h+D)*A+D^2/C^3*log(-
C*h+D)*B
h=ho
hhw=1/C^2*h*D*B-1/C*A*h+1/2/C*B*h^2-D/C^2*log(-C*h+D)*A+D^2/C^3*log(-
C*h+D)*B
fh=hh-hhw
f=fh-L
y1=solve('.16119041121863798876103059552405e-
```

13*Qo/(.37387516853299661440718376131245e-

11+.84875044348828133537223822910160e-

4*Qo)^2*log(.12934956758761407551072910611508e-2*Qo)-

.13681043300787742779975740473024e-

17*Qo^2/(.37387516853299661440718376131245e-

11+.84875044348828133537223822910160e-

4*Qo)^3*log(.12934956758761407551072910611508e-

2*Qo)+.80595205609318991872809331732529e-

14*Qo/(.37387516853299661440718376131245e-

11+.84875044348828133537223822910160e-4*Qo)^2-

.71218112073745064130731438000182e-10/(.37387516853299661440718376131245e-

11+.84875044348828133537223822910160e-4*Qo)-

.16119041121863798876103059552405e-13*Qo/(.37387516853299661440718376131245e-

11+.84875044348828133537223822910160e-4*Qo)^2*log(-

.28489287842214342017827402612009e-10+.64674783793807037755364553057542e-

3*Qo)+.13681043300787742779975740473024e-

17*Qo^2/(.37387516853299661440718376131245e-

11+.84875044348828133537223822910160e-4*Qo)^3*log(-

.28489287842214342017827402612009e-10+.64674783793807037755364553057542e-

3*Qo)-13.71600000000000000000000000000=0','Qo')

y2=double(y1)

%%%%%%%%%%%%%% Dimensionless group%%%%%%%%%%%%%%

K=(ko/muo)*(dw-do)*9.81

Kw=(kw/muw)*(dw-do)*9.81

```
Xd=L/ho %dimentionless drainage radius

%%%%%% Output the dimension critical rate%%%%%%%%%%%%%%%%%%%%%

Qo=y2 %m^3/s critical rate for whole flow system

Qc=2*Qo*24*60*60*0.3048/1.0/0.1589 %bbl/day/ft

Qd=2*Qo/(K*ho) % dimentionless rate oil

Qwd=2*Qw/(Kw*hw)% dimentionless rate water
```

APPENDIX D

NOMENCLATURE

Symbol	Description
A	drainage area
a	half the major axis of drainage ellipse
B_o	oil formation volume factor
b	the distance between the apex of the cone to the well
c	shape parameter of OWC
c_t	total compressibility
h	thickness
h_o	oil zone thickness
h_w	water zone thickness
h_c	critical cone height
h_{pc}	capillary transition zone
h_{well}	the distance between the well to the top of the reservoir
h_{wD}	dimensionless well location
H	the sum of oil zone thickness and water zone thickness
G	Green's function
K	hydraulic conductivity
k	permeability
k_o	oil zone permeability
k_w	water zone permeability
k_{ro}	oil zone relative permeability
k_{rw}	water zone relative permeability
L	horizontal well length, distance
M	end point mobility ratio

N	stock tank oil initially in place
N_p	cumulative oil production
V	the net bulk volume of reservoir rock
p	pressure
p_i	initial pressure in the oil zone
p_o	pressure in the oil zone
p_w	pressure in the water zone
p_r	reservoir pressure at the initial gas/oil contact
p_e	reservoir pressure at outer boundary
q	flow rate
q_o	oil flow rate per unit length
q_w	water flow rate per unit length
q_l	flow rate per unit length
q_c	critical oil rate per unit length
q_{cD}	dimensionless critical rate
q_{wD}	dimensionless water drainage rate
RF	recovery factor
r_w	wellbore radius
r_e	reservoir radius
r_{we}	effective wellbore radius
s	direction along interface
S_{or}	residual oil saturation
S_{wc}	connate water saturation
t	parameter
t	time
u	flow velocity
u_n	flow velocity normal to the interface

u_x	flow velocity at x direction
u_z	flow velocity at z direction
u_s	flow velocity along interface
x	x direction or dimension
x_w	wellbore radius measured at x direction or dimension
x_e	distance from wellbore to the reservoir boundary, reservoir radius
x_{eD}	dimensionless reservoir radius
y	y direction or dimension
z	z direction or dimension

Greek

Symbol	Description
γ	specific gravities
γ_o	oil specific gravities
γ_w	water specific gravities
μ	viscosity
μ_o	oil viscosity
μ_w	water viscosity
ρ	density
ρ_o	oil density
ρ_w	water density
ρ_g	gas density
Φ	potential
Φ_o	oil potential
Φ_w	water potential
∇	gradient
Δ	difference
ϕ	porosity

Functions

ln	Napierian logarithm
sinh	Hyperbolic sine
cosh	Hyperbolic cosine
tanh	Hyperbolic tangent
s	Dilogarithm $s(x) = \int_1^x \frac{\ln t}{1-t} dt$
ε	Function sign $\varepsilon(x) = x \big/ \lvert x \rvert$

VITA

Wenting Qin was born in Chongqing, China.

She obtained a Bachelor's degree from Southwest Petroleum University, in 2003.

She worked as a petroleum engineer at China National Offshore Oil Corporation (CNOOC), Tianjin, China from 2003 to 2004.

She then joined Department of Applied Earth Sciences at Delft University of Technology, The Netherlands and received a degree of Master of Science in petroleum engineering in 2006.

In September 2006, she entered the Craft & Hawkins Department of Petroleum Engineering at Louisiana State University to work towards a doctoral degree in petroleum engineering in August 2011.